CHALMERS
UNIVERSITY OF TECHNOLOGY

Implementation of the permanent deformation model PEDRO for pavement structures

Master's Thesis in the Master's Programme Infrastructure and Environmental Engineering

ANNA RÖDIN
EMMA UHRDIN ANDERSSON

Department of Civil and Environmental Engineering
Division of GeoEngineering
Research Group Road and Traffic
CHALMERS UNIVERSITY OF TECHNOLOGY
Master's Thesis BOMX02-17-09
Gothenburg, Sweden 2017

MASTER'S THESIS BOMX02-17-09

Implementation of the permanent deformation model PEDRO for pavement structures

Master's Thesis in the Master's Programme Infrastructure and Environmental Engineering

ANNA RÖDIN

EMMA UHRDIN ANDERSSON

Department of Civil and Environmental Engineering
Division of GeoEngineering
Research Group Road and Traffic
CHALMERS UNIVERSITY OF TECHNOLOGY
Göteborg, Sweden 2017

Implementation of the permanent deformation model PEDRO for pavement structures
Master's Thesis in the Master's Programme Infrastructure and Environmental Engineering

ANNA RÖDIN

EMMA UHRDIN ANDERSSON

Examensarbete BOMX02-17-09/ Institutionen för bygg- och miljöteknik,
Chalmers tekniska högskola 2017

Department of Civil and Environmental Engineering
Division of GeoEngineering
Research Group Road and Traffic
Chalmers University of Technology
SE-412 96 Göteborg
Sweden
Telephone: + 46 (0)31-772 1000

Cover:
Image from E6 Fastarp-Heberg (Trafikverket, 2017), pavement structure 12, one of the studied pavement structures.
Department of Civil and Environmental Engineering. Göteborg, Sweden, 2017

Implementation of the permanent deformation model PEDRO for pavement structures

Master's thesis in the Master's Programme Infrastructure and Environmental Engineering

ANNA RÖDIN
EMMA UHRDIN ANDERSSON
Department of Civil and Environmental Engineering
Division of GeoEngineering
Research Group Road and Traffic
Chalmers University of Technology

ABSTRACT

The lifespan of a road is dependent on several factors including the development of permanent deformations and cracking. The current design method considers cracking in the bound layers and deformations at the subgrade surface, but not the deformation in the bound layers. VTI (The Swedish National Road and Transport Research Institute) is currently developing a software, PEDRO (Permanent deformation of asphalt concrete layers for roads), that calculates the permanent deformation in bituminous layers. The aim of the thesis is to evaluate and calibrate the model PEDRO. The software was used to calculate the permanent deformation for two pavement structures located at the road E6 Fastarp-Heberg. The first structure is a reference structure built according to the, during construction, existing standard. The second structure is a FAS structure that is built according to the FAS concept. By comparing the calculated permanent deformation to the deformations measured at the road, the calibration factor used in PEDRO was calculated for each structure.

PEDRO is based on the viscoelasticity of the asphalt material and considers the dynamic viscosity and Poisson's ratio of the asphalt concrete, the amount and characteristics of the traffic and the temperature of the pavement. All input data except the viscous properties were gathered from previously conducted studies. The viscous properties were assessed in the laboratory with a test called asphalt concrete shear box, a method developed by VTI. The results of the laboratory tests were used to generate master curves, one for each asphalt concrete layer. The master curves were then used to determine the dynamic shear modulus and angular frequency for each asphalt mix, which were used to calculate the viscosity.

A new surface course was paved in 2011 but the laboratory specimens were drilled before that, and therefore the calculations were performed for 2010. The measured rutting for the reference structure was 17 mm in 2010, where 8.22 mm were caused by the permanent deformation of the bound layers. By comparing the measured permanent deformation to the one calculated in PEDRO a calibration factor of 0.1001 was found. For the FAS structure the measured rutting in 2010 was equal to 9 mm and 5.31 mm originated from the permanent deformation of the bound layers. For the FAS structure a calibration factor of 0.0668 was found.

Key words: permanent deformation, rutting, PEDRO, asphalt concrete shear box, asphalt concrete

Implementering av den permanenta deformationsmodellen PEDRO för vägkonstruktioner

Examensarbete inom masterprogrammet Infrastructure and Environmental Engineering

ANNA RÖDIN
EMMA UHRDIN ANDERESSON
Institutionen för bygg- och miljöteknik
Avdelningen för geologi och geoteknik
Väg och trafik
Chalmers tekniska högskola

SAMMANFATTNING

Livslängden på en väg beror på flera faktorer, bland annat utvecklingen av spårbildning och sprickbildning. Den nuvarande designmetoden beräknar sprickbildning i beläggningen och deformationer på undergrundens yta, men inte deformationerna i de bundna lagren. VTI (Statens väg- och transportforskningsinstitut) utvecklar för närvarande en programvara, PEDRO (Permanent deformation of asphalt concrete layers for roads), som beräknar permanenta deformationer i bitumenbundna lager. Syftet med examensarbetet är att utvärdera och kalibrera modellen PEDRO. Programvaran användes för att beräkna de permanenta deformationerna för två olika asfaltskonstruktioner vid E6 Fastarp-Heberg. Den första konstruktionen kallas referens och är byggd i enighet med den, under genomförandet, gällande standarden. Den andra konstruktionen kallas FAS och är byggd enligt FAS-konceptet. Genom att jämföra den beräknade permanenta deformationen mot den spårbildning som är uppmätt på vägen kunde kalibreringsfaktorn i PEDRO beräknas för de två konstruktionstyperna.

PEDRO är baserat på de viskoelastiska egenskaperna i asfalten och beräknar utifrån den dynamiska viskositeten och Poissons tal för asfalten, trafikmängden och trafikens karaktär samt temperaturen i vägen. All indata utom den dynamiska viskositeten inhämtades från tidigare genomförda studier. Viskositeten analyserades och beräknades i laboratoriet med ett test som kallas asphalt concrete shear box, en metod utvecklad av VTI. Resultaten av laboratorieförsöken användes för att generera masterkurvor, en för varje asfaltslager. Masterkurvorna användes sedan för att bestämma den dynamiska skjuvmodulen och vinkelfrekvensen för varje asfaltslager och dessa parametrar användes för att beräkna viskositeten.

Vägen fick en ny beläggning år 2011 men provkropparna borrades innan beläggningsarbetet så beräkningarna utfördes för år 2010. Den uppmätta spårbildning för referenskonstruktionen var 17 mm 2010, där 8,22 mm orsakades av permanenta deformationer i de bundna lagren. Genom att jämföra den uppmätta spårbildningen med den som beräknades i PEDRO erhölls en kalibreringsfaktor på 0,1001. För FAS-konstruktionen var den uppmätta spårbildning år 2010 lika med 9 mm, varav 5,31 mm härstammar från de permanenta deformationerna i de bundna lagren. För FAS-konstruktionen erhölls en kalibreringsfaktor på 0,0668.

Nyckelord: permanenta deformationer, spårbildning, PEDRO, asphalt concrete shear box, asfalt

Contents

Preface

In this thesis the model PEDRO has been used to calculate the permanent deformation in the bound layers and to estimate the calibration factors for the studied pavement structures. The thesis is part of an ongoing project performed by VTI (Swedish National Road and Transport Research Institute) aiming to calibrate the model PEDRO.

The thesis was carried out during the spring of 2017 at the department of Civil and Environmental Engineering at Chalmers University of Technology. It was performed at the Swedish Transport Administration in Gothenburg and the laboratory work was carried out at VTI in Linköping. The thesis is part of an industry-wide project: Prognosis of permanent deformation - asphalt pavements. The project work was performed with support from the Strategic Innovation Program (a joint venture of VINNOVA, Formas and the Swedish Energy Agency), the Swedish Transport Administration, SBUF, Nynas, Volvo Technology and Däckspecialisternas riksförbund. The master thesis was carried out by Anna Rödin and Emma Uhrdin Andersson, with supervision from Sven Agardh at Lund University, Carl-Gösta Enocksson at the Swedish Transport Administration and Safwat Said at VTI.

We would like to thank our supervisor Carl-Gösta Enocksson at the Swedish Transport Administration for his support and for making this study possible. Further, we would like to give thanks to Safwat Said and Abubeker Ahmed at VTI for their help with PEDRO, the laboratory tests and for all material they have provided for the thesis, and to Andreas Waldemarson at VTI for his help with the laboratory tests. Finally, we would like to thank Sven Agardh at Lund University for his supervision and Gunnar Lannér at Chalmers University of Technology for his help with all administrative questions, as well as all other who have answered our questions and helped us collect information.

Gothenburg, June 2017

Anna Rödin and Emma Uhrdin Andersson

Notations

Abbreviations

AASHO	American Association of State Highway and Transportation Officials
AADT	Annual average daily traffic
AADTh	Annual average daily traffic, heavy vehicles
ABS	Stone mastic asphalt
AG	Base mix
ATR	Automatic traffic recorder
AVC	Automated vehicle classifier traffic measurement system
BWIM	Bridge weigh in motion traffic measurement system
cc	Centre-to-centre distance
ESAL	Equivalent single axle load
FAS	Swedish asphalt pavement association
MEPDG	Mechanistic-Empirical Pavement Design Guide
PEDRO	Permanent deformation of asphalt concrete layers for roads
PMS Objekt	Pavement management systems, a pavement designing tool
PMSv3	Pavement management systems version 3, an information database
PRIMAL	Longitudinal profile reference equipment
RD	Rut depth
RST	Road surface tester
TRVK-väg	The Swedish transport administrations technical requirements Road construction
TRVR-väg	The Swedish transport administrations technical advice Road construction
VEROAD	Visco Elastic Road Analysis Delft
Viacobase	Trademark asphalt mixture
Viacobind	Trademark asphalt mixture
Viacotop	Trademark asphalt mixture
VTI	The Swedish National Road and Transport Research Institute
VViS	Road weather information system
WIM	Weigh in motion traffic measurement system

Roman upper case letters

B	constant used in master curves
D	constant used in master curves
F	force [N]
$\|G^*\|$	dynamic shear modulus [MPa]
N	number of axle loads, load repetitions
N_a	number of axle loads with axle type a
N_b	number of axle loads with axle type b
P_a	weight of axle type a [metric ton]
P_b	weight of axle type b [metric ton]
$S_{t_{day,1}}$	stiffness modulus at $t_{day,1}$ [MPa]
$S_{t_{day,2}}$	stiffness modulus at $t_{day,2}$ [MPa]
T	temperature [°C]
T_{ref}	reference temperature [°C]
V	vehicle speed [m/s]

Roman lower case letters

a	radius of contact area [m]
a_1	factor used to describe viscosity in PEDRO
a_2	factor used to describe viscosity in PEDRO
a_3	factor used to describe viscosity in PEDRO
b	constant used in master curves
b_1	regression constants used in MEPDG
b_2	regression constants used in MEPDG
b_3	regression constants used in MEPDG
c	constant used in master curves
d	sample diameter [m]
f	frequency [Hz]
f_r	reduced frequency [Hz]
h	thickness [mm]
i	$\sqrt{-1}$
k	constant used in master curves
n	factor describing age properties
$n_{sublayers}$	number of sublayers

p	constant used in master curves
t	time [s]
$t_{day,1}$	age of bituminous layer [days]
$t_{day,2}$	age of bituminous layer [days]
x	distance from loading centre [m]
x_{shift}	factor used to describe Poisson's ratio in PEDRO
y_{min}	factor used to describe Poisson's ratio in PEDRO
y_{span}	factor used to describe Poisson's ratio in PEDRO
z	depth from road surface [m]

Greek lower case letters

α_T	shift factor
β	constant used in master curves
β_1	calibration factor used in MEPDG
γ	constant used in master curves
δ	constant used in master curves
$\varepsilon_\perp$	transverse strain [m/m]
$\varepsilon_\parallel$	axial strain [m/m]
ε_{mean}	average strain [m/m]
ε_p	permanent vertical strain [m/m]
ε_r	elastic vertical strain [m/m]
$\lvert\eta^*\rvert$	dynamic viscosity [MPa s]
η_p	viscosity at peak phase angle [Pa s]
λ	factor used to describe Poisson's ratio in PEDRO
κ	constant used in master curves
ν	Poisson's ratio [-]
σ_0	contact pressure [Pa]
$\emptyset$	phase angle [degrees]
ω	angular frequency [rad/s]

1 Introduction

This master thesis seeks to evaluate a method to predict the development of permanent deformation on a road paved with asphalt concrete. A model, PEDRO (Permanent deformation of asphalt concrete layers for roads), that is currently under development for this purpose will be examined and validated. The results gained from the model will be compared to measured rut development at a motorway located in southern Sweden.

This chapter begins with an overview of why the permanent deformation is so crucial to the lifespan of the asphalt concrete layers, followed by how the lifespan is currently calculated and the drawbacks of that method. Further, the thesis will be put into context with the ongoing development of the model PEDRO. The objectives and limitations will also be reviewed along with the chosen method used to perform this study.

1.1 Background

The Swedish Transport Administration manage all national roads in Sweden. The total length of the national road network is 98500 km, and approximately 80 % of all national roads are constructed with asphalt concrete (Trafikverket, 2015a). The lifespan of the bound layers is said to be exceeded when the distresses become visible and limits the traffic flow. The most common reason for an unsatisfying pavement condition is the permanent deformation in the bitumen bound layers (Oscarsson, 2011) and therefore it becomes the most crucial distress to consider during design and construction. The current development of increasing traffic intensity, heavier trucks, alternation of truck tires and an increased construction of 2+1 roads with narrower lanes has accelerated the development of permanent deformation on Swedish roads (Said, 2016).

Today pavements are designed using PMS Objekt, a program designing pavements according to the demands and standards developed by the Swedish Transport Administration, TRVK-väg and TRVR-väg. The method calculates the number of standard axles (ESAL) that can pass on the road before damage occurs. Fatigue cracking and deformation at the subgrade surface are considered in PMS Objekt but not the permanent deformation in the bound layers which has been found to be one of the main contributors to loss in pavement condition. Further, the accuracy of the calculation is limited and the suggested pavement designs are standardised because PMS Objekt is based on empirical formulas only valid for a limited number of asphalt concrete mixes. The consequence of this is that some roads are not performing satisfactory while others are excessively constructed. By stepping away from the standard designs of pavements and creating more optimised designs, the cost for construction could be decreased without increasing the cost for maintenance. However, this demands that the calculations of the pavements lifespan are increasing in accuracy and are valid for many different design options. The consensus is that this can be achieved by calculating the distress based on mechanistic correlations (Oscarsson, 2011). If the estimation of lifespan can be made accurately, the pavement structures can be designed optimally.

1.2 Problem

There is an ongoing project conducted by VTI (The Swedish National Road and Transport Research Institute) which aims to implement a model for permanent deformation. So far only a beta-version (Version 1.03) of the model PEDRO exists, and the verification of the model is under progress. The aim of implementing PEDRO is to contribute with complementary predictions of permanent deformation in the asphalt concrete layers, and thereby enable an optimal construction and maintenance planning (Said, 2016). Several methods for calculating the permanent deformations of a road structure already exists. However, most of these models are based on linear elastic theories and static loads, which does not give a fully accurate description of the asphalt concrete's behaviour (Said, 2016) and therefore is PEDRO, a viscoelastic model, being developed. The master thesis will be part of the project conducted by VTI and examine two different pavement structures. It will compare the measured rutting of those structures to the rutting estimated in PEDRO.

When calculating the permanent deformation some pavement properties are required, along with the traffic load and distribution, and climate data. The Swedish Transport Administration have several test sections for which the pavement performance is well documented. One of these roads is E6 Fastarp-Heberg which will serve as reference road for the thesis. The road is a motorway located north of Halmstad which consists of nineteen pavement structures that are all continuously being tested and evaluated, providing a generous amount of available data. This data includes: rut depth, wear of the surface layer, pavement temperature, layer thickness and more.

1.3 Aim and objectives

The goal of the thesis is to calibrate the model PEDRO for two different pavement structures, and the results of the model will be compared to measured values of permanent deformation for the two structures. The master thesis will calibrate the model PEDRO which is being developed by VTI and focus will be on the bound layers in asphalt concrete pavement structures. Further, the results of the project should assist in the implementation of PEDRO and provide useful data for the study conducted by VTI. Specifically, the thesis should provide accurate viscosity parameters for the studied asphalt mixtures and determine the calibration factor in PEDRO for the two structures.

1.4 Limitations

The calculations will be based on two short road sections, both part of a motorway in the southern part of Sweden. To draw any conclusions regarding the validity and accuracy of PEDRO based on the results of this thesis alone will be hard. However, this thesis is part of a larger study validating the PEDRO model, and the complete study will give a better understanding of the model's accuracy. PEDRO only calculates the permanent deformation in the bound layers, and therefore focus will be solely on the bound layers. By comparing calibration factors for similar roads PEDRO can be validated. However, this is the first part of the VTI implementation project to finish and therefore a comparison of calibration factor is not possible.

The material properties are tested in the laboratory. However, the core samples are from 2011, how (or if) they have been affected by the storage is not known. This could have

a major impact on the results of the laboratory and thereby also on the calculations of the permanent deformation.

The calculations are performed for E6 Fastarp-Heberg, however not all the needed input data is available for the reference road. The used data is chosen to be as accurate as possible but may still entail some incorrect data, which affect the accuracy of the results.

1.5 Method

The thesis will be conducted in five steps. First a literature review will be performed followed by laboratory experiments to find the needed material properties. Then the laboratory results will be compiled and analysed, followed by the collection of data measured at the reference road. Finally, the results of the laboratory experiments and field data will be used in PEDRO to calculate the permanent deformation and the calibration factor.

The literature review will give an insight to the model PEDRO and the correlations and assumptions it is based on. Further, the literature study will explore the earlier research conducted on the reference road, E6 Fastarp-Heberg. It will also give some insights to the mechanisms causing permanent deformation in asphalt concrete pavements, as well as provide knowledge on the laboratory tests and how they are performed.

The laboratory experiments will be performed to determine the viscosity of the asphalt concrete. Specifically, the tested properties are the shear modulus and phase angle which describe the viscoelasticity of the material, i.e. how prone it is to permanent deformation. These parameters are determined by performing shear tests on core samples from the reference road E6 Fastarp-Heberg. The experiments are designed by VTI and will be performed at their laboratory in Linköping. Both studied pavement structures are asphalt bound pavements and two core samples per bound layer from each structure will be examined.

The measured and evaluated data of the road E6 Fastarp-Heberg will be gathered from different reports following up the pavements performance (Wiman, et al., 2009; Ekblad & Lundström, 2011) as well as from PMSv3, the Swedish Transport Administration's road survey tool. A beta version of the model PEDRO will be used to calculate the permanent deformation and the results will be compared to the measured values of rutting at E6 Fastarp-Heberg.

The project will focus on the bound layers in the pavement and the structural deformation in the unbound layers will not be included, neither will the wearing caused by studded tires. Earlier research conducted at E6 Fastarp-Heberg evaluated the origin of the permanent deformation in the two studied pavement structures (Ekblad & Lundström, 2011) and those results will be used to complement the calculated permanent deformation, combined with the measurements of wearing caused by studded tires presented in Wiman, et al. (2009).

2 Asphalt concrete

The top layers of an asphalt pavement consist of asphalt concrete with the main task of distributing the load of the traffic down onto the underlying layers. Further, the asphalt concrete should be strong and durable enough to resist damage like rutting and cracking. Asphalt concrete consists of bituminous binder, aggregates, filler and sometimes also modifier. The properties of the asphalt concrete depend on the production process, the properties of the included materials and the surrounding environment.

2.1 Manufacturing process

Specifications of material properties and amounts of the different ingredients for an asphalt concrete are stated in the Job Mix Formula, the recipe of the asphalt mixture. According to the demands by the Swedish Transport Administration the Job Mix Formula must contain the following information: type of concrete, grain size distribution curve, quality of aggregates including material extraction site, particle density for the aggregates, type of binder, amount of binder in percent of weight, and specifications of any additives among more (Trafikverket, 2011a). Today it is becoming more common to order asphalt pavements according to performance. In those cases, trademark asphalt mixtures are often used and the Job Mix Formula is not made public.

The production of asphalt concrete can be done either as Hot Mix Asphalt, Warm Mix Asphalt or Cold Mix Asphalt. The biggest difference between the three mixtures is the temperature during production. Due to the difference in temperature the Job Mix Formula is a bit different as well, to make sure the aggregates and binder are well mixed and that the asphalt concrete has sufficient durability when the road is finished.

2.2 Material properties

The material properties of the asphalt concrete depend on the material properties of the included ingredients, bitumen and aggregates. Asphalt concrete is a viscoelastic material, due to the viscoelastic nature of the bitumen (Oscarsson, 2011) but also due to the roughness and interlocking of the aggregates (Said, et al., 2013).

2.2.1 Bitumen

Within the temperature range of applications, the material properties of the bitumen alter. At temperatures of 100-150°C bitumen is a fluid, at temperatures below 0°C the material is solid and brittle and in-between it is viscoelastic (Persson, 2016), and the stiffness of the material may vary with eight orders of magnitude (Bahia, 2009). Different bitumen change between these phases at different temperatures, and a softer bitumen is able to reach lower temperatures than a harder one before becoming solid and brittle (Persson, 2016).

Hardness, softening point, viscosity and breaking point are all tested to help determine how the bitumen behave at different temperatures. The hardness is tested with a needle penetration test determining the hardness of the bitumen at a certain temperature, and the viscosity test determines the flow of the bitumen at a certain temperature (Persson, 2016). The softening point test determines at which temperature the bitumen reaches a

certain softness and the breaking point is tested with Fraas breaking point test to determine at which temperature the bitumen may suffer from low temperature fractures (Persson, 2016). However, there are some drawbacks to these testing methods: penetration, softening point and breaking point are all one point measurements and empirical based which minimises their applicability (Bahia, 2009).Viscosity is also a single point measurement but a fundamental material property, yet it is only valid for Newtonian fluids (fluids with a viscosity independent on the applied shear force, e.g. water). Bitumen can only be considered a Newtonian fluid at very high temperatures (above softening point) or at constant shear rates (accomplished by very long loading times of several hours or even days), limiting the applicability (Bahia, 2009).

Bitumen is a viscoelastic material and the viscoelastic behaviour, independent of time and temperature, must be defined by at least two properties: its entire resistance to deformation and how that resistance is divided between the elastic and the viscous parts. In the shear mode, these properties can be described by the dynamic shear modulus and phase angle (Bahia, 2009). The total resistance to deformation is described by the dynamic shear modulus, and the division between elasticity and viscosity is described by the phase angle which varies from 0° to 90°. The material composition, loading time and temperature all effect the distribution between these components (Bahia, 2009). Between summer and winter the phase angle may vary with as much as 85° (Bahia, 2009), and the same variation can be found between traffic at standstill and traffic with high speed (Andersson, et al., 1994). At low temperatures or high frequencies, the phase angle reaches the limiting value of 0° meaning that the bitumen is completely elastic (Bahia, 2009). At high temperatures, the phase angle moves towards 90° and the material demonstrates a complete viscous behaviour.

2.2.2 Aggregates

The main component in regards of volume and weight of asphalt concrete is the aggregates. They create a solid structure in the asphalt concrete that is held together by the binder, and the purpose of the aggregates is to distribute the load on the surface down to the underlying layers. Further, the aggregates give the asphalt concrete durability and resistance to permanent deformations.

The properties of the aggregates depend on the size and gradation, hardness off the stone material, shape and roughness, as well as the angularity of the particles (Parhamifar, 2016a). The properties of the material, such as mineral composition also have a big impact (Brown, et al., 2009). The size and gradation of the aggregates define if the asphalt concrete is dense or porous. A dense pavement with a continuous gradation is preferable for highly travelled roads due to better interlocking between particle and less void in the asphalt concrete (Parhamifar, 2016a). This improves the restraint to abrasion and permanent deformation. Crushed aggregates provide a good stability to the material, given the surface roughness that creates friction and thereby interlocking between the stones (Said, et al., 2013). Further, the crushed aggregates results in lower peak phase angles which limits the asphalt concretes viscous behaviour and makes it less prone to rutting (Said, et al., 2013).

The Swedish Transport Administration has several requirements for the aggregates used in asphalt concrete. The demands include specifications of the distribution curves for the fractions and requirements of the properties of the aggregates (Parhamifar, 2016a). The aggregates must pass a few standard tests where the required performance for each test depend on the chosen asphalt mixture (Lind, 2011). The tests include: the flakiness index, proportion of aggregates with crushed surface, and the three abrasion tests Nordic abrasion test, Los Angeles test and Micro Deval test (Lind, 2011). The flakiness index test determines the ratio between the length and thickness of the aggregates, indicating if the grains are prone to breaking or not (Parhamifar, 2016b). The proportion of aggregates with crushed surface determines the roughness of the aggregates (Trafikverket, 1990). The three abrasion tests methods are similar in the way they grind an aggregate sample with steel balls, to test the durability and resistance to abrasion of the material (Pavement Interactive, 2011). The Nordic abrasion test and the Micro Deval test are performed in water.

2.3 Modified asphalt concrete

Bitumen is commonly conceived as a secondary product during refining and therefore the will to produce higher-quality bitumen is limited (Bahia, 2009). Thus, to increase the performance of the asphalt concrete and to meet the demands set by climate, traffic and pavement structure modified asphalt concrete was introduced. Modification can improve the rigidity, elasticity, brittleness, storage ability, durability and resistance to accumulated damage (Bahia, 2009). There are different kinds of modifiers and they can be divided into the following groups: thermosetting polymers, elastomeric polymers, thermoplastic polymers, chemical modifiers and extenders, fibres, antistripping, natural binders, and fillers (Papagiannakis & Masad, 2008).

The most commonly used modifiers are polymer modifiers (Bahia, 2009). A polymer modified asphalt concrete usually becomes more viscous and get a better elastic recovery, but the hardness of the binder seems not to be affected by the modification (Yildirim, 2005). However, there are drawbacks to the modification; lack of compatibility and separation during storage or application can lead to an inadequately performing pavement (Yildirim, 2005). There are many different polymer modifiers and they affect the asphalt concrete's properties in varying ways, and they can be combined to improve several different properties (Bahia, 2009). Styrene-butadiene-styrene, an elastomeric polymer (Papagiannakis & Masad, 2008), is the most commonly used modifier today and it has good compatibility, improve the elasticity properties and provide beneficial properties during low temperatures (Yildirim, 2005). The use of polymer modified binders has proven successful both in field and laboratory environments, however the laboratory tests lack the ability to determine which modifier is preferable in different circumstances (Yildirim, 2005). Testing of elastic recovery is today used to evaluate the performance of a polymer modified binder but there is a lack of correlation between the elastic recovery and resistance to rutting (Yildirim, 2005).

2.4 Ageing

The properties of an asphalt concrete are constantly changing due to ageing. Ageing refers to the change in the asphalt mixture and/or composition due to the influence of temperature and oxygen, which increase the stiffness of the bitumen and makes it harder and more brittle (Oscarsson, 2011; Papagiannakis & Masad, 2008). The main processes occurring during ageing are oxidation, evaporation, exudation and physical hardening (Read & Whiteoak, 2003). During the manufacturing and construction, the exposure to air will cause the bitumen to oxidise and induce evaporation of volatiles, causing the asphalt concrete to age (Collop & Cebon, 1995). After construction, the asphalt concrete is exposed to long term oxidation, however the exposure is limited mainly to the surface (Agardh, 2005). The oxidation process is usually limited to the first years of the pavement's life (Oscarsson, 2011). By minimising the void content of the asphalt concrete the ageing of the pavement can be highly reduced (Read & Whiteoak, 2003).

There are a few tests developed to determine the ageing properties of bitumen. The Rolling Thin Film Oven Test is used to predict the ageing properties of a bitumen during the manufacturing of asphalt concrete, which is the first phase of ageing (Persson, 2016; Papagiannakis & Masad, 2008). The test is performed by comparing an aged bitumen to a virgin bitumen, and commonly it is the retained penetration depth and softening point increase that is measured. The Pressure Ageing Vessel is used to calculate the ageing properties of the bitumen in an asphalt pavement, the second stage of the ageing process (Papagiannakis & Masad, 2008). The test is performed by putting the sample in a hyperbaric chamber at high temperature, trying to simulate the ageing of 7 to 10 years, and then comparing the sample to a virgin bitumen (Persson, 2016). The test is mostly used in the US.

3 Permanent deformation of pavement structures

Permanent deformation or rutting is a depression in the pavement caused by the load of the passing vehicles and it gradually increases with every passing vehicle (Said & Hakim, 2014). Rutting is caused by a few different factors and mechanisms, and the main causes of rutting can be divided into wearing from studded tires, consolidation due to post-compaction of the different layers, and structural deformation and lateral movement of the materials (Ekblad & Lundström, 2011). The studded tires rip off small particles of the pavement and the loss of material in the wheel path causes rutting. The consolidation and compaction is caused by a densification of the different layers due to the traffic load. The lateral movement imply a shift of the material, primarily in the bitumen bound layers, creating upheavals on the sides of the wheel path, see Figure 1, and it is also caused by the traffic load (Said & Hakim, 2014). The structural deformation is related to the depression in the subgrade and the unbound layers.

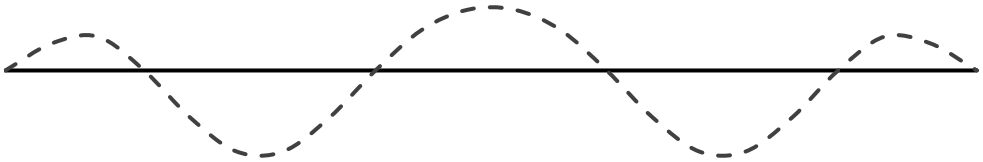

Figure 1. Schematic picture of lateral displacement

According to Kaloush and Witczak (2002) the development of rutting in the bitumen bound layers can be divided into three parts: initial, secondary and tertiary, see Figure 2. The initial development of rutting is mainly caused by the repeated loading, compacting the pavement and increasing the materials density (Kaloush & Wiczak, 2002). This initial deformation usually last one to two years after construction (Wiman, et al., 2009) and may be caused by inadequate compaction during construction (Said, et al., 2016). When the material is fully compacted the development of rutting is in the secondary phase. The repeated heavy vehicle loading induce shear stresses in the material that result in lateral movement, where the material moves from the wheel path and build upheavals on the sides of the wheel path (Said & Hakim, 2014). During the secondary phase the permanent deformation is still increasing, but at a lower rate. When moving into the tertiary phase the deformation rate promptly increases, suggesting the failure of the material (Said, et al., 2011).

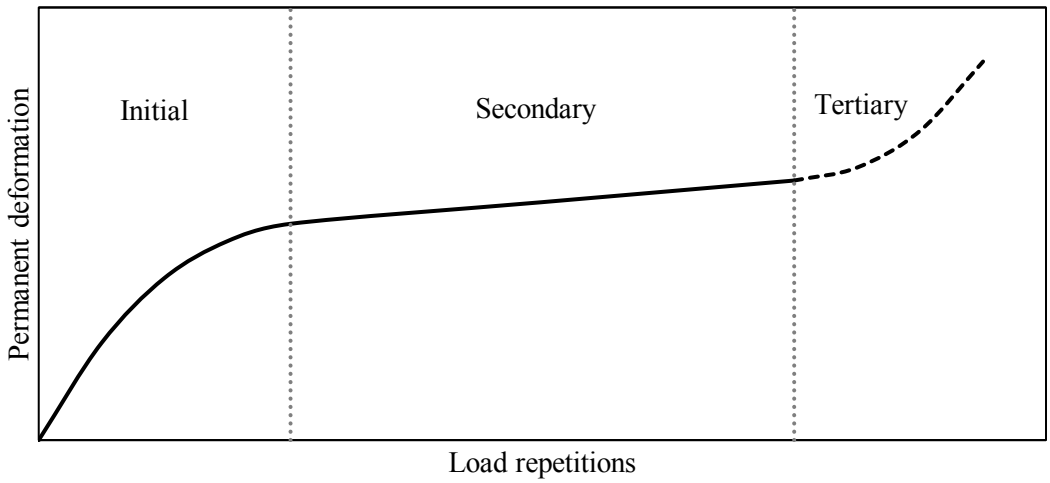

Figure 2. Typical curve of the development of permanent deformation in an asphalt concrete pavement.

The severity of the rutting is dependent on the properties of the asphalt mixture, combined with the traffic load and climate (Said & Hakim, 2014). Asphalt concrete is a viscoelastic material and it has been found that the viscous properties combined with the shear properties of the asphalt concrete are the main reasons why the pavement is prone to rutting (Said & Hakim, 2014; Björklund, 1984).

3.1 Asphalt concrete properties

How prone the asphalt concrete is to permanent deformation is mainly dependent on the viscoelasticity of the material. A less viscoelastic, i.e. harder, asphalt concrete is more resistant to permanent deformation (Oscarsson, 2011) and Poisson's ratio and the dynamic viscosity are usually used to describe these properties. The viscoelastic properties of asphalt concrete are mainly the effect of the viscoelastic behaviour of the bitumen, but the properties of the aggregates are also of importance. Large aggregate size, high angularity and high surface roughness all improve the resistance to permanent deformation since all these properties improve the interlocking between the aggregates (Oscarsson, 2011; Kim, 2009).

3.1.1 Poisson's ratio

When a material is exposed to a straining force, it will become elongated in the direction of the force and retain a thickness reduction perpendicular to the force. Poisson's ratio describes the relationship between how much the material elongates in one direction and reduces in thickness in the other, see equation (1) (Burström, 2011). For asphalt concrete Poisson's ratio varies with temperature and load frequency, i.e. the angular frequency (Gudmarsson, 2014), and gradually changes with an increased number of load repetitions (Said & Hakim, 2014). Poisson's ratio is approximately 0.35 at room temperature (Björklund, 1984).

$$\nu = \frac{\varepsilon_{\perp}}{\varepsilon_{\parallel}} \quad (1)$$

where:

ν = Poisson's ratio

$\varepsilon_{\perp}$ = transverse strain [m/m]

$\varepsilon_{\parallel}$ = axial strain [m/m]

3.1.2 Dynamic viscosity

The viscosity of an asphalt concrete is dependent on the temperature and loading time (Said, et al., 2013) and can be determined by the dynamic shear modulus and phase angle. A high dynamic shear modulus is preferable since it makes the material more resistant to deformation, and a low phase angle is preferable since it makes the material more elastic and recoverable (Bahia, 2009). At peak phase angle the material behaviour of the asphalt concrete is at its maximum viscosity making it the most receptive to permanent deformation (Said & Hakim, 2014). The viscosity can be calculated using equation (2) (Papagiannakis & Masad, 2008).

$$|\eta^*| = \frac{|G^*|}{\omega} \quad (2)$$

where:

$|\eta^*|$ = dynamic viscosity [MPa s]

$|G^*|$ = dynamic shear modulus [MPa]

ω = angular frequency [rad/s]

3.1.3 Ageing

When asphalt concrete ages it becomes harder and more brittle, which can be described by the change in the material's stiffness. To consider the ageing during the design phase the stiffness modulus is used and the Swedish Transport Administration have guidelines regarding the magnitude of the stiffness (Winnerholt, 2011b). The stiffness increases when the pavement ages (Winnerholt, 2011b) and the ageing process can be described with equation (3) (Said, 2005).

$$S_{t_{day,2}} = S_{t_{day,1}} \cdot \left(\frac{t_{day,2}}{t_{day,1}}\right)^{n} \quad (3)$$

where:

$S_{t_{day,1}}$= stiffness modulus at $t_{day,1}$ [MPa]

$S_{t_{day,2}}$= stiffness modulus at $t_{day,2}$ [MPa]

$t_{day,1}$, $t_{day,2}$ = ages of the bituminous layer [days]

n = factor describing age properties

3.2 Climate

The main climate factor affecting the rutting is the temperature since high temperatures makes the asphalt concrete soft and increases its proneness to rutting. Even though the climate in Sweden is generally cold the pavement surface can reach temperatures up to 50°C (Said, et al., 2011). The use of harder bitumen could lower the impact from high temperatures. However, a switch to a harder bitumen could induce other distress mechanisms such as fatigue cracking, especially during winter when the temperature is significantly lower (Oscarsson, 2011). It has been found that the use of polymer additives could decrease the dependence on temperature (Read & Whiteoak, 2003), thereby the rutting can decrease without increasing the risk of inducing other distress mechanisms such as cracking.

3.3 Traffic

There are many different factors connected to the traffic that effect the development of permanent deformation in a pavement structure. The axle load, wheel configuration, contact pressure, speed, lateral wander and amount of traffic are all of importance when considering the deformation in a bituminous pavement (Said, et al., 2016; Agardh, 2005).

3.3.1 Axle load

The damage caused by a vehicle is empirically related to the fourth power of its axle weight, resulting in heavy traffic being the primary cause for deterioration. This correlation between axle weight and loss of serviceability is usually expressed with the forth power law, equation (4), and was developed in the AASHO road test (AASHO Committee on Design, 1961). The test was conducted for axel loads varying from 3 ton to 13 ton.

$$N_a = N_b \left(\frac{P_b}{P_a}\right)^4 \quad (4)$$

where:

N_a = number of axle loads with axle type a

N_b = number of axle loads with axle type b

P_a = weight of axle type a [metric ton]

P_b = weight of axle type b [metric ton]

The load a road is exposed to during its lifetime is usually expressed in the number of standard axles (ESALs) that passes during that time. How many ESALs an actual axle corresponds to can be calculated with the forth power law, setting P_a to the weight of one ESAL. One ESAL is defined as a dual configured axle with a load of 100 kN and 800 kPa in contact pressure, see Figure 3 (Winnerholt, 2011a). In Sweden heavy vehicles are usually considered to correspond to 1.3 ESALs in average.

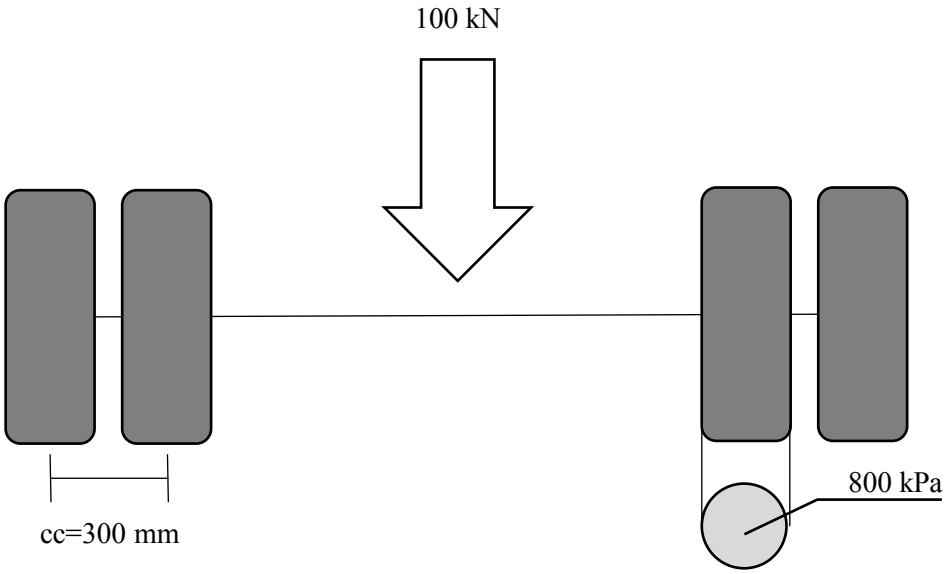

Figure 3. Schematic picture of an ESAL

Calculations of distress are usually adapted to the single axle, but many heavy vehicles use alternative axle configurations, with both single, tandem and tridem axles. However, the effect of the alternative axle configurations will most likely not affect the layers close to the surface (Agardh, 2005), see Figure 4, and therefore they are not addressed further in this report.

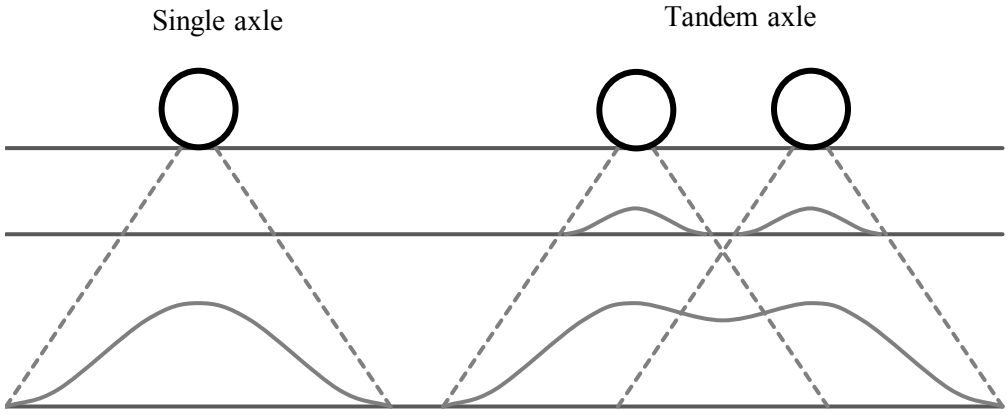

Figure 4. Superposition of stress distributions under single and tandem axle configurations

3.3.2 Wheel configuration

It has previously been proved that the wheel configuration has a major impact on the stresses induced in the pavement, which in turn affect the damage on the pavement (Said, et al., 2016; European Commission, 2001). The wheel configuration of one axle can be either widebase or dual, as seen in Figure 5. The smaller contact area of the widebase tire induces a larger pressure on the pavement surface causing greater stresses

and more damage compared to the dual configuration with the same axle load (Verstraeten, 1995). However, as greater dimensions of the widebase tires have been introduced the damage caused by them has decreased and is getting closer to the damage caused by the dual configuration (European Commission, 2001).

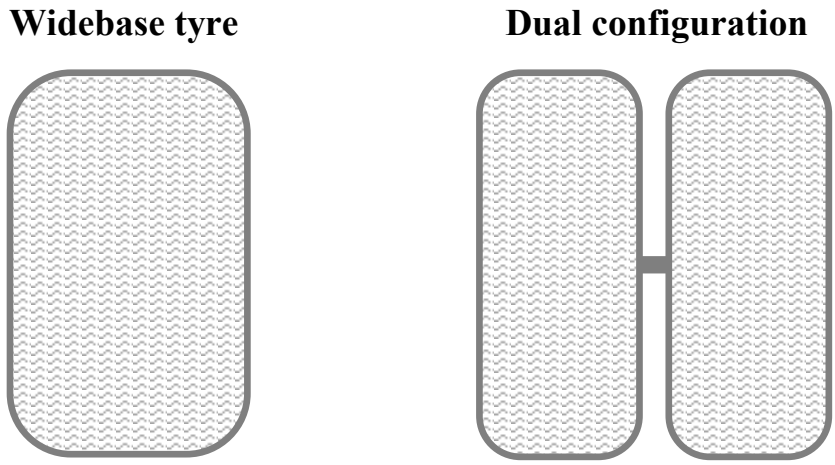

Figure 5. Schematic picture showing difference between widebase and dual configuration

3.3.3 Tire contact pressure

The tire contact pressure is dependent on both the axle load, wheel configuration and the tire contact area, which depends on the tire inflation pressure. An increased tyre inflation pressure will result in a smaller contact area and thereby increase the contact pressure and the induced stresses in the pavement. However, Said & Hakim (2014) stated that the tire inflation pressure is of less importance for the permanent deformation than the tire load, over the range of applicable tire pressures and loads.

3.3.4 Speed

Since viscoelasticity is a time-dependent property the vehicle speed is of importance for the response in the pavement and thereby also the development of permanent deformation (Agardh, 2005). Slow moving vehicles have a higher influence on the development of permanent deformation, which intersections and bus stops are a confirmation of. Experiments have been conducted to prove this correlation, with the conclusion that the speed's effect on the deterioration is minimal at the speeds typical in rural areas but an important factor to consider in urban areas (Ullidtz & Ekdahl, 1998).

3.3.5 Lateral wander

Lateral wander means that the vehicles travelling on the road use slightly diverse wheel paths, resulting in the weight of the traffic being somewhat distributed over the width of the pavement surface (McGarvey, 2016). This distribution of the traffic results in a slower progression of permanent deformation compared to if all vehicles were driving in the same wheel path, see Figure 6 (Said, et al., 2016). The width of the lateral wander depends mainly on the width of the lane, and it has been found that road designs with narrow lanes, e.g. 2+1 roads, have amplified rutting compared to other roads of the same age (Carlsson, 2009; Erlingsson, et al., 2012). Further, it has been found that the difference between the damage caused by widebase and dual configurations increase with a decreasing lateral wander (Said, et al., 2016).

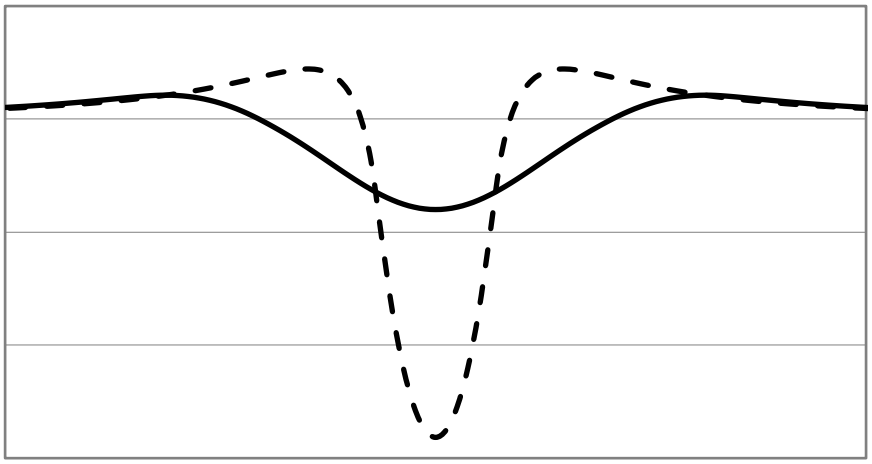

Figure 6. Effect of lateral wander on the development of permanent deformation

3.3.6 Amount of traffic

The permanent deformation of a pavement structure is highly dependent on the amount of traffic travelling on the road during its lifespan. For a road with multiple lanes in each direction, the amount of traffic in the lanes are rarely the same which results in a higher distress in some lanes. Generally, the lane distribution differs with traffic amount, and with an increasing amount of traffic the distribution over the lanes becomes more equal. However, most of the heavy traffic will travel in the right lane. For an AADT of 2000 the amount of trucks in outer lane was found to be 94 %, and for an AADT of 10000 the amount is 81 % (Darter, et al., 1985).

4 Calculation models for permanent deformation

There are several different models that can be used to predict the permanent deformation of an asphalt concrete pavement. Most models use elastic properties, but recently some models looking at viscoelastic properties has emerged. Three different models are presented in this chapter, where the model PEDRO is the one used to perform all the calculations in the thesis.

4.1 VEROAD

A model used for predicting stresses, strains and permanent deformations in asphalt pavements has been developed at Delfts University of Technology, and is called VEROAD (Visco Elastic Road Analysis Delft). The model consists of several programs that calculate how a moving wheel load affect an asphalt pavement using a viscoelastic analysis (Nilsson, 1999). An overview of the available programs in the VEROAD model, and how they are connected, is presented in Figure 7.

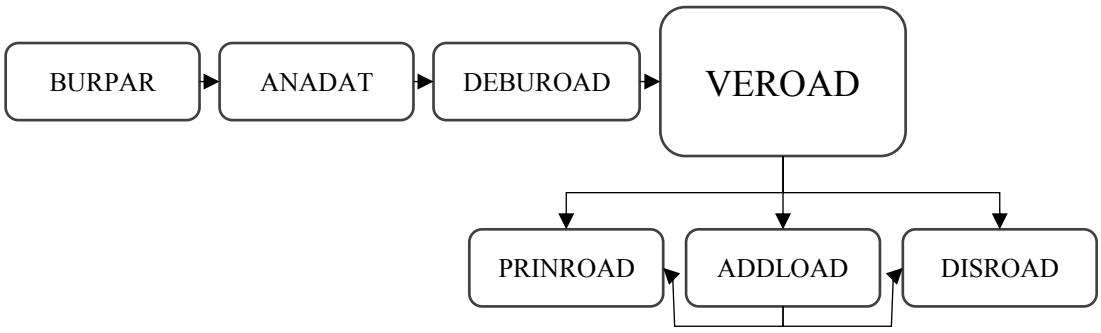

Figure 7. Schematic overview of the VEROAD model (Nilsson, 1999)

VEROAD uses the linear elastic bulk modulus and the linear elastic shear modulus to describe how the viscoelastic material behaves. The shear modulus is described by a material model called Burgers' model, which combines elastic springs with viscous dashpots to get a model that describes the linear viscoelastic behaviour (Nilsson, 1999). A schematic picture of the material model is presented in Figure 8. VEROAD calculates the time depended displacements, stresses and strains, in three dimensions (Nilsson, 1999).

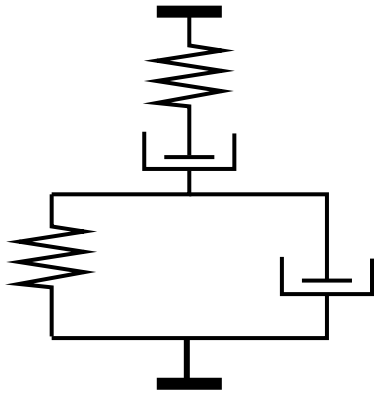

Figure 8. Burgers' model

4.2 MEPDG

A mechanistic-empirical model called the Mechanistic-Empirical Pavement Design Guide, or MEPDG, has been developed by the National Cooperative Highway Research Program, USA (NCHRP, 2004). The model calculates the condition of the surface described by a number of distress types. MEPDG estimates the permanent deformation based on plastic strain and it uses vertical strains to model response and distresses in pavements (NCHRP, 2004). The MEPDG takes permanent deformation in the unbound layers into account (NCHRP, 2004) which PEDRO and VEROAD do not.

In MEPDG, the permanent or plastic strain in the asphalt layers is a function of the number of load repetitions, temperature, vertical elastic strain in the pavement and the elastic material properties (NCHRP, 2004). The model has been developed from laboratory tests and correlates the compressive elastic strain to a permanent strain with equation (5) (NCHRP, 2004). When using the MEPDG model, the quality of the input data can be chosen from three different quality levels. The highest level requires precise measured data, the second incomplete measured data and the last level estimated data (NCHRP, 2004). The model functions similarly for all three levels.

$$\varepsilon_p(N) = \beta_1 \cdot b_1 \cdot T^{b_2} \cdot N^{b_3} \cdot \varepsilon_r \quad (5)$$

where:

ε_p = permanent vertical strain [m/m]

β_1 = calibration factor

T = temperature [°C]

N = number of axle loads, load repetitions

ε_r = elastic vertical strain from response model [m/m]

b_1, b_2, b_3 = regression constants

The model is based on linear elastic multilayer theory (NCHRP, 2004) and the pavement structure is divided into multiple sublayers to calculate the permanent strain and deformation more precisely. The strains are added together with regards to the sublayers' thickness (NCHRP, 2004). By using the sum of the permanent strain for each sublayer a total permanent deformation can be calculated. The total permanent deformation is calculated according to equation (6) (NCHRP, 2004). The model calculates a maximum deformation but does not produce a surface profile.

$$RD = \sum_{i=1}^{n_{sublayers}} \varepsilon_p^i \cdot h^i \quad (6)$$

where:

RD = total rut depth [mm]

ε_p = permanent vertical strain, per sublayer [m/m]

h = thickness, of sublayer [mm]

$n_{sublayers}$ = number of sublayers

4.3 PEDRO

One model that is currently being developed in Sweden is PEDRO (Permanent Deformation of asphalt concrete layers for Roads). PEDRO is based on a method developed by Björklund (1984) which assumes that the asphalt concrete is viscoelastic and will react accordingly when exposed to traffic load. Since the viscous part is the main contributor to rutting the viscoelasticity is an important factor to consider. To be able to use Björklunds (1984) assumption, the model PEDRO use the material properties dynamic viscosity at peak phase angle and Poisson's ratio. The dynamic viscosity at peak phase angle describes the material behaviour when the asphalt concrete reaches the least resistance to permanent deformation (Said, et al., 2013). Poisson's ratio describes how the asphalt concrete reacts when charged with compressive and tensile forces, and it is associated with the elasticity and shear modulus of the material.

PEDRO calculates the deformation that occurs when asphalt concrete is pushed to the side of the wheel by calculating the surface profile. It only uses the vertical stresses caused by the wheels, and not stresses in the other directions, since this is the largest force that affects the pavement for a free rolling wheel (Said & Hakim, 2014). The model is based on equation (7) that calculates the vertical strain at a chosen point (Said, et al., 2011). To get a surface profile, the model runs the equations for a set number of points across the lane width. Since the equation is for the passing of one axle, the number of total passing axles are added to get a rut depth at a certain time after the construction (Said & Hakim, 2014).

$$\varepsilon_p = \frac{\sigma_0 \cdot (1-2\nu)}{V \cdot \eta_p} \cdot Re\left[\sqrt{(z+ix)^2 + a^2} - (z+ix)\right] + \frac{\sigma_0 \cdot z}{V \cdot \eta_p} \cdot Re\left[1 - \frac{z+ix}{\sqrt{(z+ix)^2+a^2}}\right] \quad (7)$$

where:

ε_p = permanent vertical strain [m/m]

σ_0 = contact pressure [Pa]

ν = Poisson's ratio

V = vehicle speed [m/s]

η_p = viscosity at peak phase angle [Pa s]

z = depth from road surface [m]

x = distance from loading centre [m]

i = $\sqrt{-1}$

a = radius of contact area [m]

PEDRO considers how the material changes over time but does not include any other damage to the road, such as cracking (Oscarsson, 2011). It calculates both the initial and the secondary parts of the rutting development (Said & Hakim, 2014). As stated previously in this report, the initial part of rutting includes compaction of the bound layers (decrease in volume), which the first term of equation (7) calculates using Poisson's ratio (Said & Hakim, 2014). The second term calculates the shear deformation, i.e. the deformation at constant volume (Oscarsson, 2011). The viscosity at peak phase angle is used for both parts of the equation (Said & Hakim, 2014).

5 Field tests

In the following chapter the different measurement methods for rut depth will be presented, along with measurement methods for traffic volume and load and how climate data is gathered. The chapter should give an insight to how the data used in this study has been collected and measured and help identify any shortcomings and potential errors of the data.

5.1 Rut depth measurements

Estimating the rut depth of a road can be done both by measuring it directly out on the road or by using a method to evaluate the road surface. There are numerous methods available to evaluate the surface profile and the two most commonly used on Swedish roads are described below.

The most precise field measurement tool is called PRIMAL (longitudinal profile reference equipment) which consists of a laser beam at a fixed height and a moving measuring wheel that measures the road surface compared to the laser beam (Ekblad & Lundström, 2011). The PRIMAL method gives one cross section of the road for every 20 mm making it possible to get a precise surface profile (Said, et al., 2016). This measuring method is time consuming and thereby require an untraveled road.

A faster method to measure the road surface is to use a RST-car (road surface tester). A RST-car is a car that uses lasers to measure the condition of the road without the need to stop the normal traffic. The surface is measured at 15 or 17 points across the width of the road for every 100 mm of the road length (Lindström, 2015). Because the measurements can be performed while the traffic is running, RST-cars are used primarily on network level and the PRIMAL method is preferred on object level.

When the surface profile is determined the rut depth can be calculated. There are many ways to calculate the rut depth, but the most common method is the wire line method (Oscarsson, 2011). In the wire line method a straight line is drawn above the ruts, as if a wire is stretched out over the road's profile, and the distance from the bottom of the rut to the line is measured, see Figure 9. Either the average rut depth for each of the wheel paths or the maximum rut depth of both wheel paths is calculated, depending on the purpose of the calculation (Oscarsson, 2011). In PMSv3, the Swedish Transport Administration's road survey tool, the average rut depth for both the left and right wheel paths and the maximum rut depth over a length of 100 m is presented, measured with an RST-car (Trafikverket, 2017).

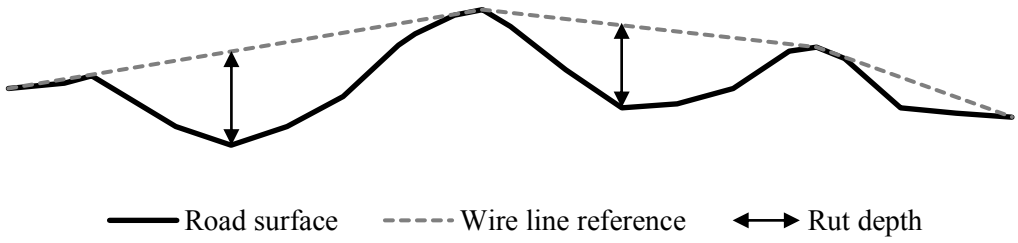

Figure 9. Schematic picture showing how to measure rut depth using the wire line method

5.2 Traffic measurements

The amount of traffic and the vehicles characteristics are important parameters to know when calculating the permanent deformation. There are a few different methods available to collect this data on site and three commonly used monitoring devices are the automatic traffic record (ATR), the automated vehicle classifier (AVC) and the weigh in motion (WIM) system (Papagiannakis & Masad, 2008). These devices are installed in the driving lanes and they record data while the traffic flows as normal.

The different systems function differently, and therefore there is a variation in what data they collect. The ATR measures the vehicle length and speed, and can therefore only be used as a vehicle counter. The AVC measure traffic volumes according to vehicle classification which is defined by the number of axles per axle configuration (Papagiannakis & Masad, 2008). The AVC classify the vehicles by measuring the number of axles and their spacing. According to Papagiannakis & Masad (2008) a variation in vehicle speed can result in errors of the classification. The WIM collect the same information as the AVC as well as the axle load of each passing axle. The benefit of the WIM system is its ability to respond and recover quickly enabling it to measure correctly even at motorway speeds (Papagiannakis & Masad, 2008).

In Sweden, a system called Metor 2000 has been used to measure the amount of traffic (Lundström, 2001) and the collected information includes vehicle type and speed (Trafikverket, 2015c) making the system an AVC monitoring system. Commonly the measurements are performed at a predefined interval and the AADT is estimated using these values because continuously measuring the traffic of the entire road network would be too costly (Trafikverket, 2015c).

The testing of a bridge weigh in motion (BWIM) system has been performed since 2002 (Vägverket, 2010). Measurements of the axle loads and gross weight have been executed on 14 different locations for one week at a time for several years (Winnerholt & Persson, 2006) (Vägverket, 2007) (Winnerholt, 2008) (Winnerholt, 2009) (Vägverket, 2010).

5.3 Climate measurements

The Swedish Transport Administration have their own road weather information system, VViS (Trafikverket, 2011b). The weather stations are placed along the national road network in places were the risk for icy roads is high. The weather stations measure air temperature, the pavement temperature 2 mm under the road surface, air humidity, the wind speed and direction as well as precipitation.

6 Reference road – E6 Fastarp-Heberg

The Swedish Transport Administration has a few roads in Sweden where different pavement structures are tested. These road sections are continually examined after construction to increase the knowledge on performance of different pavement structures. E6 Fastarp-Heberg is one of these roads and the long, thorough and intense follow-ups since the opening in 1996 makes it unique in Sweden (Ekblad & Lundström, 2011; Wiman, et al., 2009). The road is located a few kilometres north of Halmstad and 23 km south-east of Falkenberg. It consists of 19 different parts constructed with different pavement structures in the south going direction (Wiman, et al., 2005). The location of the studied pavement structures can be seen in Figure 10.

Figure 10. Map of the locations of the studied pavement structures (Google, 2017)

6.1 Pavement structure

In this study, sections 12 and 13 from E6 Fastarp-Heberg are analysed. The bound layers are constructed for a design period of 20 years (Vägverket, 1994). Section 12 is a so-called reference structure and is constructed according to the standards at the time of construction, the pavement structure can be seen in Figure 11a. The aggregates used in the bound layers are quartzite (Wiman, et al., 2005) and the largest aggregate size is 16 mm for the wearing course (ABS16) and 22 mm for the bearing course (AG22) (Trafikverket, 2017). Section 13 is constructed according to the FAS concept, where the bearing course of the reference structure has been replaced by a 115 mm bituminous bearing course and an 80 mm binder course. The pavement structure of Section 13 is shown in Figure 11b. How the bituminous layers in the pavement structure have been modified is not accounted for since the FAS concept was ordered after pavement performance (Viman, 2005). The aggregates used for the asphalt concrete in section 13 are porphyry (Wiman, et al., 2005) and the largest aggregate size is 16 mm for the

Viacotop and Viacobind, the Viacobase have a largest aggregate size of 22 mm (Ulmgren & Lundström, 2006).

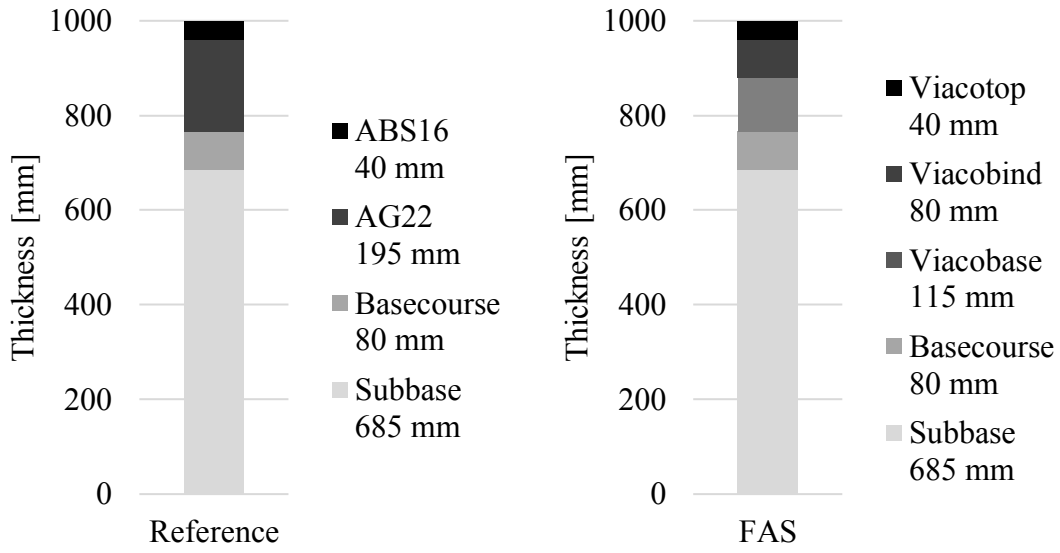

Figure 11. Pavement structure of a) the reference structure and b) the FAS structure

The construction took place in late 1996 and the paving was conducted in December 1996 (Trafikverket, 2017). In September 2011, an additional 26 mm thick wearing course was added onto the pavement of both structures (Trafikverket, 2017). However, the core samples used in the laboratory experiments where drilled earlier in 2011 and therefore there are no available specimens of the new coating.

6.2 Pavement performance data

The condition of E6 Fastarp-Heberg has been measured since the opening and focus has been on measuring the profile of the surface (Wiman, et al., 2009). Surface profile measurements have been performed twice every year, once during spring and once during autumn, using the surface profile measuring device PRIMAL (Wiman, et al., 2005). An RST-car has also been used to measure the surface profile yearly during autumn.

6.2.1 Measured rut depth

The development of permanent deformation, from PRIMAL measurements, is presented in Figure 12 (Wiman, et al., 2009; Ekblad & Lundström, 2011). Measurements with the PRIMAL method performed in 2010 show a permanent deformation of 17 mm for structure 12 and 9 mm for structure 13 (Ekblad & Lundström, 2011). These values are average values based on measurements performed at two different locations on each structure. The measurements performed between 1997 and 2006 are the average of at least nine different measuring locations per structure (Wiman, et al., 2009). The prognosis made by Wiman, et al. (2009), based on the measurements from 1997 to 2006, is also presented in the figure.

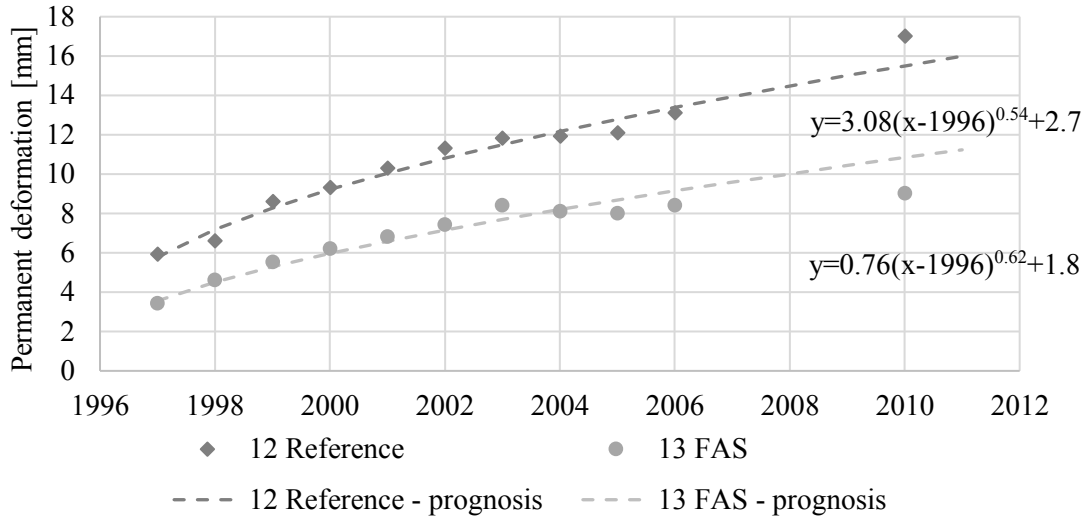

Figure 12. Permanent deformation based on PRIMAL measurements

In 2011 before the new surface coating was paved, the rutting was measured using a RST-car, pavement structure 12 had 11.74 mm in rut depth and for pavement structure 13 the rutting was measured to 8.05 mm (Trafikverket, 2017). The values are the average values calculated of the maximum rutting per 20 m. In Figure 13 the development of permanent deformation, based on the RST-car measurements, are presented (Trafikverket, 2017). Wiman, et al. (2009) found that the RST-car measurements were in average about 68 % of the PRIMAL measurements.

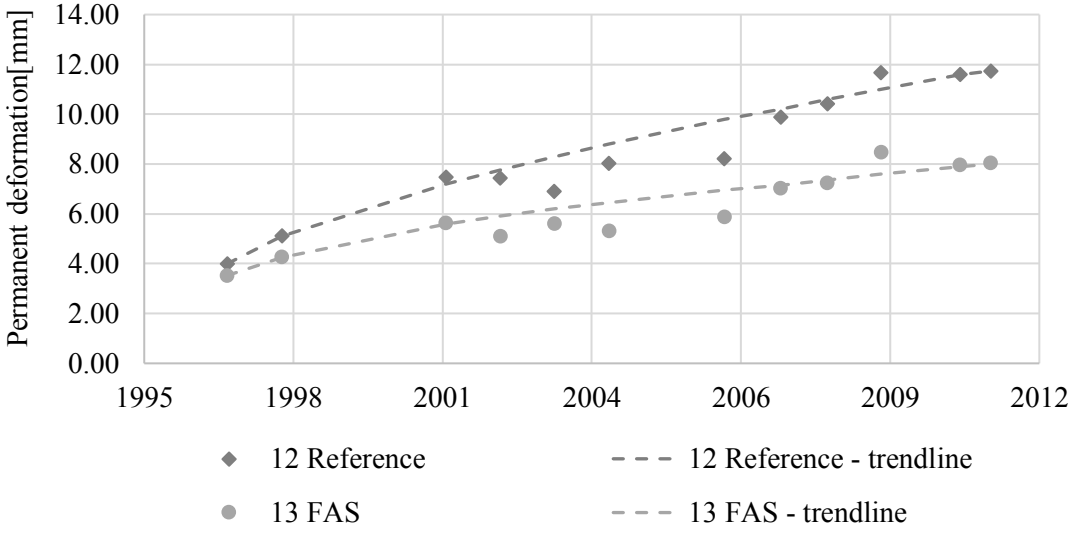

Figure 13. Permanent deformation based on RST-car measurements

The values presented in Figure 12 and Figure 13 are the total measured deformations and not the accumulated development of permanent deformations, i.e. the deformations caused by construction are included.

6.2.2 Wearing caused by studded tires

Measurements of the development of wearing caused by studded tires have been performed yearly since 1996 up till 2003, with one measurement in the autumn and one in the following spring using a laser-profilometer developed by VTI. To perform the calculations of the wearing it is assumed that the pavement is so stiff during the winter that no permanent deformation occurs (Ekblad & Lundström, 2011). The results of these measurements have been compiled by Wiman, et al. (2005) and are presented in Figure 14. From the measured values a linear regression model for the accumulated wearing caused by studded tires have been produced. Values for 2010 were calculated from the prognosis, and are 4.78 mm and 3.69 mm for structure 12 and 13 respectively.

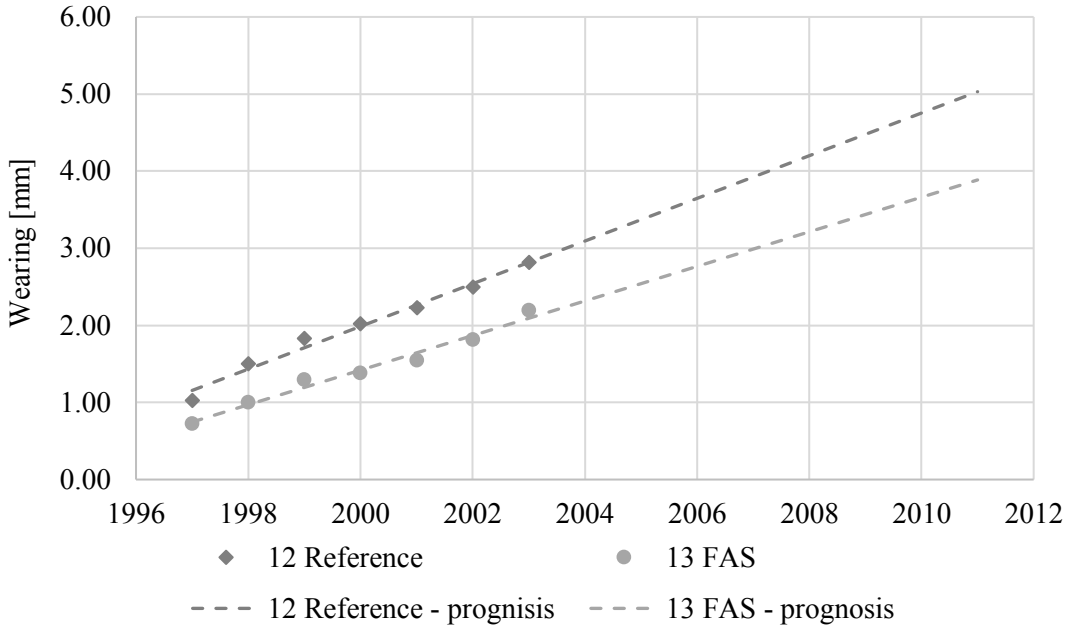

Figure 14. Total wearing caused by studded tires

6.2.3 Compaction of unbound layers

Ekblad & Lundström (2011) conducted a study to identify the cause of rutting for structure 12 and 13. Their conclusion was that the rutting for pavement structure 13 is caused by compaction and lateral displacement of the bound layers combined with wearing of studded tires. However, for pavement structure 12 they found that part of the rutting was not explained by permanent deformation of the bound layers and wearing of studded tires, 4 mm remained unaccounted for which were assumed to be caused by deformation in the unbound layers. Ekblad & Lundström (2011) based their calculations on measurements from 2010, and since the wearing of studded tires was only measured up to 2003 they used linear extrapolation to get the wearing of studded tires up to 2010. All calculations are performed for the right wheel path, which generally has a smaller amount of permanent deformation given that the lateral placement of passenger cars and heavy vehicles usually concide for the left wheel path.

6.3 Climate data

The climate in the area has been measured regularly for several years at the climate station VViS1336. The climate station is placed just south of the analysed pavement structures, as shown in Figure 15.

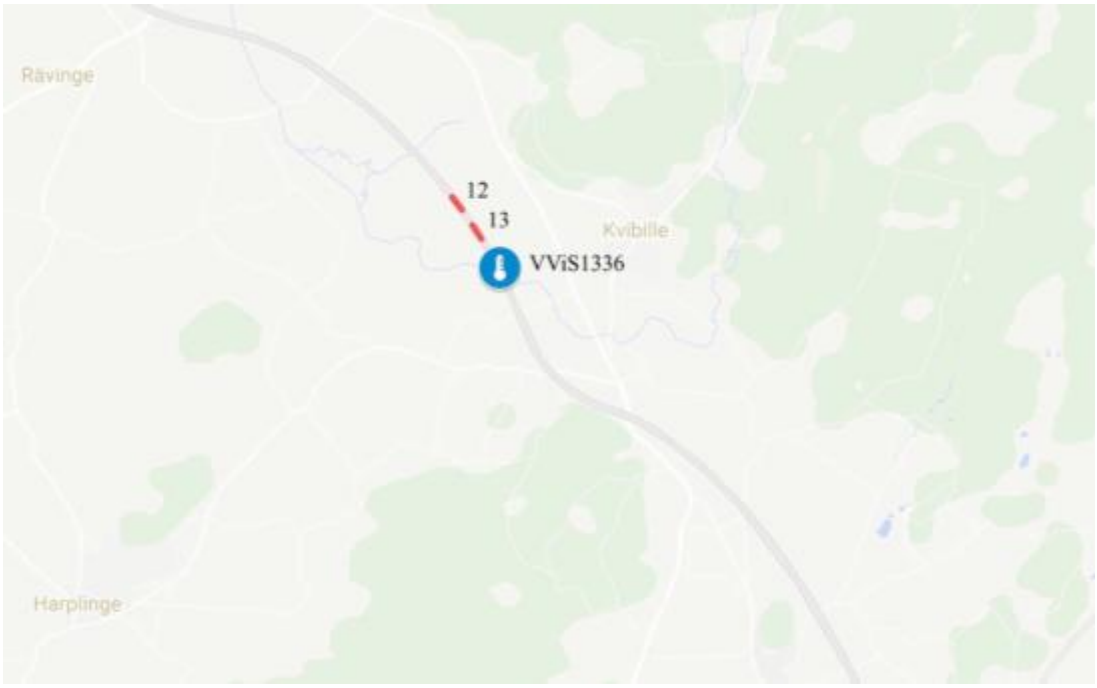

Figure 15. Map showing location of climate station VViS1336 in relation to the analysed pavement structures (Google, 2017)

The pavement temperature is the far most important climate parameter effecting the development of permanent deformation (Said & Hakim, 2014). Therefore, it is the only climate parameter considered in this study. The station VViS1336 measures the temperature at the pavement surface continuously every half hour (Trafikverket, 2011b). The coldest noted temperature from 2014 to 2016 is -14.5°C in January 2016, and the highest is 48.5°C in July 2014 (Trafikverket, 2015b).

6.4 Traffic data

As stated earlier the development of permanent deformation is dependent on the traffic volume, the vehicle configuration, the speed and lateral wander. The data needed to describe these factors for E6 Fastarp-Heberg are presented in this chapter.

6.4.1 Traffic volume

The amount of traffic and their weight is most accurately measured with a BWIM system. However, there is no measured BWIM data for E6 Fastarp-Heberg but results from other locations can be used to estimate these characteristics for the reference road (Oscarsson, 2011). Of the available national BWIM measurement locations, E6 Löddeköpinge is the closest one. Löddeköpinge is located approximately 130 km south of the reference road (Google, 2017). An alternative to the BWIM data is the use of AADT and the load equivalent factor, however this method is considered less accurate.

The traffic growth rate is not included in the BWIM data and was therefore estimated separately. Traffic measurements at E6 Fastarp-Heberg performed 1996, 1998, 2002, 2006, 2010 and 2014 (Trafikverket, 2016) were used in the calculation. The collected data and the estimated traffic growth is presented in Figure 16. An exponential trend line is adapted to the measured data, to get the traffic growth in percentage. The traffic growth is derived from the trend line, and is equal to 4.09 %.

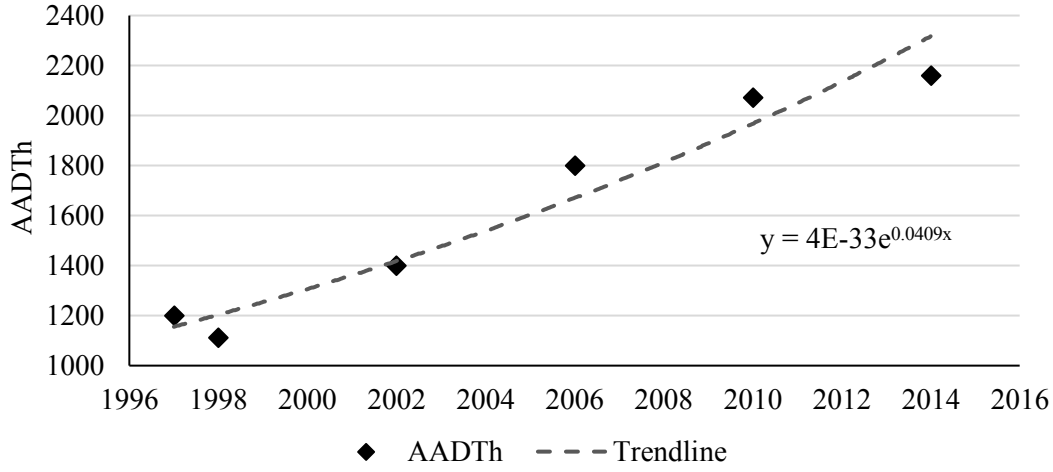

Figure 16. AADTh from the Swedish Transport Administration's measurements with an exponential trend line

6.4.2 Vehicle configuration

The most important factors to consider of vehicle configurations are the wheel configuration and the contact pressure. The amount of dual configured wheels was measured in 2011 in a master thesis (Almqvist, 2011). The study was performed on E18 Hummelsta and found that 52 % of all wheels on heavy vehicles have a dual configuration. The tire width and centre to centre distance are also important factors to consider, those factors were examined in another study from the same thesis. The study was performed in Västerås in 2011 and found that 48 % of all dual tires had a width of 315 mm and 34 % had a width of 265 mm, the average minimum centre to centre distance for these widths are 315.5 mm (Doublecoin, 2012). For the single tire configuration, the most common tire width was 385 mm, representing 84 % of all widebase tires.

The contact pressure is difficult to measure. However, there is a correlation between the contact pressure and the tire load and tire contact area. The tire contact area is in turn dependent on the tire type and width, as well as tire inflation pressure. The recommended tire inflation pressure varies with the tire type and load, but is generally around 800 kPa (Goodyear, 2012).

6.4.3 Vehicle speed and lateral placement

The vehicle speed at E6 Fastarp-Heberg was measured in 2014 and the average speed for the heavy traffic on the road was 103 km/h for the vehicles without trailer and 84 km/h for those with (Trafikverket, 2016). The average daily amount of heavy vehicles without trailer was 830 and the amount with was 1335 and this results in an average speed of the heavy vehicles of 91.2 km/h.

As stated earlier the lateral wander is highly dependent on the lane width and the reference road have a lane width of 3.5 m (Wiman, et al., 2009). McGarvey (2016) conducted a study to find the standard deviation of the lateral wander for different roads and lane widths, and a selection (the motorways included in the study) of the results can be seen in Table 1.

Table 1. Vehicular Lateral Wander (McGarvey, 2016)

Road	**Lane width [m]**	**Standard deviation [mm]**			
		Heavy vehicle track width 1.8 m		**Heavy vehicle track width 2.1 m**	
		Left	**Right**	**Left**	**Right**
E6 Uddevalla	3.65	308	332	256	254
E4 Linköping	3.70	372	405	224	228
E4 Linköping	3.65	315	357	218	222

7 Laboratory test – Asphalt concrete shear box

One part of the master thesis is to perform laboratory tests on asphalt concrete samples from the reference road, to get accurate values of the material's viscosity. The chosen laboratory test method is developed by Said, et al. (2013) and is called asphalt concrete shear box. The method is used to obtain the dynamic shear modulus and phase angle of an asphalt concrete sample which are needed to determine the viscosity. The shear modulus describes the relationship between the shear stress and strain of a sample (Burström, 2011) and consists of two components, the storage modulus and loss modulus, the phase angle describes the division of these two modules (Said, et al., 2013). The phase angle is calculated as the time difference between the stress and strain and it goes from 0° to 90°, a phase angle over 45° means that the material is more viscous than elastic and the vice versa for a phase angle under 45°. When calculating the viscosity, the angular frequency is at peak phase angle.

7.1 Method

Cylindrical samples of the asphalt concrete are tested in a device that consists of two plates on which the sample is glued using epoxy glue and two strain gauges are used to measure the two plates movements in relation to each other, see Figure 17 (Said, et al., 2013). The cylindrical samples can either be made in the laboratory, or drilled from a road. The diameter of the sample can be 100 – 150 mm, and the sample should not be thicker than ¼ of the diameter (Said, et al., 2013). The strain gauges measure the shear deformation of the sample, with an accuracy of 60 nm ($60 \cdot 10^{-9}$ m) (Said, et al., 2013).

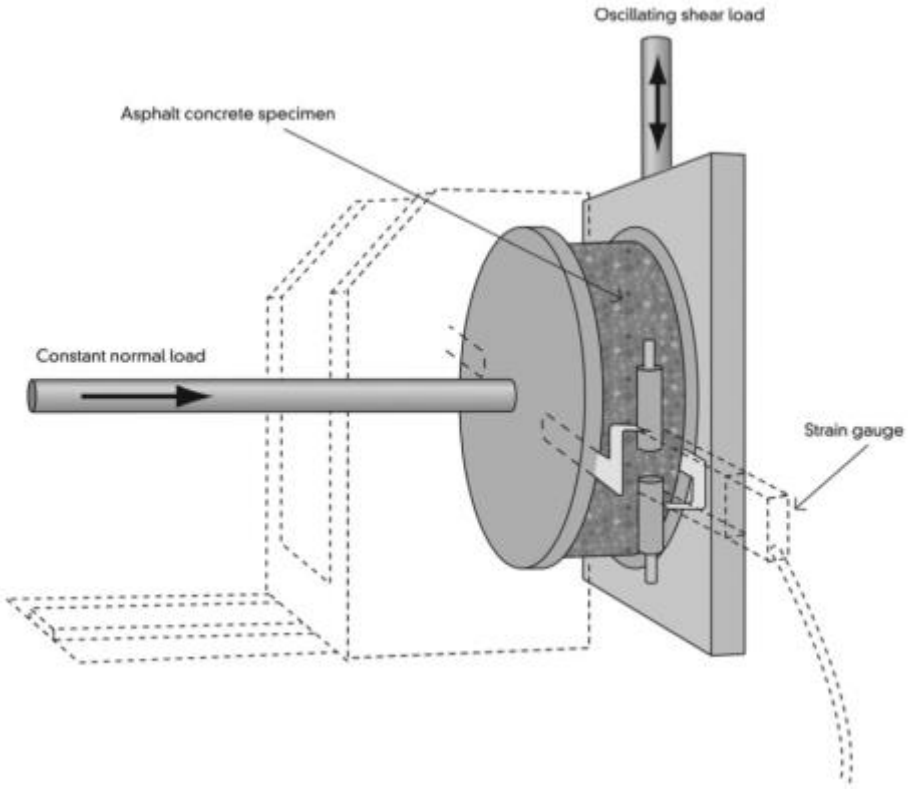

Figure 17. Schematic picture showing the device used for the asphalt concrete shear box (Said, et al., 2013)

One of the plates has a constant normal pressure of 5.5 bar and the other plate is sheared vertically over different frequencies to test the shear modulus of the sample. The vertical load varies with different frequencies at several different temperatures to get results for all applicable temperatures and traffic loads (Said, et al., 2013). The sample will be cooled down to the lowest temperature and run through all the frequencies, starting with the highest. Then the temperature is increased and the test is performed again for all frequencies, and this is repeated for all test temperatures. A high frequency represents a short loading time which is why the test start with a high frequency and then decrease for each temperature (Said, et al., 2013). The lower the sample temperature the better the resistance to permanent deformation and therefore the test start with a low temperature.

7.2 Expected outcome

The test results can be used to generate master curves for the shear modulus and phase angle. A master curve presents the shear modulus and the phase angle for the reference temperature and an example is shown in Figure 18 (Said, et al., 2013; Papagiannakis & Masad, 2008; Ahmed, et al., 2013). "The master curve allows the estimation of mechanical properties over a wide range of temperatures and times (or frequencies), which could be realised in the field but are not practical to simulate in the laboratory" (Papagiannakis & Masad, 2008). The master curves differ depending on the binder and aggregate in the sample, for example a harder binder would give the peak phase angle at a lower frequency, i.e. longer loading time (Said, et al., 2013).

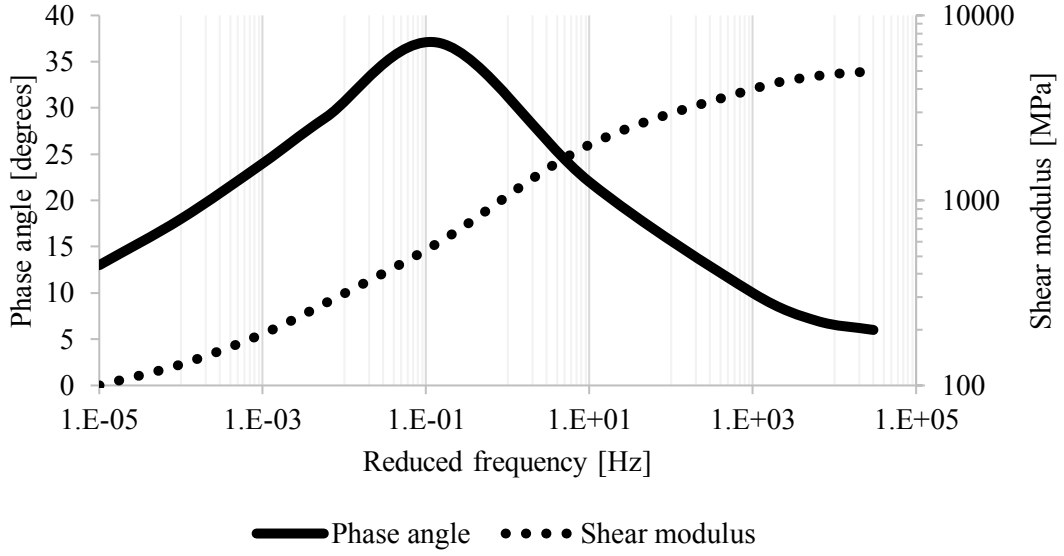

Figure 18. Example of master curve

When the phase angle reaches its maximum value, the material is most receptive to deformations (Said & Hakim, 2014). For this reason, the values used for further analysis is the shear modulus and viscosity corresponding to the frequency at peak phase angle (Said, et al., 2013). Since the parameters of the material are dependent on the temperature, the peak phase angle will occur at different frequencies for different reference temperatures (Said, et al., 2013).

7.3 Working process

3 core samples per pavement structure were available to testing. The core samples were divided into 4 disks from each core, resulting in a total of 12 sample disks available for laboratory testing from each pavement structure. The reference structure was divided into three disks of ABS16 and nine disks of AG22. For the FAS structure the number of disks produced was three Viacotop discs, three Viacobind disks and six Viacobase disks. Two disks from each asphalt concrete mix were tested including one extra from the Viacotop layer due to unreliable test results, resulting in 11 tested sample disks. For AG22, each sample core had three layers but only two specimens were tested, those specimens came from the bottom and middle layers. The bottom layer was chosen because those layers often show different properties due to unsatisfactory compaction. The middle and top layer are assumed to have similar properties and therefore only one specimen from those two layers was tested. The Viacobase is also divided into two layers and one specimen from each layer were tested to account for any differences between the layers.

The laboratory tests were performed according to the method described earlier and a more thorough laboratory working process can be found in Appendix I – Laboratory working process. The tests were performed for 8 different frequencies and 4 different temperatures. The tested frequencies were 16 Hz, 8 Hz, 4 Hz, 2 Hz, 1 Hz, 0.5 Hz, 0.1 Hz and 0.05 Hz, and the tested temperatures around -5°C, 10°C, 30°C and 50°C. The deformation was measured at both the front and back of the specimen, and the shear force was measured as well. The laboratory protocol with tested temperatures and specimen specifications is presented in Appendix II – Laboratory protocol.

Master curves were generated for all asphalt mixes of the two studied pavement structures. The test was performed for each layer separately, and the results for each asphalt mix were added into the same master curve to get an average result for that specific mix. The FAS pavement structure has three bituminous layers which results in three master curves and the reference structure has two bituminous layers giving two master curves, thus resulting in a total of five master curves. The master curves were then used to obtain the angular frequency and dynamic shear modulus at peak phase angle, which can be used to calculate the dynamic viscosity.

7.3.1 Analysis of laboratory results

The results of the laboratory experiments were measurements of the deformation and shear force. Since the shear force is applied in a sinus formation all measured results was fitted to sinus curves, an example is shown in Figure 19.

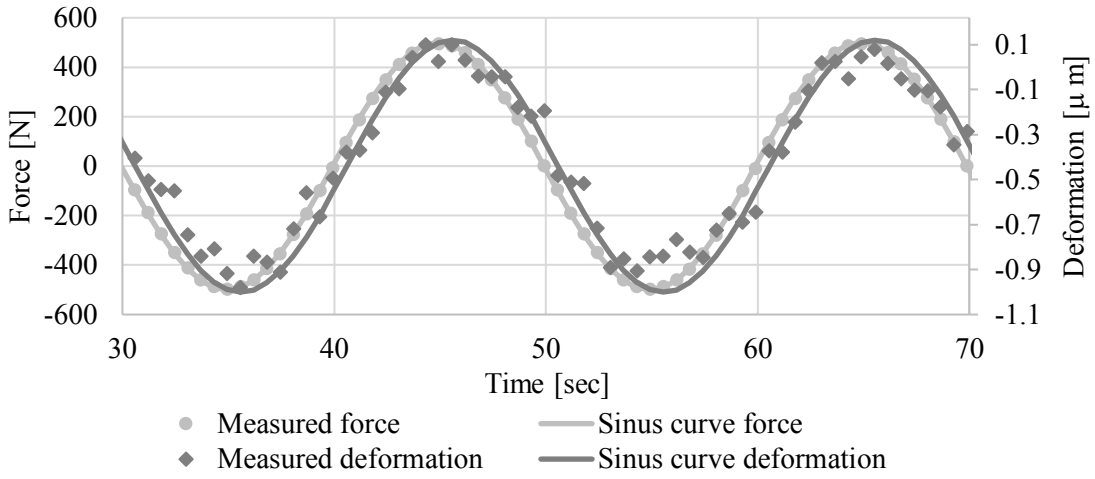

Figure 19. Adaption of sinus curves

The amplitude of the sinus curve for the deformation is the same as the maximum deformation at the applied frequency and temperature. The strain was calculated using the deformation and the specimen thickness. The strain was then used to calculate the dynamic shear modulus for each tested frequency and temperature using equation (8) (Ahmed, et al., 2013). The time difference between the force and deformation was determined by calculating the difference in shifting along the x-axle for the two sinus curves, and was used to calculate the phase angle according to equation (9) (Ahmed, et al., 2013).

$$|G^*| = \frac{4 \cdot F}{\pi \cdot d^2 \cdot \varepsilon_{mean}} \quad (8)$$

$$\emptyset = 360 \cdot \frac{\Delta t}{2 \cdot \pi} \quad (9)$$

where:

$/G^*/$ = dynamic shear modulus [MPa]

F = force [N]

d = sample diameter [m]

ε_{mean} = average strain [m/m]

$\emptyset$ = phase angle [degrees]

f = frequency [Hz]

Δt = difference in time [s]

7.3.2 Generating master curves

The calculated values for dynamic shear modulus and phase angle were plotted and two curves (master curves), equation (10) and (11), were fitted to the calculated values. Any measurements diverging severely from the average were not considered in the fitting of the master curves. Equation (12) and (13) calculate the shift factor for the master curves according to the Arrhenius-equation (Ahmed, et al., 2013), adapting the results to the reference temperature. The reference temperature was set to 10°C during the calculations.

$$\log(|G^*|) = \delta + \frac{\beta}{1+e^{\kappa-\gamma\cdot\log(f)}} \quad (10)$$

$$\emptyset = D \cdot \left(1 - \frac{e^{\left(\frac{\log(f)-p}{B}\right)}}{1+e^{\left(\frac{\log(f)-p}{B}\right)}}\right) + c \cdot \left(\frac{1}{1+\left(\frac{\log(f)-p}{b}\right)^2}\right) \quad (11)$$

$$\log(f_r) = \log(\alpha_T) + \log(f) \quad (12)$$

$$\log(\alpha_T) = k \cdot \left(\frac{1}{T+273} - \frac{1}{273+T_{ref}}\right) \quad (13)$$

where:

$|G^*|$ = dynamic shear modulus [MPa]

f = frequency [Hz]

f_r = reduced frequency [Hz]

α_T = shift factor

$\emptyset$ = phase angle [degrees]

T = temperature [°C]

T_{ref} = reference temperature [°C]

$\delta, \beta, \kappa, \gamma, b, c, k, p, B$ and D = constants

7.3.3 Interpretation of master curves

The final step of the laboratory work was to read the dynamic shear modulus and frequency from the master curve, both at peak phase angle. The frequency was used to calculate the angular frequency with equation (14).

$$\omega = 2 \cdot \pi \cdot f \quad (14)$$

where

ω = angular frequency [rad/s]

f = frequency [Hz]

The master curves were adapted to one reference temperature, but the frequency at peak phase angle and shear modulus for other temperatures can be determined with Arrhenius-equation. Thereby it is possible to determine the viscosity for other temperatures with the same master curve.

7.4 Results

The laboratory tests provided measurements of deformation from two sides of each specimen and the magnitude of the applied shear force. The measurements were used to generate five master curves presented in Figure 20, and all master curves are presented individually in Appendix III – Master curves combined with the measurements.

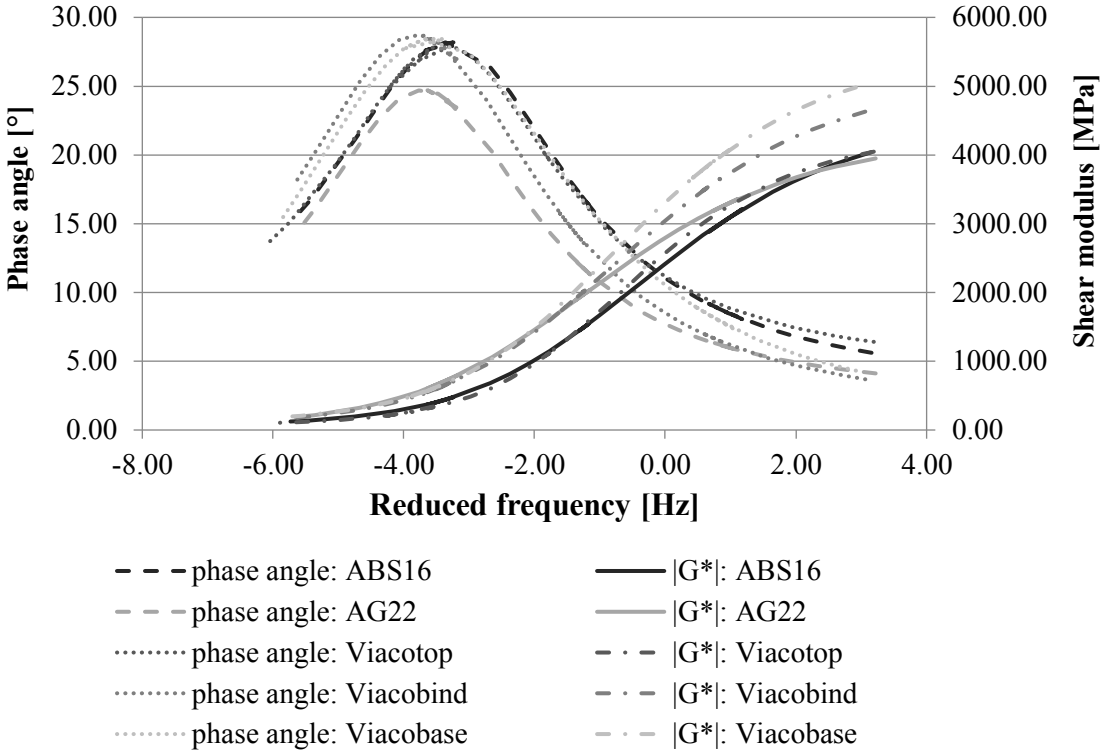

Figure 20. Master curves for all tested layers, at reference temperature 10°C

The master curves were used to determine the dynamic shear modulus and frequency at peak phase angle for 10°C. The results of those calculations are presented in Table 2.

Table 2. The frequency and dynamic shear modulus at peak phase angle for all tested specimen, at reference temperature 10°C

	Phase angle [°]	**Frequency [Hz]**	**Angular frequency [rad/s]**	**Dynamic shear modulus [MPa]**
Reference structure				
ABS16	28.18	$5.7604 \cdot 10^{-4}$	$3.6193 \cdot 10^{-3}$	476.54
AG22	24.70	$2.3000 \cdot 10^{-4}$	$1.4452 \cdot 10^{-3}$	603.21
FAS structure				
Viacotop	27.92	$3.1094 \cdot 10^{-4}$	$1.9537 \cdot 10^{-3}$	336.74
Viacobind	29.53	$1.4867 \cdot 10^{-4}$	$9.3413 \cdot 10^{-4}$	486.55
Viacobase	28.44	$2.0640 \cdot 10^{-4}$	$1.2968 \cdot 10^{-3}$	549.64

The angular frequency and the dynamic shear modulus where used to calculate the dynamic viscosity using equation (2). The results of those calculations are presented in Table 3.

Table 3. Results of calculations of dynamic viscosity at reference temperature 10°C

	Dynamic viscosity [MPa s]
Reference structure	
ABS16	$1.3167 \cdot 10^5$
AG22	$4.1740 \cdot 10^5$
FAS structure	
Viacotop	$1.7236 \cdot 10^5$
Viacobind	$5.2086 \cdot 10^5$
Viacobase	$4.2383 \cdot 10^5$

One of the tested specimen were conflicted with a testing error. The error occurred in the control system prior to the testing of an ABS16 specimen and resulted in a static negative force of 1500 N in the bar providing the shear force during the tests. The specimen showed lower dynamic shear modulus compared to the other tested ABS16 specimen. However, it is not known if this difference is caused by the testing error or if it is correlated to some variations in the specimens and therefore the results are not excluded from the calculations.

One of the Viacotop specimen showed abnormal results and therefore an additional specimen was tested for the Viacotop layer. The test results for the specimen is presented in Appendix III – Master curves combined with the master curve for the other two tested specimens to demonstrate the difference in the laboratory results. Exactly why the specimen showed abnormal results is not known but there was a power outage the morning of the testing and all equipment had to be restarted, which could be the cause of the abnormal results.

8 Calculation of permanent deformation

The second part of the master thesis include the calculation of the permanent deformation for the two studied pavement structures. For the calculation of the permanent deformation a beta-version of the software PEDRO was used. The implementation of the software is not yet complete and to get precise results from PEDRO calibration is needed which is what this thesis aims to do for the two studied pavement structures.

8.1 Software structure

The input fields in the software are divided into four input tabs. The input tabs are general data, material data, traffic data and climate data. Once all input data has been filled in the software can run and when the calculations are done the results are presented in the results tab. The layout of each tab can be seen in Appendix IV – Software structure.

8.1.1 Input

The pavement structure input data in the general tab include the layer thickness and mix type, construction and test dates, and a calibration factor that consider the material properties, traffic characteristics and climate factors etc. The selection of mix type will in a future version of the software adapt the values used for viscosity and Poisson's ratio. However, this function is not available in the current version since these parameters are being determined in the ongoing implementation. In these calculations the material data will be put in manually.

The material properties are divided into four factors describing the viscosity and four factors describing Poisson's ratio. The viscosity parameters are a_1, a_2, a_3 and n. The factor n describes the ageing properties and how they affect the viscosity. The factors a_1, a_2 and a_3 describe the shear properties. The factors describing Poisson's ratio is y_{span}, y_{min}, λ and x_{shift}. The difference between these parameters and a fixed Poisson's ratio is that these parameters are sigmoidal functions that take into consideration how Poisson's ratio alters with temperature.

The traffic input data includes the amount of traffic, vehicle characteristics and traffic distribution. The amount of traffic can be calculated in PEDRO either with BWIM data or by specifying AADTh (Annual average daily traffic of heavy vehicles), amount of heavy vehicles in outer lane, standard axle load and load equivalent factor. Further, the annual traffic growth and design period are included here independent of the chosen input for amount of traffic. The vehicle characteristics include the contact pressure, percent of dual wheels, vehicle speed, lateral wander and dual wheel centre to centre distance. The tire contact pressure can be accounted for either by defining a contact pressure or by using a tire contact area model where the tire type and the tire pressure are defined. The daily traffic distribution is defined by the four factors d_1, d_2, d_3, and d_4 which are constants describing the traffic distribution over 24 h.

The input temperature used in the model is the temperature distribution of the bituminous layers. The input is made either by selecting one of the predefined regions or by putting in the monthly average temperatures manually.

8.1.2 Results

The results tab provides the results for the entire design period. A table presents the development of permanent deformation for every year, both for each layer separately as well as the total deformation for all layers. A graph show the development of permanent deformation over the chosen timespan, both for each layer individually and the total permanent deformation. A second graph show the transversal profile of the pavement surface, both for each layer and the entire pavement structure. The numerical results in the table are the maximum depression calculated from the original surface level and does not include the upheavals in the current version.

8.2 Working process

The viscosity parameters determined in the laboratory experiments are used as material input data in PEDRO and the compilation of the results was the first step of the working process. However, the viscosity data is only one part of the input data necessary for the calculations in PEDRO. Therefore, the second step of the working process was to gather all other needed input data.

The road was paved in September 2011 and the last rutting measurement before that was performed in May 2011. PEDRO calculates the rutting for the entire design period but the results after the new surface was paved are neglected since the new paving is not evaluated in the laboratory. Given the higher accuracy from the PRIMAL data those measurements were used for comparison and the calculations were performed for 2010 given the used data from Ekblad & Lundström (2011).

Once all the data was gathered the calculations and calibration could be performed. An iteration process was performed to find the accurate calibration factor. The first set of calculations were performed with the calibration factor 1 and the obtained results were used to calculate a new calibration factor, and this process was repeated until the calculated and measured rutting matched. Since the measured deformation includes the upheavals, the results were exported to Excel and a manual calculation of the rut depth, including upheavals, was performed.

The final step of the working process included an analysis of the traffic data. The traffic input data was changed from BWIM data to ESALs and the calculations were performed the same way as earlier, by iteration of the calibration factor.

8.3 Determination of viscosity parameters

In PEDRO, the factors a_1, a_2 and a_3 are used to describe the viscosity properties and they were determined from the dynamic viscosity at different temperatures. As described earlier the same master curve can be used to obtain the dynamic viscosity for other temperatures than the reference temperature. The correlation between the logarithmic viscosity and temperatures is a second-degree polynomial function, as seen in equation (15).

$$\log|\eta^*| = a_1 \cdot T^2 + a_2 \cdot T + a_3 \quad (15)$$

where

$|\eta^*|$ = dynamic viscosity [MPa s]

T = temperature [°C]

a_1, a_2 and a_3= factors used to describe viscosity in PEDRO

By plotting the logarithmic viscosity and temperature in excel, the equation, and thereby factor a_1, a_2 and a_3, were obtained. The factors are presented in Table 4.

Table 4. Viscosity factor a_1, a_2 and a_3

	a_1	**a_2**	**a_3**
Reference structure			
ABS16	0.0004	-0.1323	6.4099
AG22	0.0004	-0.1323	6.9110
FAS structure			
Viacotop	0.0004	-0.1323	6.5269
Viacobind	0.0004	-0.1323	7.0072
Viacobase	0.0004	-0.1402	6.9952

8.4 Input data

In the following chapter, the choice of input data to the different tabs in PEDRO are presented according to each tab. All specific data for E6 Fastarp-Heberg is presented in chapter 6 Reference road – E6 Fastarp-Heberg, and the viscosity parameters are calculated in chapter 8.3 Determination of viscosity parameters. A compilation of the used input data is presented in Appendix V – Input data.

As stated earlier, the mix type input is neglected since the determination of those properties is a part of the ongoing implementation. The calibration factor is set to 1 in the first run of the model, and then recalculated and altered during the calibration process.

The material properties tab is divided into two parts, one for viscosity and one for Poisson's ratio. For the viscosity parameter four factors are needed. The factor n describes the ageing properties of the asphalt concrete, the used value is default in PEDRO and is based on earlier conducted research (Said, 2005). The factors a_1, a_2 and a_3 describe the shear properties and are derived from the master curves produced from the laboratory results. For Poisson's ratio, the default values in PEDRO are used.

The traffic tab is divided into three parts, one for traffic amount and load, one for vehicle characteristics and one for the daily traffic distribution. The chosen method for defining the traffic data is regional BWIM data. The reason for this choice is that the BWIM data is considered more accurate compared to the use of ESALs. E6 Löddeköpinge is chosen as data source for the BWIM data because it is the closest located measuring site and it is the same motorway.

The chosen method for the calculations of contact pressure is the tire contact area model. This model requires the manual input of tire type and inflation pressure for both

dual and widebase tires. The measuring of contact pressure is difficult whereas accurate data for tire type and inflation pressure is easier to find. The tire types currently available in PEDRO are presented in Table 5. The tire types used in the calculations are selected according to the most common tire widths found by Almqvist (2011). The tire pressures used in the calculations are based on the recommendations from Goodyear (2012).

Table 5. Truck tire types available in PEDRO

	Tire type
Dual configuration	G159A 11R22.5
	BF12 295/80R22.5
Single configuration	WTT 6.00R9
	G165 425/65R22.5
	G425/65R22.5

For the lateral wander an average value is used based on the results from McGarvey (2016). The used values for the daily traffic distribution are the default values in PEDRO. These values are average for Swedish roads and are based on the values presented in Vägverket (1994).

For the climate data there are two available input options. Since the VViS station (1336) located at E6 Fastarp-Heberg does not measure the pavement temperature at all the needed depths, one of the predefined measuring locations was selected. Measuring location Falkenberg (VViS 1329), located approximately 25 km north of the reference road, was chosen for the climate input data. Of all the available locations with the needed pavement temperature data it is located closest to the reference road.

8.5 Results

The calculations were performed separately for the two studied pavement structures. The results for the reference structure are presented first, followed by the results for the FAS structure. The calculated permanent deformation is compared to the measured values presented in chapter 6.2 Pavement performance data.

8.5.1 Reference structure

The measured rutting in 2010 at section 12 at E6 Fastarp-Heberg was 17 mm. The rutting caused by studded tires was approximately 4.78 mm in 2010 and the study performed by Ekblad & Lundström (2011) found that approximately 4 mm of the permanent deformation was caused by the compaction of unbound layers. Ekblad & Lundström (2011) performed their calculations for the right wheel path but their results are assumed to be accurate for the left wheel path in order to perform the calculations. This leaves 8.22 mm of rutting caused by permanent deformation of the bound layers which is used for comparison. The correct calibration factor was calculated by an iteration process comparing the calculated rutting to the measured one and the result from the iteration process is presented in Table 6. The calibration is performed for 2010 and no comparison is made to measurements of any other year.

Table 6. Results from iteration process, reference structure

Iteration number	Calibration factor	Depression [mm]	Upheaval [mm]	Total deformation [mm]
1	1	70.904	11.237	82.141
2	0.1001	7.097	1.125	8.222

The result of the iteration process was a calibration factor of 0.1001. A schematic figure of the permanent deformation of the final calculation is presented in Figure 21. The negative values of permanent deformation are equal to the upheavals and account for approximately 14 % of the total rut depth.

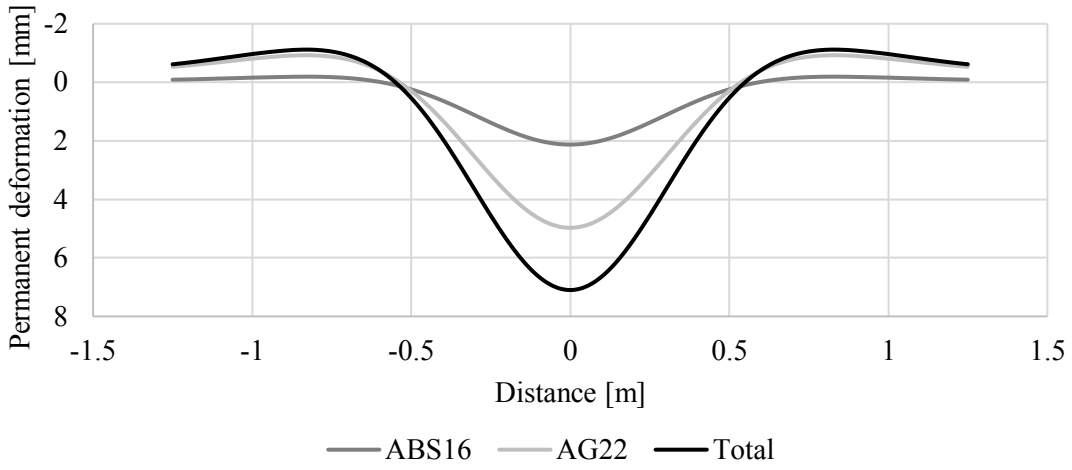

Figure 21. Calculated permanent deformation of reference structure

After calibrating the program with the measured values from 2010 the accumulated permanent deformation was calculated for each year, the results are presented in Figure 22. The figure show the development of permanent deformation for each layer as well as the complete structure from construction until 2010.

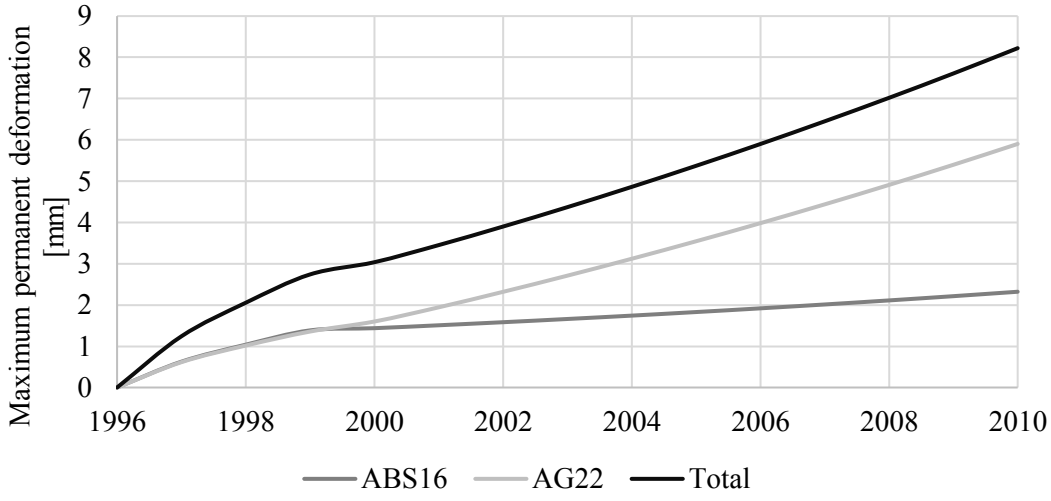

Figure 22. Calculated rut depth 1996-2010, reference structure

8.5.2 FAS structure

The measured rutting in 2010 for the FAS pavement structure is equal to 9 mm. The rutting caused by studded tires was in 2010 approximately 3.69 mm and no deformation of the unbound layers was found in the study performed by Ekblad & Lundström (2011). Therefore the conclusion is that the permanent deformation in the bound layers was 5.31 mm in 2010. Just like for the reference structure, the calibration factor was calculated through an iteration process and the results are presented in Table 7. The comparisons performed to find the calibration factor are made with measurements from 2010.

Table 7. Results from iteration process, FAS structure

Iteration number	Calibration factor	Depression [mm]	Upheaval [mm]	Total deformation [mm]
1	1	68.261	11.245	79.506
2	0.0668	4.560	0.751	5.311

The iteration process gave a calibration factor of 0.0668. In Figure 23 the calculated profile of the permanent deformation is presented. The upheavals are approximately 14 % of the total deformation and are represented by the negative permanent deformation in Figure 23.

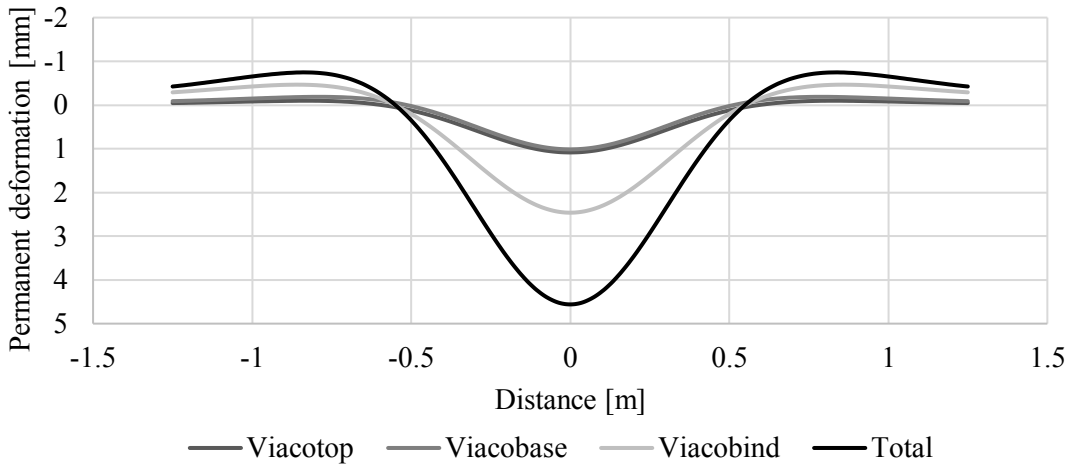

Figure 23. Calculated permanent deformation of FAS structure

Once the calibration was performed the development of permanent deformation was calculated and those results are presented in Figure 24. The results show the development for each layer and all layers combined for a timespan from construction until 2010.

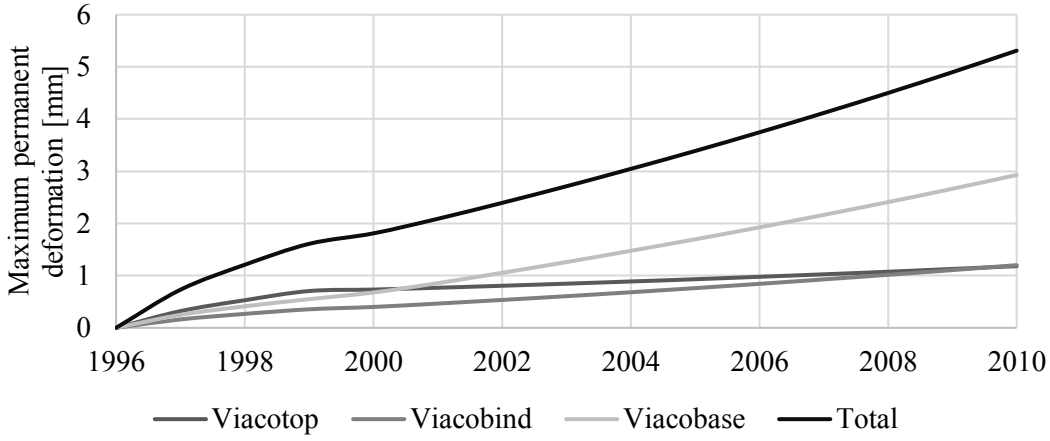

Figure 24. Calculated rut depth 1996-2010, FAS structure

8.6 Comparison of traffic input data

An analysis was performed to see how large impact the choice of traffic input data had on the results. The analysis was performed by altering the input data from BWIM to ESALs and calculating the calibration factor, both for the reference structure and the FAS structure.

8.6.1 Input data

In PEDRO, the amount of traffic is defined as the traffic flow the year of construction and then the annual traffic growth is used to increase the traffic each year. However, to enable the comparability between the prior calculations and these calculations traffic data is used for E6 Löddeköpinge for the measuring period of 2006-01-01 to 2010-01-01. The BWIM data was measured between 2004 and 2009 for the same road section.

The AADTh in the north going direction was 2690 ± (7 %) and the amount in the other direction was 2580 ± (7 %) (Trafikverket, 2016). Since the studied pavement structures are placed in the south going direction the AADTh for that direction was used. The distribution of the traffic in the two lanes is dependent on the total amount of traffic on the road. With an AADTh of 2580 the amount of trucks in outer lane is approximately 93 % (Darter, et al., 1985).

The load equivalent factor describes how many ESALs a heavy vehicle corresponds to. It takes the weight and axle configuration into consideration to calculate the total amount of ESALs. The load equivalent factor is usually calculated for each heavy vehicle category with the forth power law, described in equation (4), and then summarised according to each category's portion of the total traffic (Kawa, et al., 1998). The load equivalent factor has been estimated for the reference road using the BWIM data collected between 2004 and 2009 at E6 Löddeköpinge. The used load equivalent factor of 1.36 is an average value for the entire measuring period (Winnerholt & Persson, 2006), (Vägverket, 2007), (Winnerholt, 2008), (Winnerholt, 2009), (Vägverket, 2010).

8.6.2 Reference structure

The measured rutting used for comparison and iteration is the same as earlier, 8.22 mm. The calculated calibration factor is equal to 0.1666 and the results of the calculations are presented in Table 8. Note that this calibration factor is about 160 % the size of the calibration factor of the BWIM data at 0.1001.

Table 8. Results of calculation with ESALs, reference structure

Iteration number	Calibration factor	Depression [mm]	Upheaval [mm]	Total deformation [mm]
1	1	42.849	6.500	49.349
2	0.1666	7.139	1.083	8.222

8.6.3 FAS structure

The comparison was made with the same measured deformation as earlier, which was 5.31 mm. The calculations resulted in a calibration factor equal to 0.1113, the results are presented in Table 9. The calibration factor from the BWIM calculations was 0.0668 and the calibration factor gained when calculating with ESALs is approximately 170 % of the factor gained with BWIM.

Table 9. Results of calculation with ESALs, FAS structure

Iteration number	Calibration factor	Depression [mm]	Upheaval [mm]	Total deformation [mm]
1	1	41.213	6.504	47.717
2	0.1113	4.587	0.724	5.311

9 Uncertainties

The insecurities involved in the study include the measurements of permanent deformation, the input data in PEDRO, the laboratory methods, as well as the correlations used for the calculations in PEDRO. In this chapter, all known insecurities are accounted for.

9.1 Rut depth measurements

When comparing the PRIMAL measurements, the measurement from 2010 for the reference structure showed higher values compared to the prognosis from 2006. This is demonstrated in Figure 25. The difference could be caused by some alterations in the performed measurements, or indicate the failure of the pavement structure.

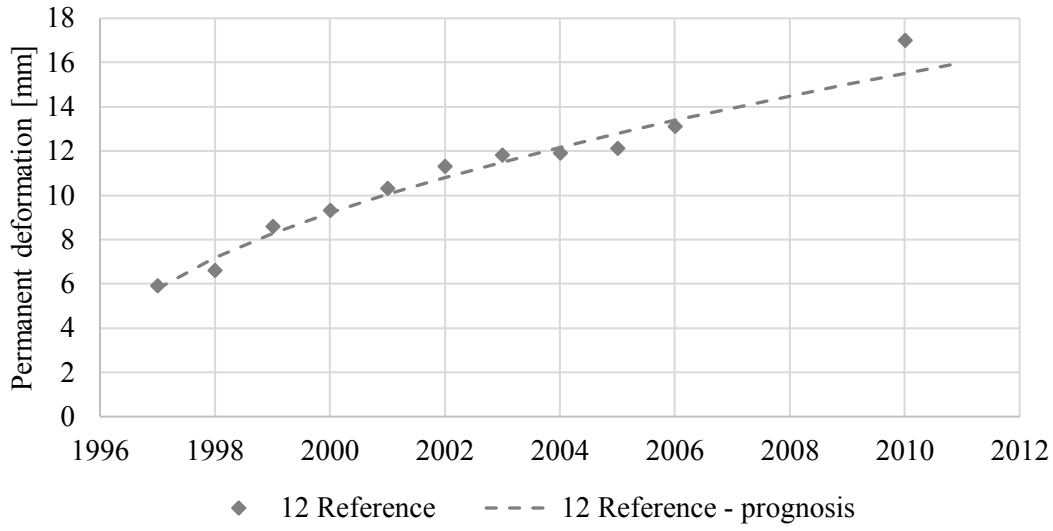

Figure 25. Comparison of measured rut depth for the reference structure

The first potential explanation for the diverging value for 2010 is that the measurements have been performed differently. It is known that the 2010 measurements are based on two profiles, while the earlier measurements are based on at least nine profiles. This makes the 2010 measurements more dependent on the chosen profiles and more susceptible to any extreme values. The data could also indicate that the development of permanent deformation had reached the third tertiary development phase, i.e. the failure of the structure, which is not accounted for in PEDRO. However, the measurements performed with the RST-car show that the development of permanent deformation is still in the second phase. Therefore, it is believed that there is a difference between the performance of the measurements.

Further, all calculations in PEDRO are performed for the left wheel path. However, the calculations of compaction of the unbound layers are performed for the right wheel path (Ekblad & Lundström, 2011) but are assumed to be accurate for both wheel paths in the performed calculations. In general, the development of rutting each year in the right wheel path is 65 % of the development in the left wheel path (McGarvey, 2016) and if this affect the level of compaction of the unbound layers is not considered.

Finally, the presented values of measured rutting are all total rutting and not excluding the deformations occurring during construction. The development of permanent

deformations could be considered more accurate to use, but Ekblad & Lundström (2011) did not adapt their measurements and in order to use their data, the total deformations were used.

9.2 Input data

The input data include two different kinds of insecurities. Firstly, not all needed input data was available for E6 Fastarp-Heberg and therefore the used data come with some uncertainties concerning its applicability to the reference road. Secondly, all measurements and tests come with uncertainties and limitations and it is important to recognise these uncertainties and limitations since they may affect the final results.

9.2.1 Pavement data

The construction dates and test dates are used to calculate the age of the asphalt concrete. The construction date is set according to the information from the previous studies conducted at E6 Fastarp-Heberg. Since two tests were performed per asphalt mix there are two test dates per mix and therefore the test date is an adaption. Given the very long time span of over 20 years between construction and testing, those few days between the tests should be insignificant. The layer thicknesses originate from the design documents and the real layer thicknesses may vary from those values and throughout the road sections. However, it is believed that the average layer thicknesses are close to those of the design documents.

The factors describing Poisson's ratio are not adapted for the specific asphalt mixes in this study but are general values for asphalt concrete. How much Poisson's ratio alters with different asphalt mixes or the age of the asphalt concrete has not been examined, and therefore it is hard to determine the size of the error. The factor n describing the change in viscosity due to ageing is not adapted to the different asphalt mixes either. How the ageing has effected the different mixes is not known and therefore the factor remained unchanged.

9.2.2 Traffic data

The BWIM data used for the calculations was measured at E6 Löddeköpinge, 130 km south of the reference road. In between E6 Löddeköpinge and E6 Fastarp-Heberg there is a junction splitting E6 which continues north towards Gothenburg and E4 going north towards Stockholm. Therefore, it is likely that a significant amount of the traffic passing by E6 Löddeköpinge will turn of E6 and onto E4, and not pass the reference road. The AADTh for E6 Fastarp-Heberg is equal to 2160 vehicles while E6 Löddeköpinge have an AADTh of 3420 vehicles, which is 58 % more. Since the chosen source for traffic data has a larger AADTh than the reference road it is likely that the results from the calculations will be slightly overestimated.

An option for the calculations of the traffic load would be to combine the BWIM data from E6 Löddeköpinge with BWIM data from E6 Kungsbacka. However, the BWIM data from E6 Kungsbacka are from a regional measurement and are therefore not included in PEDRO. The option to import BWIM data to PEDRO is not available yet which is why this option could not be performed.

The annual traffic growth is based on measurements performed at E6 Fastarp-Heberg. The measurement was performed with the Metor 2000 measuring system. According to the literature these measuring devices can be sensitive to variations in vehicle speed, where large speed variations can cause measuring errors (Papagiannakis & Masad, 2008). However, the vehicle speeds are considered to have minor variations, limiting the risk of error.

The traffic distribution factors originate from Vägverket (1994) and are average for Swedish roads. How much the daily traffic distribution varies over different roads and sections or if the distribution has changed over the past 20 years is not known. However, the general consensus is that any change in the daily traffic distribution is small, both between different roads and over the years.

9.2.3 Vehicle data

None of the vehicle specific data is available for E6 Fastarp-Heberg, except for the average vehicle speeds. The data used to estimate the lateral wander is based on measurements at E6 Uddevalla and E4 Linköping. They are both motorways with lane widths 0.15-0.2 m wider than E6 Fastarp-Heberg, this could result in an overestimated lateral wander at E6 Fastarp-Heberg. However, they are the only examined motorways in Sweden and the effect of restricted lane widths have mostly been noticed on 2+1 roads, where lane widths typically are more restricted and the side verge limited. Hence, the error caused by an incorrect lateral wander is considered small.

The measurement of wheel configuration is based on measurements at Västerås and E18 Hummelsta, which are both located approximately 500 km north of E6 Fastarp-Heberg. It is possible that there are some differences in the wheel configuration of the heavy traffic in the, by Almqvist (2011), studied area compared to E6 Fastarp-Heberg. However, it is the only study of that kind performed on the Swedish collection of heavy vehicles. Further, the options available in PEDRO did not match the most common tire widths found by Almqvist (2011). However, since focus was not on estimating permanent deformation cause by different tire types and widths, these limitations were not examined further. Further, it is not considered how the vehicle characteristics have changed since the road opening in 1996 since it would require thorough knowledge on the heavy vehicle fleets composition over the years.

9.2.4 Climate data

In PEDRO, temperature measurements from Falkenberg were used which were conducted at three different depths of the pavement; 0.02 m, 0.065 m and 0.14 m. The temperature measuring station closest to the studied pavement structures, VViS 1336, only measured the temperature at 0.002 m depth and could therefore not be used in PEDRO. However, to evaluate the accuracy of the used data, the measured data at 0.02 m depth at Falkenberg was compared to the measured data at VViS station 1336. The measurements are presented in Appendix VI – Temperature data. The temperature at the VViS station is at average 1.5°C higher. However, the temperature at the VViS station is measured closer to the surface which typically results in a higher temperature but it is believed that the Falkenberg weather station is in average a little bit colder than the reference road which will give underestimated results. The size of the potential error was not further examined.

9.3 Laboratory tests

Limitations in the laboratory tests include the time restriction preventing all layers and specimens from being tested, the long storage time at the laboratory, and the errors and limitations correlated to the performance of the laboratory tests.

9.3.1 Limited amount of tested specimen

Time limitations during the laboratory testing prevented all layers from being tested and it was assumed that all layers with the same mix type have the same properties. However, it is not unlikely that the bottom layer is less compacted compared to the following layers and this could affect the performance of that layer. For the asphalt mix AG22 of the reference structure specimens from layer 1 and 2 were tested (layer 3 was not tested) and there was no indication of difference in compaction. The Viacobase of the FAS structure consists of two layers and one specimen per layer was tested. There is a difference in phase angle between the two specimens, but if that is the effect of a difference between the layers or general variety between the specimens cannot be evaluated from these results. Further specimens from each layer would need to be tested to verify a difference between the layers. However, due to time limitations of this project the number of tested samples is considered enough to get accurate results and the differences are considered a general variation between the specimens, like variations in bitumen or void content.

9.3.2 Storage and ageing

The core samples used for the laboratory tests were drilled in 2011 and have been stored in the laboratory since. The difference in how the specimens aged in the laboratory compared to how they would have aged in the road is not known and it is hard to draw any conclusions regarding the ageing and how it has been affected. However, it is possible that the exposure to oxygen increased for the underlying layers while other weather related ageing processes were limited.

9.3.3 Testing errors

Prior to the testing of one of the ABS16 specimen, an error occurred in the controlling equipment. The bar used to induce shear force had reached a static force of -1500 N. The test was performed as usual and the phase angle showed normal results, however the shear modulus showed lower values compared to the other tested specimen of ABS16. This could be the result of the testing error, but also a general variation between the specimens. To limit the uncertainties considering the testing error another specimen should have been tested of ABS16. However, there was not time to perform the test and the difference in shear modulus was considered a normal specimen variation.

One Viacotop specimen showed abnormal test results compared to all other tested specimen, not explainable by the general variation between the specimens. Therefore, a third Viacotop specimen was tested to confirm the material properties and increase the reliability of the laboratory results. As mentioned earlier there was a power outage before the testing begun and the equipment had to be restarted. If something had happened to the specimen while in the testing box prior to or during the power outage is not known but it is the only known source of irregularity during the performance of

the tests. The other possible explanation would be some irregularities in or damage caused earlier to the specimen but no such thing was detected when the specimen was selected for the laboratory tests.

9.3.4 Divergent test results

When adapting the master curves to the laboratory results, some values deviated from the fitted curves. The diverging values occurs more frequently for the phase angle and can be found in the master curves of AG22, Viacotop, Viacobind and Viacobase. This could be caused by a bad fitting of the test results to the sinus curves, since a small change in the fit along the x-axle have a large impact on the phase angle. However, if a value for the phase angle stands out it is excluded from the fitting of the master curve which should limit the effect of the diverge values. There are some divergent values of the shear modulus as well, all from the tests performed at low temperatures and high frequency, and these values can be found in the master curve of AG22 and Viacobase. The deformations in this scenario are small and small deformations are hard to measure correctly with the equipment. A way to avoid these kinds of measurement errors would be to apply a higher force.

For a few of the asphalt mixes there are variations in the shear modulus between the tested specimens, see ABS16, Viacotop, Viacobind and Viacobase. For ABS16 and Viacotop the difference in shear modulus at cold temperatures are as high as 1000 MPa, for the Viacobind and Viacobase the difference is 500 MPa. These differences are most likely caused by variations between the specimens like differences in bitumen content or void content. In these cases, the master curves are fitted in between the two measured curves. For the Viacobase there is also a difference between the phase angle. The peaks coincide but the value of the phase angle differs with approximately 5° between the specimens. This is also believed to be caused by variations between the specimens.

9.4 Limitations of PEDRO

Given that PEDRO is still in the development phase, the amount of available choices for the input data are limited. For example, the contact pressure is most accurately calculated using tire type and tire pressure, however the options of tire types are few. The same limitation is valid for the traffic data; BWIM is the most accurate data but the data is only available for a few locations in Sweden. The available amount of climate stations in PEDRO are also limited, but the VViS data can be used to estimate the temperature throughout the pavement using a VTI software. However, this software is not easily available which limits the applicability of the VViS climate data.

In PEDRO, it is assumed that the correlation between viscosity and ageing is the same as for stiffness and ageing. The stiffness modulus describes the viscoelastic behaviour of asphalt concrete, and is equivalent to the quotient between tensile stress and strain (Domone & Illston, 2010). The viscosity is determined by a correlation between dynamic shear modulus and the phase angle, and the dynamic shear modulus is equal to the quotient of the dynamic stress and strain (Ahmed, et al., 2013). Both the stiffness and dynamic modulus are dependent on stresses and strains in the material and if the different stresses and strains react equally to the material ageing, the correlation between viscosity and ageing should be equal to the correlation of stiffness and ageing.

PEDRO calculates the permanent deformation based on the vertical strain and does not consider dynamic loads. However, it has been found that the longitudinal and transversal contact stresses cannot be considered insignificant (Yang, et al., 2016). The results of the study performed by Yang, et al. (2016) are presented in Figure 26. How this effects the results of PEDRO is not further investigated.

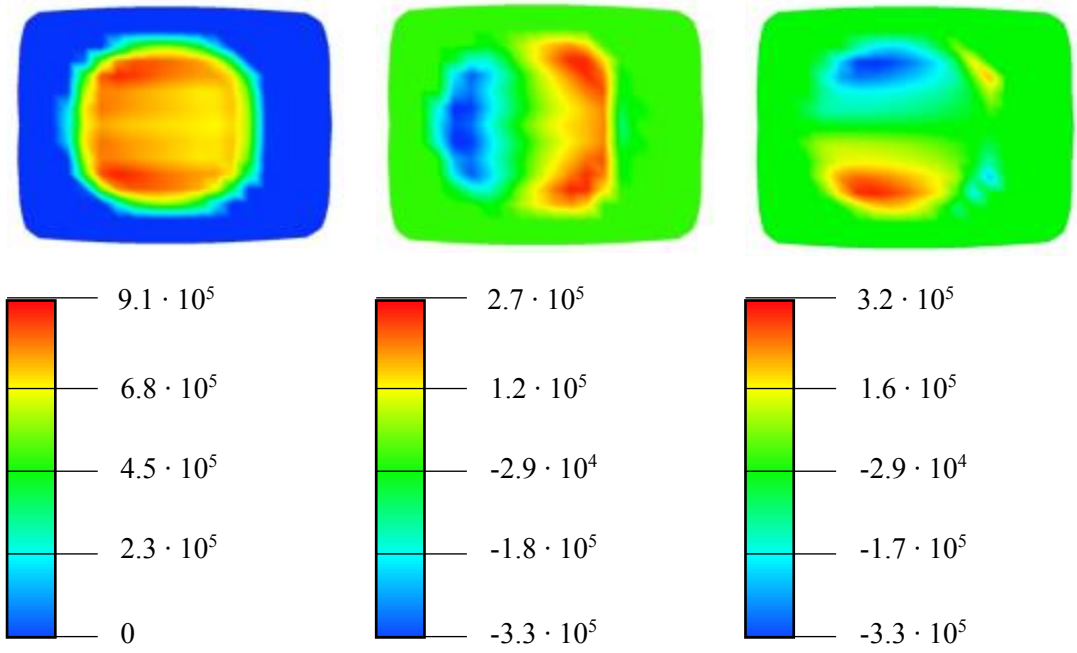

Figure 26. Tire contact stress under the free rolling state, (a) vertical stress, (b) longitudinal stress, (c) transversal stress. (Yang, et al., 2016)

10 Evaluation of results

In the following chapter both the results of the laboratory and the results of the calculations in PEDRO will be evaluated. The laboratory results are evaluated by comparing the two studied pavement structures. For PEDRO the results for the reference structure and the FAS structure are evaluated individually by comparison to measured profiles. Then the resulting calibration factors are evaluated by comparing the two structures and finally the comparison of traffic input data is evaluated.

10.1 Laboratory

When comparing the master curves the two surface layers, ABS16 and Viacotop, they show similar properties and the resulting viscosity also showed a small difference of $0.41 \cdot 10^5$ MPa s. For the base courses, AG22 and Viacobase, the variation in the master curves was larger but when looking at the resulting viscosity the difference was even smaller compared to the surface layers at only $0.06 \cdot 10^5$ MPa s. Considering the FAS structure only had about 60 % of the permanent deformations measured at the reference structure the differences in viscosity were smaller than expected which also affected the results in PEDRO.

No studies were found in which the viscosity of aged asphalt pavements had been evaluated in the laboratory, which limited the possibility to evaluate the laboratory results further. However, a comparison was made to the master curves presented by Said, et al. (2013) who evaluated the viscosity on 4 specimens manufactured at the laboratory. Their results showed similar dynamic shear modulus but higher phase angles. The values of importance for maximum viscosity are those at maximum phase angle. The specimens in this study had a frequency at maximum phase angle of approximately $1 \cdot 10^{-4}$ Hz while Said, et al. (2013) had values of about $1 \cdot 10^{-3}$ Hz. The shear modulus varies less between this study and the one performed by Said, et al. (2013), our specimens had a shear modulus at peak phase angle of approximately 500 MPa while the specimen from Said, et al. (2013) study were approximately 700 MPa. Further, their measurements showed higher conformity, and less variation or abnormal values as can be seen in our master curves presented in Appendix III – Master curves. Still, their specimens were not aged and had been stored in a controlled environment which effect the outcome of the laboratory.

10.2 PEDRO

For the primarily calculations, comparisons were made with measured surface profiles for 2011 performed by VTI. To be able to compare the measured surface profiles to the ones calculated in PEDRO the deformations in the unbound layers and the wearing caused by studded tires needed to be subtracted. The compaction in the unbound layers was estimated by adapting a curve to the results of Ekblad & Lundström (2011). Their calculations were performed for the right wheel path but are assumed to be accurate for both wheel paths, and therefore the estimated curve intersect with their results in the centre of both wheel paths. Data from McGarvey (2016) was used to estimate the lateral position of the passenger cars so the wearing caused by studded tires could be allocated over the entire lane width. The lateral position of passenger cars (McGarvey, 2016) were combined with the linear extrapolation of the wearing, performed in chapter 6.2.2

Wearing caused by studded tires. Since McGarvey (2016) found that the left wheel path often correlated for the passenger cars and the heavy vehicles, the maximum wearing caused by studded tires and the maximum rut depth of the left wheel path are assumed to coincide.

10.2.1 Reference structure

For the reference structure both wearing caused by studded tires and compaction of the unbound layers needed to be subtracted to make the data comparable. The results of those estimations, combined with the remaining rutting (permanent deformation in the bound layers) and the measured surface profile are presented in Figure 27.

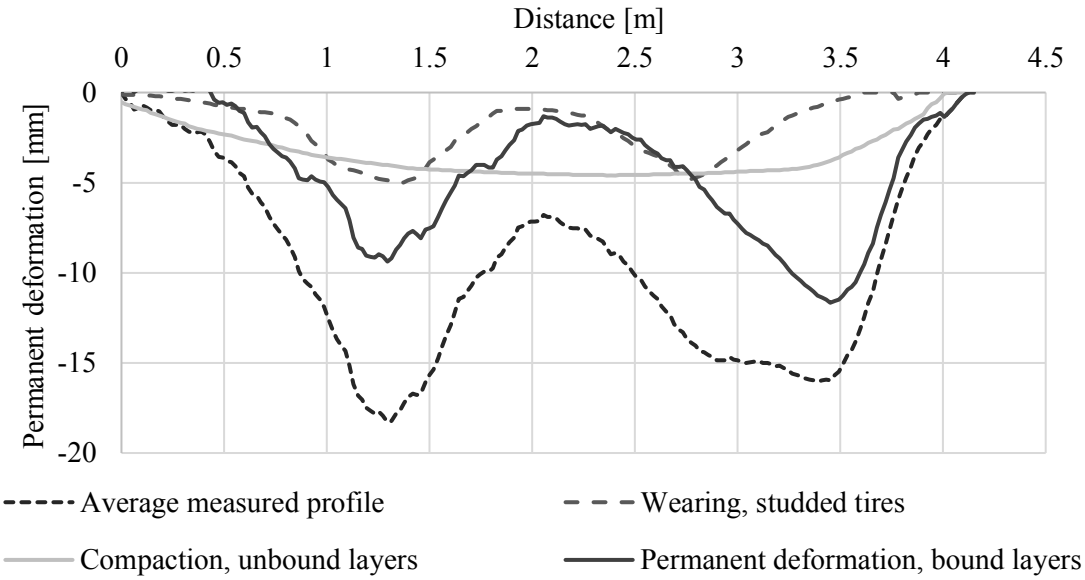

Figure 27. Measured surface profile from 2011, estimated compaction of unbound layers and wearing from studded tires as well as remaining permanent deformation of the bound layers, reference structure

For the compaction of the unbound layers the estimated curve was fitted to the, by Ekblad & Lundström (2011), calculated compaction. However, the compaction of the unbound layers is distributed according to an estimated curve which is not based on any measurements. It is known that the load is more spread out in the underlying layers compared to the surface layers and therefore the compaction of the unbound layers was assumed to be more evenly distributed over the entire lane width without a clear peak. It is possible that the curve should have somewhat steeper slopes and that the compaction should be even larger in the middle thereby resulting in no permanent deformation of the bound layers between the wheel paths. However, since the unbound layers are not considered in this study the distribution of their compaction is not further examined.

The profile showing only the permanent deformation of the bound layers was compared to the calculated profile from PEDRO and the results are presented in Figure 28. Important to notice is that the PEDRO profile is calculated for 2010 while the measured profile is from June 2011 (before the new paving).

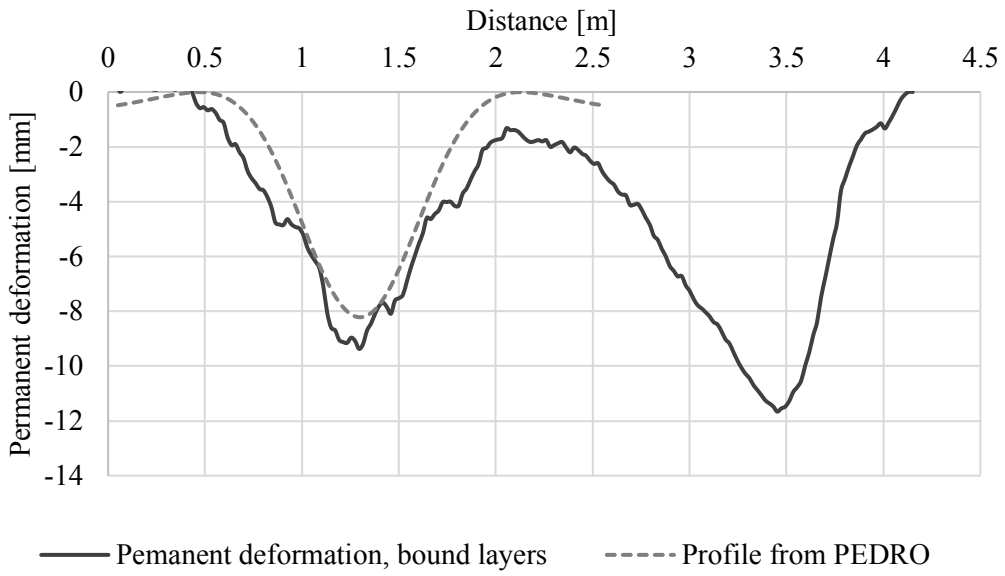

Figure 28. Comparison of measured permanent deformation of the bound layers (2011) to calculated surface profile (2010), reference structure

The measurements show a permanent deformation in the bound layers of 9.37 mm compared to 8.22 mm which is the value used to calculate in PEDRO; the difference being 1.15 mm. This could be the cause of additional deformations occurring between 2010 and 2011, another possible reason for this difference could be that the lateral position for passenger cars is based on measurements from E6 Uddevalla. E6 Uddevalla has a lane width of 3.65 m, while the reference road has a lane width of 3.5 m and this might overestimate the lateral wander and thereby underestimate the wearing.

Further, the permanent deformation of the bound layers is larger for the right wheel path than the left wheel path. These results were unexpected and induce some doubts regarding the accuracy of the obtained profile of the permanent deformation of the bound layers.

10.2.2 FAS structure

For the FAS structure only the wearing caused by studded tires needed to be considered. The results of the estimation of the wearing, combined with the the remaining rutting (permanent deformation in the bound layers) and the measured surface profile are presented in Figure 29.

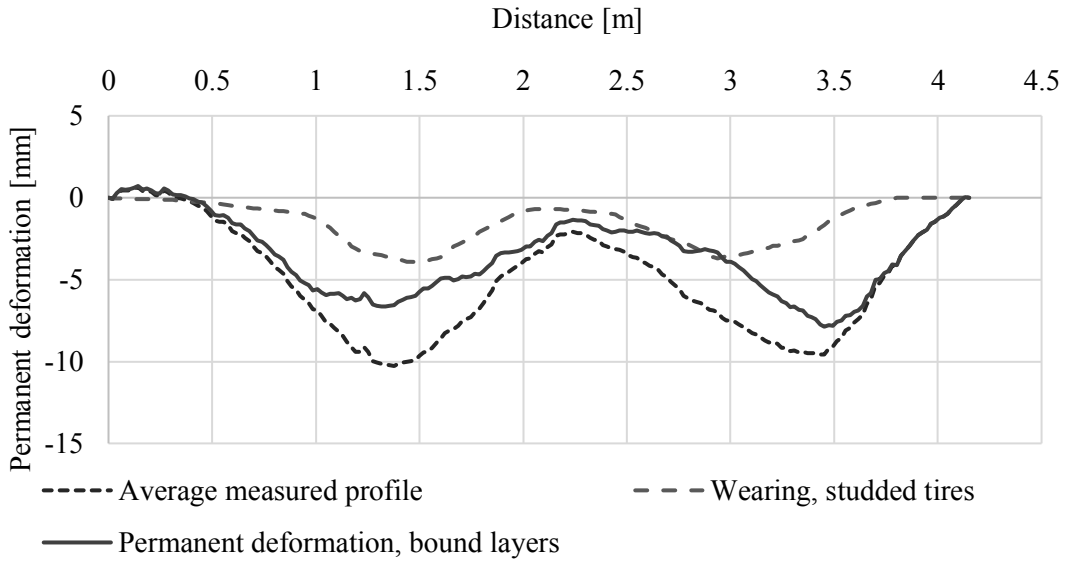

Figure 29. Measured surface profile from 2011, estimated wearing from studded tires as well as remaining permanent deformation of the bound layers, FAS structure

A comparison was made between the permanent deformation of the bound layers and the calculated profile from PEDRO, the results are presented in Figure 30. Again, the profile is calculated for maximum rutting of 2010 while the measured profile is based on average values from June 2011.

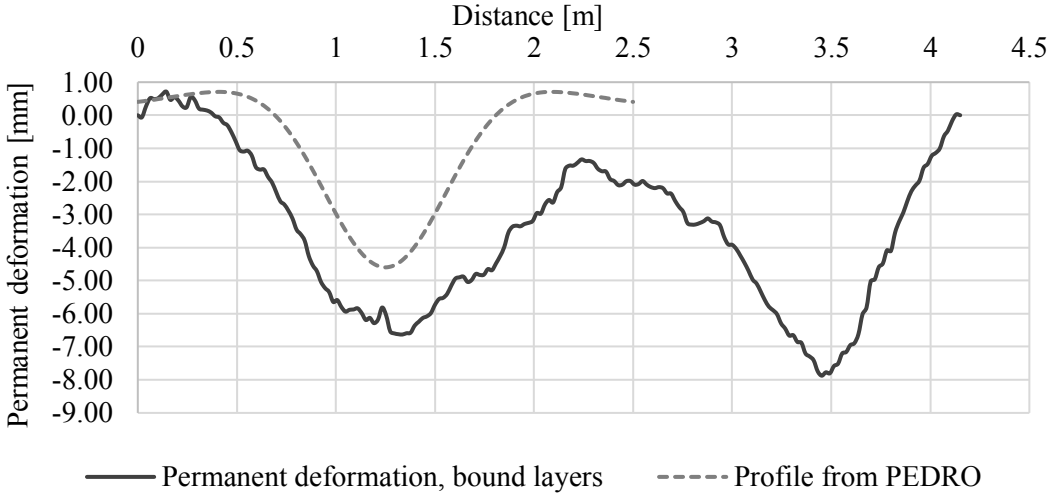

Figure 30. Comparison of measured permanent deformation of the bound layers (2011) to calculated surface profile (2010), FAS structure

The difference between the results from PEDRO and the measured permanent deformation in the bound layers is equal to 2.03 mm. Just like for the reference structure, the right wheel path show larger deformations in the bound layers compared to the left wheel path which induce some insecurities to the profile of permanent deformation in the bound layers. Ekblad & Lundström (2011) found no deformation in the unbound layers but the profile indicates that those results may be inaccurate. If there is no deformation in the unbound layers the area between the wheel paths should not show any depression but the measured profile show a depression of 1.38 mm in-

between the wheel paths. Had the permanent deformations in the unbound layers been accounted for in the calculations, the deformation in the bound layers would have been smaller at about 4 mm and thereby the calibration factor would have decreased to approximately 0.05.

Further, the measured profile is wider compared to the profile calculated in PEDRO and the match between the measured and calculated profiles is less good compared to the results of the reference structure. It is likely that the fit had been better if deformations in the unbound layers had been accounted for.

10.2.3 Calibration factor

The calibration factor affect all input parameters in PEDRO and is therefore dependent on all parameters. Given that the two pavement structures were constructed simultaneously and are placed one after the other, being exposed to the same traffic and weather, the two structures should have the same or similar calibration factors. However, the reference structure has a calibration factor of 0.1001 and the FAS structure one of 0.0668. The average calibration factor is 0.0835 and for the FAS structure that factor give a calculated deformation 25 % larger than the measured one, for the reference structure the error is slightly smaller. Since the viscosity is the only parameter that differ between the two structures it is likely that any error in the relation of the factors is caused by an incorrect viscosity. Given the many insecurities and limitations regarding the laboratory results, additional tests should be performed to further increase the accuracy of the viscosity.

The compared surface profiles gave unexpected results, where the surface profile for the FAS structure contradicted the assumption from Ekblad & Lundström (2011) that the structure had no deformation in the unbound layers. Had this been accounted for the calibration factor would have been reduced to approximately 0.05, which would increase the difference between reference and FAS further.

10.2.4 Comparison of traffic input data

Considering the uncertainties in the input data an analysis was performed to investigate what was believed to be the biggest input insecurity, the traffic data. In the analysis, the BWIM data was replaced by amount of ESALs and the load equivalent factor. The load equivalent factor is based on the BWIM measurements performed at E6 Löddeköpinge and the traffic volume is based on measurements from the same time period at the same location. The calculations with ESALs gave a calibration factor about 160-170 % of the calibration factor from the calculations with BWIM. This highlights the limitations of calculations based on ESALs and the load equivalent factor, but can be useful when trying to determine what calibration factor to use for the different kinds of input data.

Earlier research has found that calculations with ESALs usually gives about 50 % of the rut depth compared to BWIM data (Said & Hakim, 2012), which is equal to a calibration factor two times higher for the ESALs. Thereby, the results from the comparison of traffic data coincides with the result from the earlier research, indicating that the calculations are accurate.

11 Conclusion

The calculated calibration factors using BWIM data was 0.1001 for the reference structure and 0.0668 for the FAS structure and other similar roads should have calibration factors in the same range. The difference in calibration factor was larger than expected where the average calibration factor gave an error of 25 %. The surface profiles further increased the uncertainties of the results, especially considering the assumption of no permanent deformation in the unbound layers of the FAS structure. The calculations with ESALs gave calibration factors of 160-170 % the size of the ones gained with BWIM data.

To increase the accuracy of the results additional specimens of the asphalt concrete mixes should be evaluated to ensure the viscoelastic properties of the materials, since the performed number of tests were limited by the available time for the study. Further it would be interesting to evaluate if the abnormal results are the outcome of a limited measurement sensitivity and a too small applied force or if other aged pavement structures show the same inconclusive laboratory test results.

Since this thesis only examines two pavement structures that share many factors it is hard to draw any conclusions regarding the accuracy of the model. To be able to further validate the model the results should be compared to other roads and their calibration factors. Since the thesis is part of a larger project implementing PEDRO, these results can later be put in relation to results from the other studies and thereby the credibility of these results can be evaluated.

PEDRO, a viscoelastic model used to predict permanent deformation in asphalt bound layers, is a user friendly and straight forward software but the current version has some limitations. Most of the input fields lack thorough definition which increase the risk of misconception of what data to use and include. Further, the options to import data to the software is not available yet which limits the ability to further increase the accuracy of the calculations by using custom data.

12 References

AASHO Committee on Design, 1961. *AASHO Interim Guide for the Design of Flexible Pavement Structures,* s.l.: American Association of State Highway Officials.

Agardh, S., 2005. *Rut Depth Prediction on Flexible Pavements: Calibration and Validation of Incremental-Recursive Models,* Lund: Lund Institute of Technology.

Ahmed, A. W., Biligiri, P. K. & Hakim, H., 2013. An Algorithm to Estimate Rational Values of Phase Angles and Moduli of Asphalt Mixtures. *International Journal of Pavement Reserach and Technology,* 6(6), pp. 745-754.

Almqvist, Y., 2011. *Nedbrytning av vägar: Jämförelse mellan axlar med singel- respektive tvillingmontage.,* Stockholm: Kungliga Tekniska Högskolan.

Andersson, D. A. et al., 1994. *Binder Characterization and Evaluation, Volume 3: Physical Characterization,* Washington D.C.: The Strategic Highway Research Program, National Research Council.

Bahia, H. U., 2009. Modeling of Asphlat Binder Rheology and Its Application to Modified Binders. In: Y. R. Kim, ed. *Modeling of Asphalt Concrete.* Reston: American Society of Civil Engineeris, pp. 11-61.

Björklund, A., 1984. *Creep induced behaviour of resurfaced pavements. VTI Rapport 271A,* Linköping: VTI.

Brown, E. R. et al., 2009. *Hot Mix Asphalt Materials, Mixture Design, and Construction.* 3rd ed. Lanham(Maryland): NAPA Research and Education Foundation.

Burström, P. G., 2011. *Byggnadsmaterial: Uppbyggnad, tillverkning och egenskaper.* Upplaga 2:7 ed. Lund: Studentlitteratur AB.

Carlsson, A., 2009. *Uppföljning av mötesfria vägar, VTI Rapport 636-2009,* Linköping: VTI.

Collop, A. & Cebon, D., 1995. A Model of Whole-Life Flexible Pavement Performance. *Journal of Mechanical Engineering Science, IMechE,* Volume 209, pp. 389-407.

Darter, M., Elliot, R. & Hall, K., 1985. *Revison of AASHTO Pavement Overlay Design Procedures,* s.l.: NCHRP.

Domone, P. & Illston, J., 2010. *Viscosity, stiffness and deformation of bituminous materials.* 4th edition ed. Boca Raton: Taylor & Francis Group.

Doublecoin, 2012. *Doublecoin: TBR Dual Matching and Spacing Data.* [Online] Available at: www.doublecointires.com
[Accessed 24 February 2017].

Ekblad, J. & Lundström, R., 2011. *Spårbildning i asfaltsbeläggningar på provvägen E6 Fastarp-Heberg,* Upplands Väsby: SBUF.

Erlingsson, S., Said, S. & McGarvey, T., 2012. *Influence of heavy traffic lateral wander on pavement deterioration.* Malmö, EPAM 2012: 4th European Pavement and Asset Management Conference.

European Commission, 2001. *COST 334: Effects of Wide Single Tyres and Dual Tyres. Version 29,* Luxemborg: European Communities 1999.

Goodyear, 2012. *Hitta däck för lastbilar och bussar.* [Online]
Available at: http://www.goodyear.eu/se_se/truck/tires/
[Accessed 7 March 2017].

Google, 2017. *Google Maps.* [Online]
Available at: maps.google.se
[Accessed 23 February 2017].

Gudmarsson, A., 2014. *Resonance Testing of Asphalt Concrete,* Stockholm: KTH Royal Institute of Technology.

Kaloush, K. E. & Wiczak, M. W., 2002. *Simple performance test for permanent deformation of asphalt mixtures,* Washington D.C.: Transportations Research Board.

Kawa, I., Zhang, Z. & Hudson, W. R., 1998. *Evaluation of the AASHTO 18-Kip Equivalency Concept,* Texas: Texas Department of Transportation.

Kim, Y. R., 2009. Modeling of Asphalt Concrete. In: Y. R. Kim, ed. *Modeling of Asphalt Concrete.* Reston: American Society of Civil Engineers, pp. 1-7.

Lind, K., 2011. *TRVKB 10 Bitumenbundna lager,* Borlänge: Trafikverket.

Lindström, F., 2015. *Vägytemätning Mätstorheter. TDOK 2014:0003,* Göteborg: Trafikverket.

Lundström, M., 2001. *Mätprincip för METOR 2000,* s.l.: Vägverket.

McGarvey, T., 2016. *Vehicle lateral position depending on road type and lane width: Vehicle position surveys carried out on the Swedish road network,* Linköping: VTI.

NCHRP, 2004. *Guide for the Mechanistic-Empirical Design of New and Rehabilited Pavement Structures,* Champaign, Illinois: National Cooperative Highway Reasearch Program.

Nilsson, R., 1999. *A viscoelastic approach to flexible pavement design,* Stockholm: KTH Royal Institute of Technology.

Oscarsson, E., 2011. *Mechanistic-Empirical Modeling of Permanent Deformation in Asphalt Concrete Layers,* Lund: Lund University.

Papagiannakis, A. T. & Masad, E. A., 2008. *Pavement Design and Materials.* 1:st edition ed. Hoboken: John Wiley & Sons, Inc.

Parhamifar, E., 2016a. *Asphalt Pavements.* Göteborg: Lund Institute of Technology.

Parhamifar, E., 2016b. *Laboratory Instructions.* Lund: Lund University.

Pavement Interactive, 2011. *Los Angeles Abrasion.* [Online]
Available at: www.pavementinteractive.org/article/los-angeles-abrasion/
[Accessed 7 February 2017].

Persson, K., 2016. *BITUMEN: Properties and testing.* Gothenburg: TOTAL Nordic.

Read, J. & Whiteoak, D., 2003. *The Shell bitumen handbook 5th Edition, Shell UK Oil Products Limited.* 5th Edition ed. London: Thomas Telford Publishing.

Said, S., 2016. *Projektbeskrivning: Prognostisering av spårtillväxt-asfaltsbeläggning.* Linköping: VTI.

Said, S. F., 2005. Aging Effect on Mechanical Characteristics of Bituminous Mixtures. *Transportation Research Record: Journal of the Transportation Research Board,* Issue 1901, pp. 1-9.

Said, S. F., Ahmed, A. W. & Carlsson, H., 2016. *Evaluation of rutting of asphalt concrete pavement under field-like conditions.* Prague, 6th Eurasphalt & Eurobitume Congress.

Said, S. F. & Hakim, H., 2012. *Influence of Traffic Variables on Rut Formation in Asphalt Concrete Layers.* Stockholm, HVTT12.

Said, S. F. & Hakim, H., 2014. Asphalt concrete rutting predicted using the PEDRO model. *International Journal of Pavement Engineering,* 17(3), pp. 245-252.

Said, S. F., Hakim, H. & Eriksson, O., 2013. Rheological Characterization of Asphalt Concrete Using a Shear Box. *Journal ofT and Evaluation,* 41(4), pp. 602-610.

Said, S. F., Hakim, H., Oscarsson, E. & Hjort, M., 2011. Prediction of flow rutting in asphalt concrete layers. *International Journal of Pavement Engineering,* 12(6), pp. 519-532.

Trafikverket, 1990. *Bestämning av krossytegrad hos bär-och förstärkningslager ,* s.l.: Trafikverket.

Trafikverket, 2011a. *TRVKB 10 bitumenbundna lager. TRV 2011:082,* Borlänge: Trafikverket.

Trafikverket, 2011b. *Vägväderinformationssystem, VViS.* [Online]
Available at: trafikverket.ineko.se
[Accessed 3 March 2017].

Trafikverket, 2015a. *Så sköter vi vägar.* [Online]
Available at: www.trafikverket.se/resa-och-trafik/vag/Sveriges-vagnat/
[Accessed 24 January 2017].

Trafikverket, 2015b. *VViS.* [Online]
Available at: http://vvis.trafikverket.se/
[Accessed 03 March 2017].

Trafikverket, 2015c. *Vägtrafik- och hastighetsdata.* [Online]
Available at: www.trafikverket.se/tjanster/trafiktjanster/Vagtrafik--och-hastighetsdata/
[Accessed 20 February 2016].

Trafikverket, 2016. *Vägtrafikflödeskartan.* [Online]
Available at: vtf.trafikverket.se
[Accessed 22 February 2017].

Trafikverket, 2017. *PMSV3 - information om belagda vägar.* [Online]
Available at: pmsv3.trafikverket.se
[Accessed 24 February 2017].

Ullidtz, P. & Ekdahl, P., 1998. *Full-scale Testing of Pavement Response.* Trondheim, Proceedings of the Fith International Conference on the Bering Capacity of Roads and Airfields.

Ulmgren, N. & Lundström, R., 2006. *The SMA-principle applied to Wearing, Binder and Base Course Layers - the VIACO-concept.* Qubéc, 10th International Conference on Asphalt Pavements, ISAP.

Vägverket, 1994. *Vägutformning 94 Del 4,* Borlänge: Vägverket.

Vägverket, 2007. *BWIM-mätningar 2006: Sammanfattning,* Borlänge: Vägverket.

Vägverket, 2010. *BWIM-mätningar 2009: Sammanfattning,* Borlänge: Vägverket.

Verstraeten, J., 1995. *Bituminous materials with a high resistance to flow rutting.* s.l., PIARC technical committee on flexible roads.

Viman, L., 2005. *Provsträckor på E6, Fastarp-Heberg: Laboratorieprovning av bitumenbundna lager. Uppföljning efter 7 års trafik. VTI notat 35-2005,* Linköping: VTI.

Wiman, L. G., Carlsson, H., Viman, L. & Hultqvist, B.-Å., 2005. *Prov med olika överbyggnadstyper: Observationssträckor på väg E6, Fastarp-Heberg. Resultatrapport efter 7 års uppföljning 1996-2003. VTI notat 25-2005,* Linköping: VTI.

Wiman, L. G., Carlsson, H., Viman, L. & Hultqvist, B.-Å., 2009. *Prov med olika överbyggnadstyper: Uppföljning av observationssträckor på väg E6, Fastarp-Heberg 1996-2006. VTI rapport 632,* Linköping: VTI.

Winnerholt, T., 2008. *BWIM-mätningar 2007: Sammanfattning,* Borlänge: Vägverket.

Winnerholt, T., 2009. *BWIM-mätningar 2008: Sammanfattning,* Borlänge: Vägverket.

Winnerholt, T., 2011a. *TRVK Väg,* Stockholm: Trafikverket.

Winnerholt, T., 2011b. *TRVR Väg,* Stockholm: Trafikverket.

Winnerholt, T. & Persson, L., 2006. *BWIM-mätningar 2004-2005: Projektrapport,* Borlänge: Vägverket.

Yang, W., Tiecheng, S., Yongjie, L. & Chundi, S., 2016. Prediction for Tire-Pavement Contact Stress under Steady-State Conditions based on 3D Finite Element Method. *Journal of Engineering Science and Technology Review,* 9(4), pp. 17-25.

Yildirim, Y., 2005. Polymer modified asphalt binders. *Construction and Building MATERIALS,* 21(1), pp. 66-72.

Appendix

Appendix I – Laboratory working process

Step 1

Separate the core samples into disks of maximum 40 mm, each disk consistent of one asphalt concrete layer.

Step 2

Measure the thickness and diameter of each disk sample.

Step 3

Use epoxy glue to glue the disk sample to two loading steel plates. The loading steel plates should be mounted onto guided plates.

Step 4

Let the glue harden for 24 h.

Step 5

Remove the guided plates from the specimen. Put the specimen in the shear box and mount one deformation measuring device to the back of the specimen, then fasten the specimen to the right side of the shear box. The measuring device should continuously show values close to zero during the entire installation.

Step 6

Fasten the specimen to the left side and then mount the second deformation measuring device to the front of the specimen, the measured value should be approximately zero until the installation is finished. Change the setting from position mode to force mode and check that the force of the shearing side is approximately zero, adjust if necessary.

Step 7

Mount the compression bar. Place the temperature sensor in the testing box with connection to the shear box to create conditions as close to those of the sample disk as possible. Close the door. Set the temperature to the lowest testing temperature.

Step 8

When the temperature in the testing box reach the desired temperature the actual testing can start. Fill in the amplitude for each frequency according to the table below*. Make one final check that the force of the shearing side is close to zero, adjust it if necessary.

Amplitude of force [N]		Degrees [°C]			
		-5	**10**	**30**	**50**
Frequency [Hz]	**16**	2200	1500	600	250
	8	2200	1500	600	250
	4	2200	1500	600	250
	2	2000	1000	500	200
	1	2000	1000	500	200
	0.5	2000	1000	500	200
	0.1	1800	1000	500	200
	0.05	1800	1000	500	200

Step 9

Put the static side force to 5.5 bar. Check that the deformation measuring devices show approximately zero and adjust them if necessary. Then start the test, the deformations in the front and in the back and the shear force should be recorded. Note the temperature before and after the test, since these values are not recorded automatically.

Step 10

Once the test is finished, release the side force and change the temperature to the next testing temperature. Once the desired temperature is reached, repeat step 8 and 9.

Step 11

When the specimen is tested for all temperatures, change the setting from force mode to position mode and dismount the specimen. Perform the dismounting backwards compared to the installation.

*For specimen 13L1-11, alternative forces were used for the testing at -2.46°C which are listed below, for all other performed tests the forces stated previously were used.

Frequency [Hz]	16	8	4	2	1	0.5	0.1	0.05
Amplitude of force [N]	2200	2000	1900	1600	1400	1200	1000	1000

Appendix II – Laboratory protocol

The specimens are numbered after the pavement structure, layer and drill hole. The thickness, diameter, test date and tested temperatures for all specimens was notated.

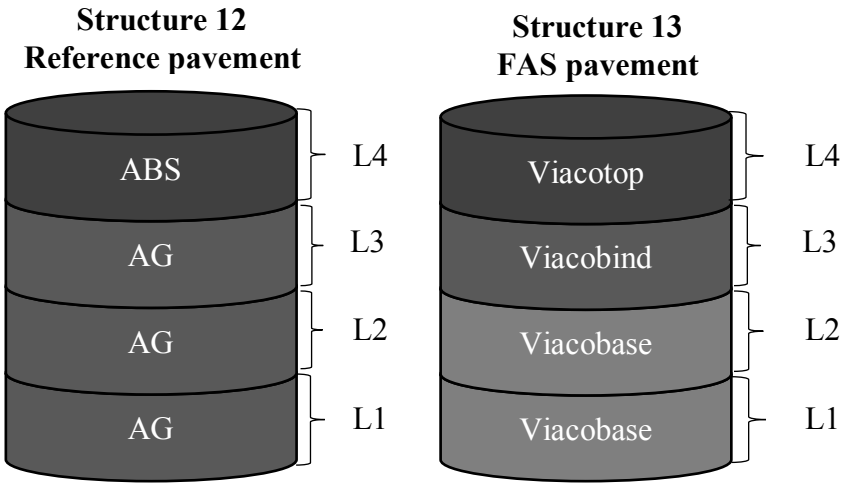

Specimen	Test date	Temperature [°C]	Thickness [mm]	Diameter [mm]
12L1-19	2017-03-02	-5.35	38.6	150
		10.70		
		30.05		
		49.85		
12L2-19	2017-03-01	-5.35	38.5	149.9
		11.35		
		30.45		
		51.25		
12L4-2	2017-03-03	-4.90	33.9	150.1
		10.10		
		30.30		
		50.60		
12L4-11	2017-03-07	-3.90	33.5	150
		10.00		
		31.35		
		49.35		
13L1-11	2017-04-28	-2.46	38.5	149.8
		11.18		
		31.86		
		49.35		

Specimen	Test date	Temperature [°C]	Thickness [mm]	Diameter [mm]
13L2-11	2017-03-10	-5.20	38.5	150
		10.05		
		31.18		
		51.43		
13L3-3	2017-04-18	-4.21	38.6	150.5
		12.82		
		30.83		
		49.79		
13L3-11	2017-03-09	-5.65	38.5	150.3
		10.15		
		31.80		
		53.00		
13L4-3	2017-04-20	-5.15	33.9	150.2
		14.55		
		35.89		
		53.88		
13L4-4	2017-03-08	-5.70	33.8	150.3
		14.65		
		31.95		
		50.25		
13L4-18	2017-03-06	-4.80	33.8	150.2
		10.35		
		31.20		
		49.45		

Appendix III – Master curves

For each layer, the generated master curves are presented in a figure and the constants used for their equations, equation (10) to (13), are presented in a table. Finally, the correlation between the temperature and viscosity is presented.

Reference structure – ABS16

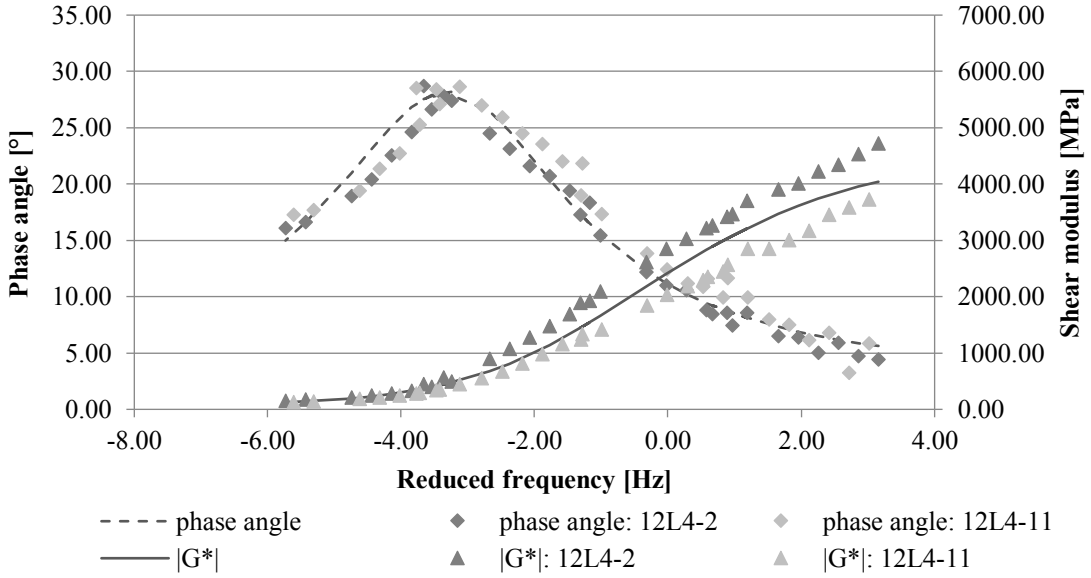

p	-3.30
b	2.25
c	24.70
D	7.00
B	20.00
δ	3.66
β	-1.95
κ	1.80
γ	-0.56
k	10000.07

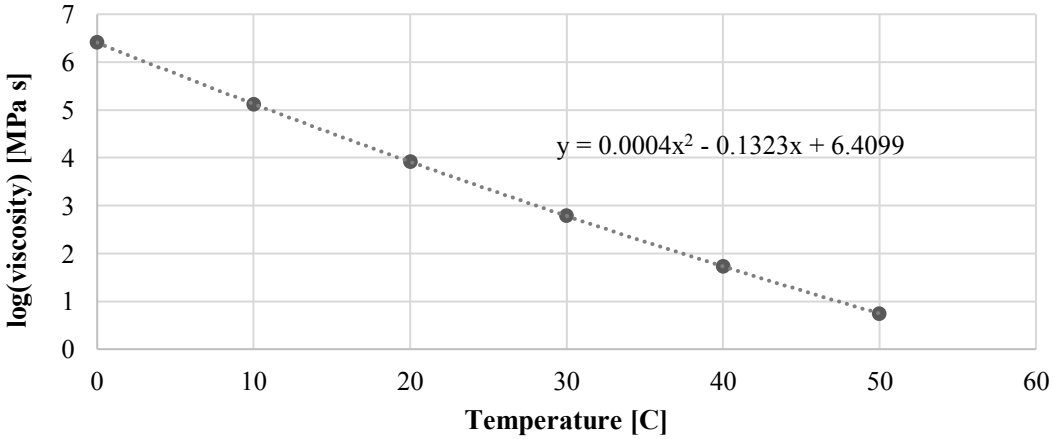

Reference structure – AG22

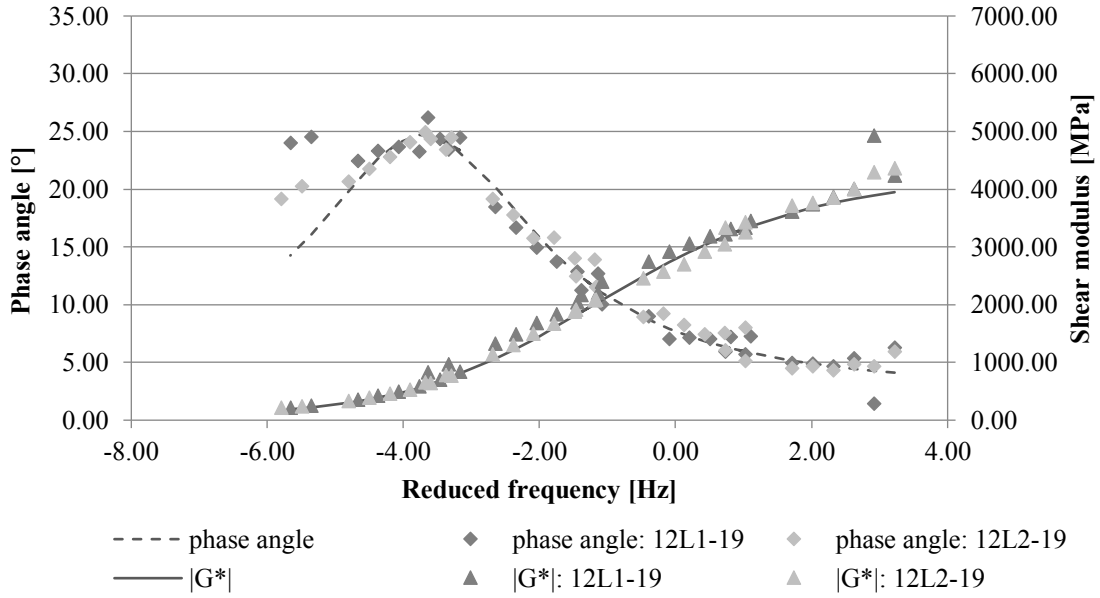

p	-3.70
b	2.10
c	22.50
D	4.44
B	3091.99
δ	3.63
β	-1.90
κ	2.23
γ	-0.56
k	10000.40

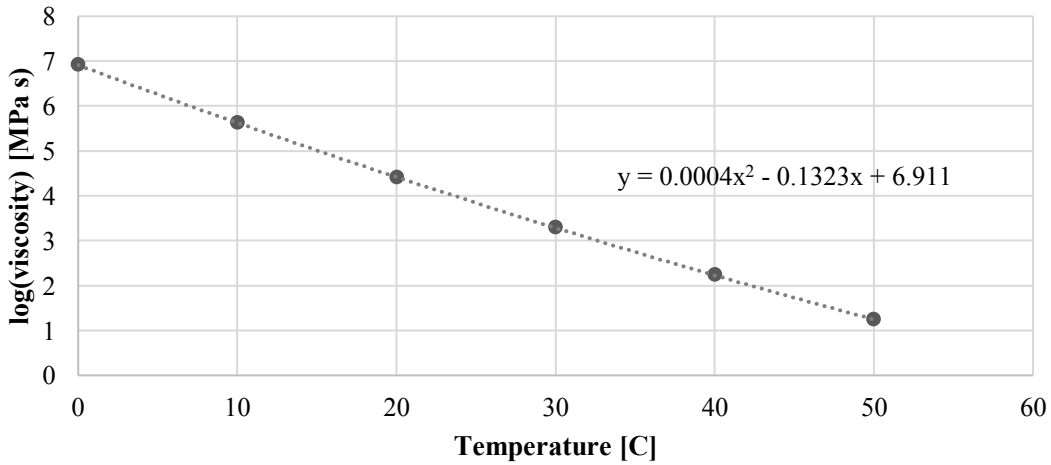

FAS structure – Viacotop

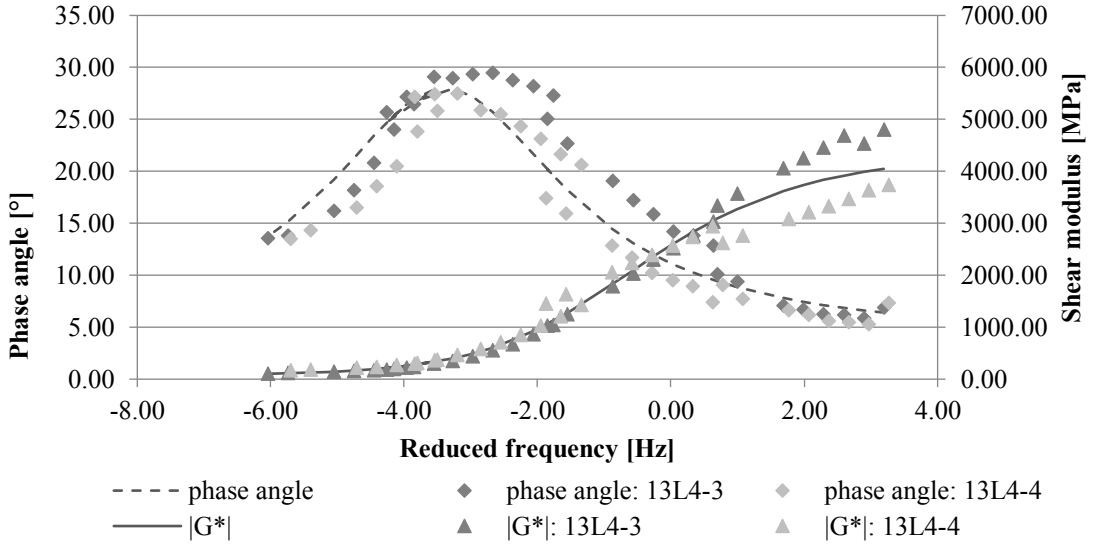

p	-3.38
b	2.20
c	24.00
D	8.00
B	2000.00
δ	3.64
β	-1.80
κ	1.95
γ	-0.69
k	10000.51

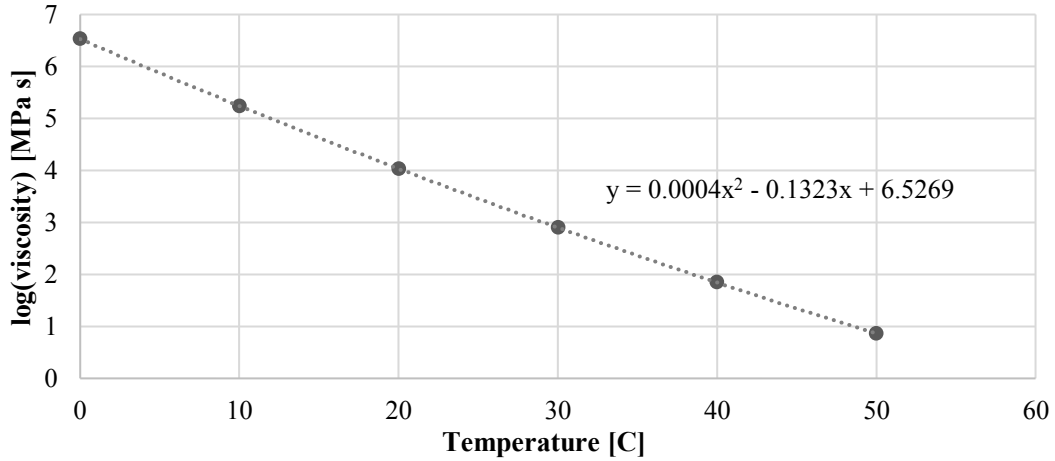

Below are the excluded measurements of specimen 13L4-18, combined with the master curves for the Viacotop layer.

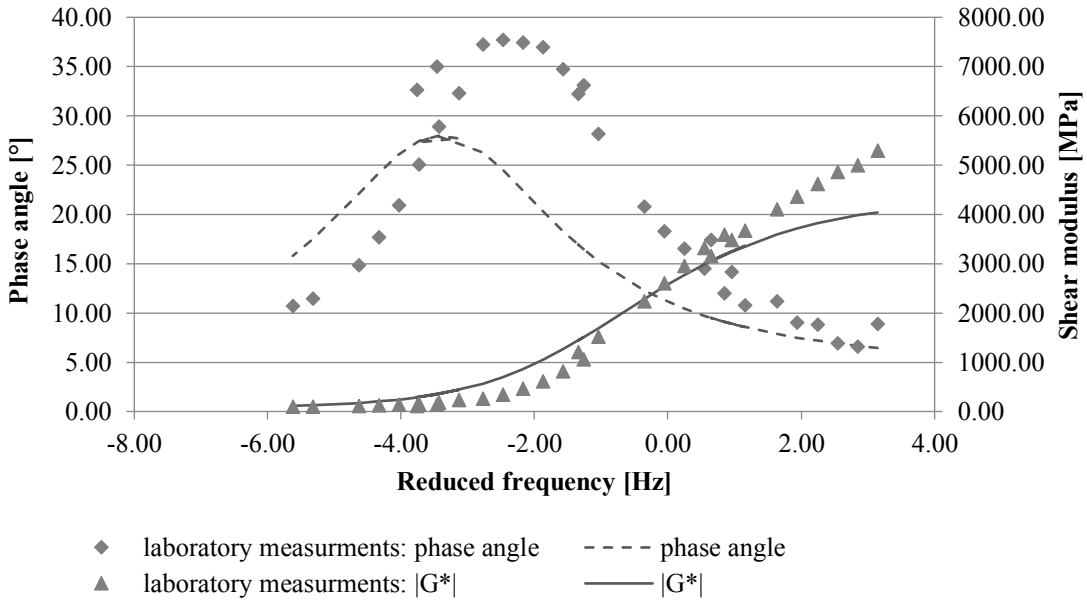

FAS structure – Viacobind

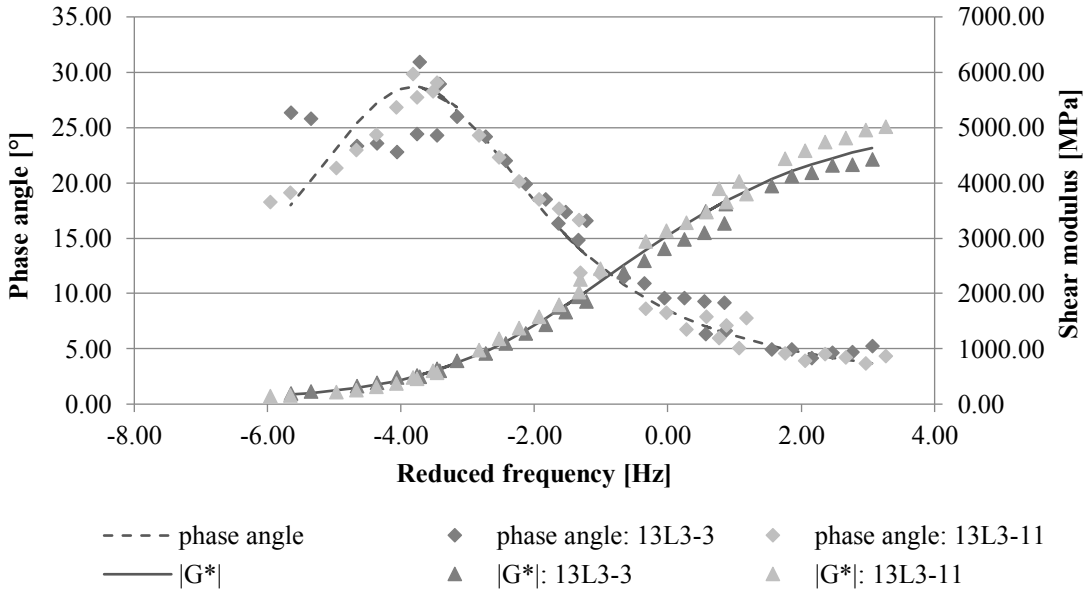

p	-3.80
b	2.35
c	28.00
D	1.50
B	1000.00
δ	3.71
β	-1.94
κ	2.02
γ	-0.56
k	10000.59

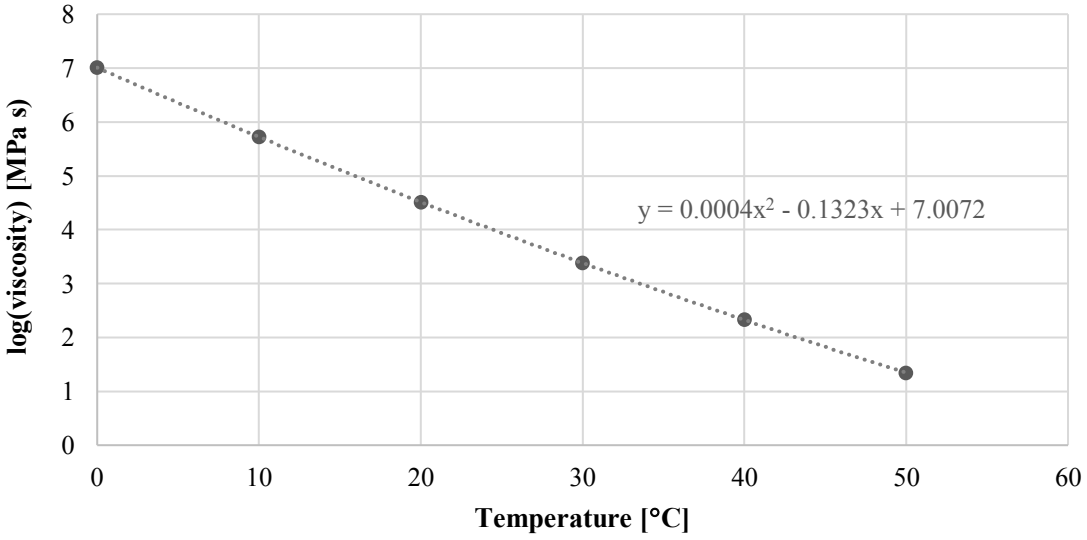

FAS structure – Viacobase

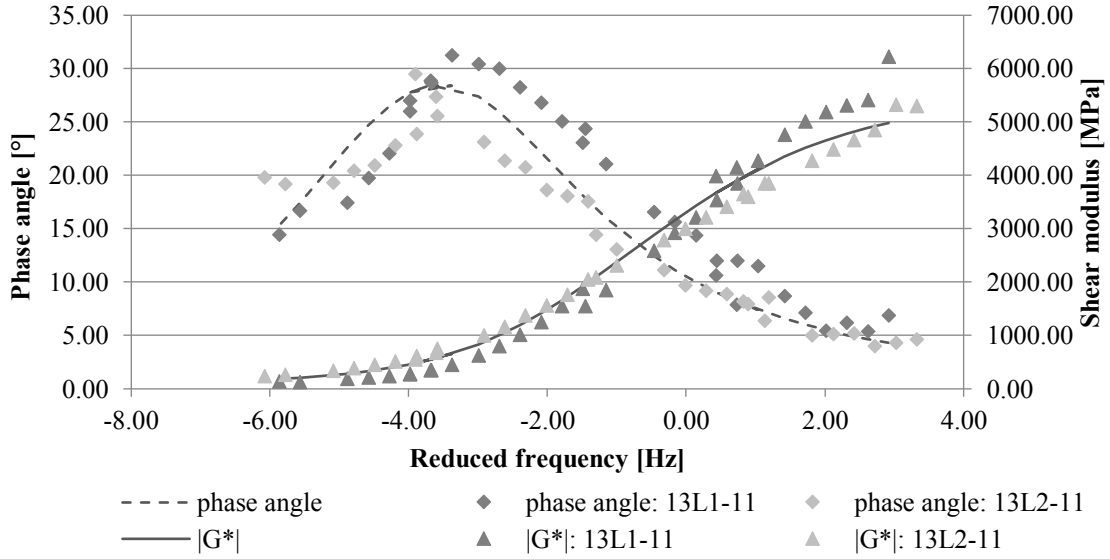

p	-3.60
b	2.80
c	31.00
D	-5
B	3
δ	3.74
β	-1.77
κ	1.95
γ	-0.60
k	10600.85

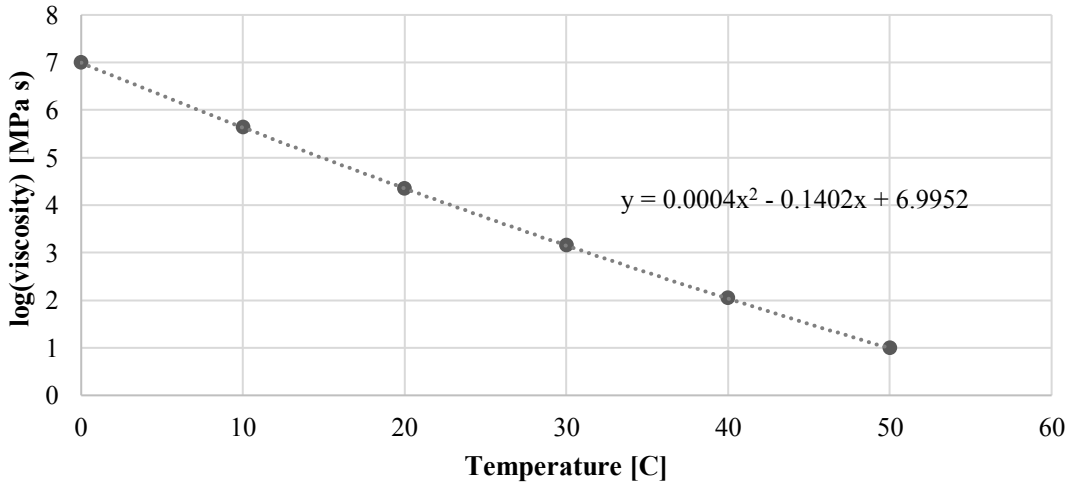

Appendix IV – Software structure

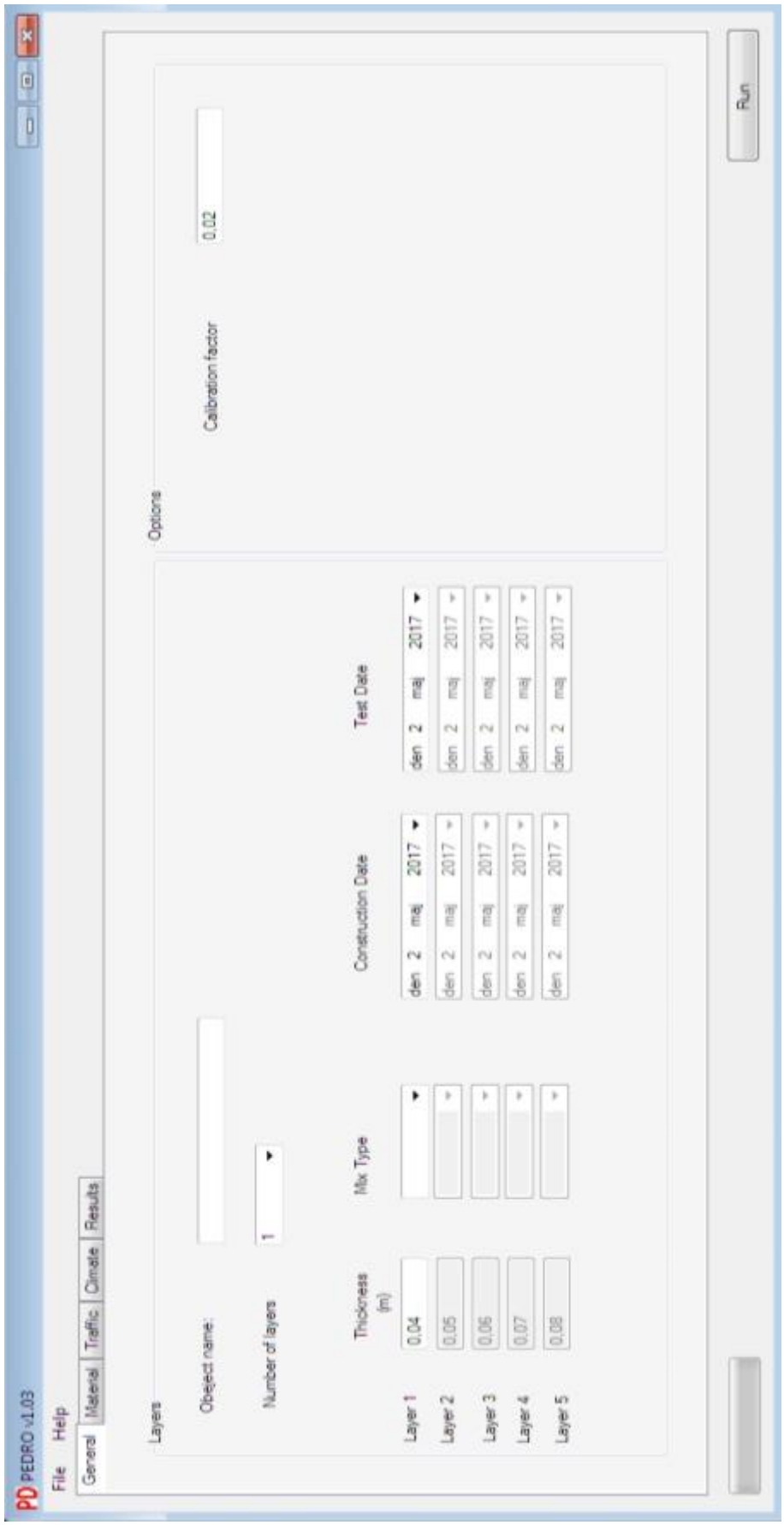

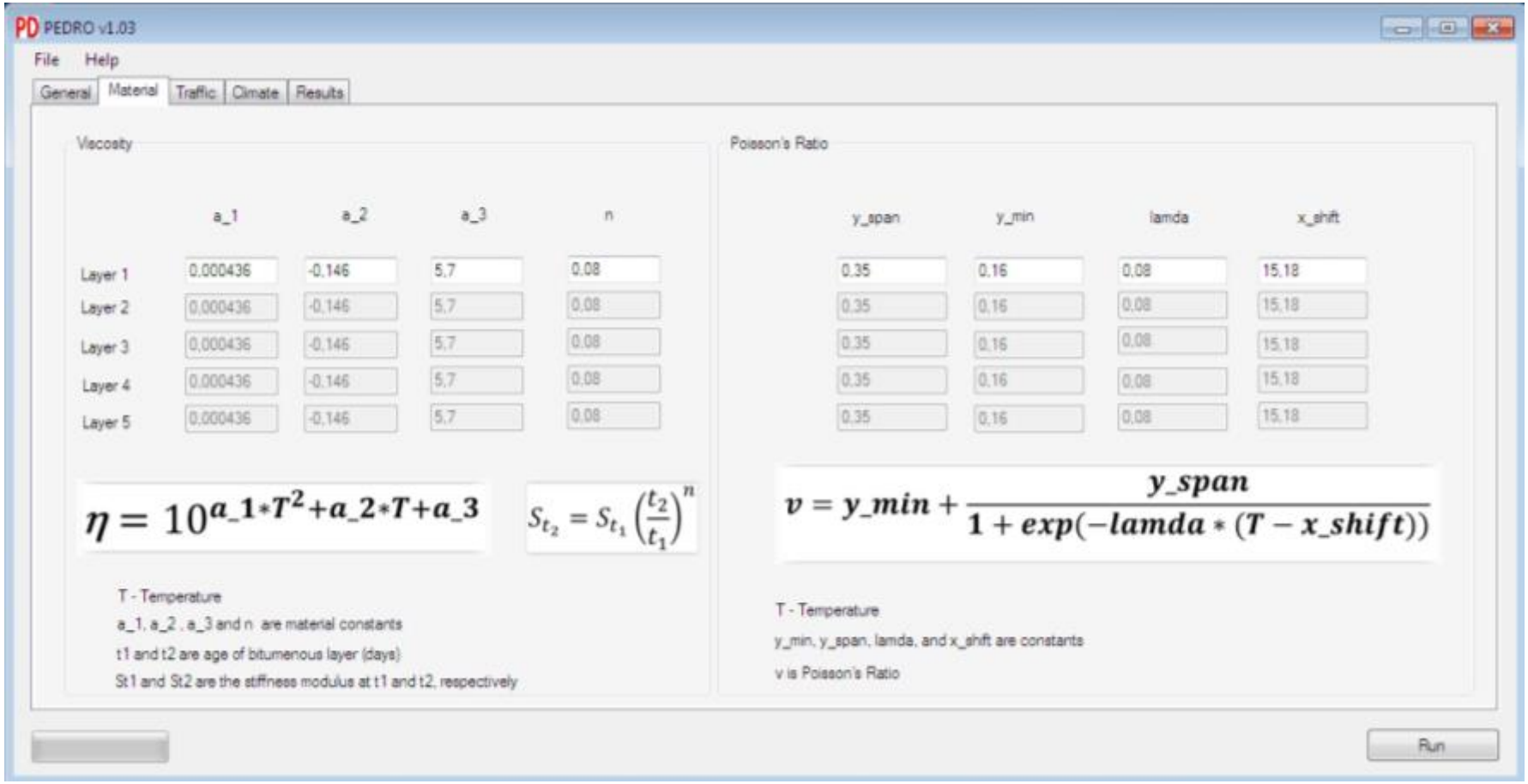
PEDRO v1.03
File
Help
General
Material
Traffic
Climate
Results
Viscosity
a_1
a_2
a_3
n
Layer 1
Layer 2
Layer 3
Layer 4
Layer 5
0.000436
-0.146
5.7
0.08
$\eta = 10^{a\_1*T^2+a\_2*T+a\_3}$
$S_{t_2} = S_{t_1}\left(\frac{t_2}{t_1}\right)^n$
T - Temperature
a_1, a_2 , a_3 and n are material constants
t1 and t2 are age of bitumenous layer (days)
St1 and St2 are the stiffness modulus at t1 and t2, respectively
Poisson's Ratio
y_span
y_min
lamda
x_shift
0.35
0.16
0.08
15.18
$v = y\_min + \frac{y\_span}{1 + exp(-lamda * (T - x\_shift))}$
T - Temperature
y_min, y_span, lamda, and x_shift are constants
v is Poisson's Ratio
Run

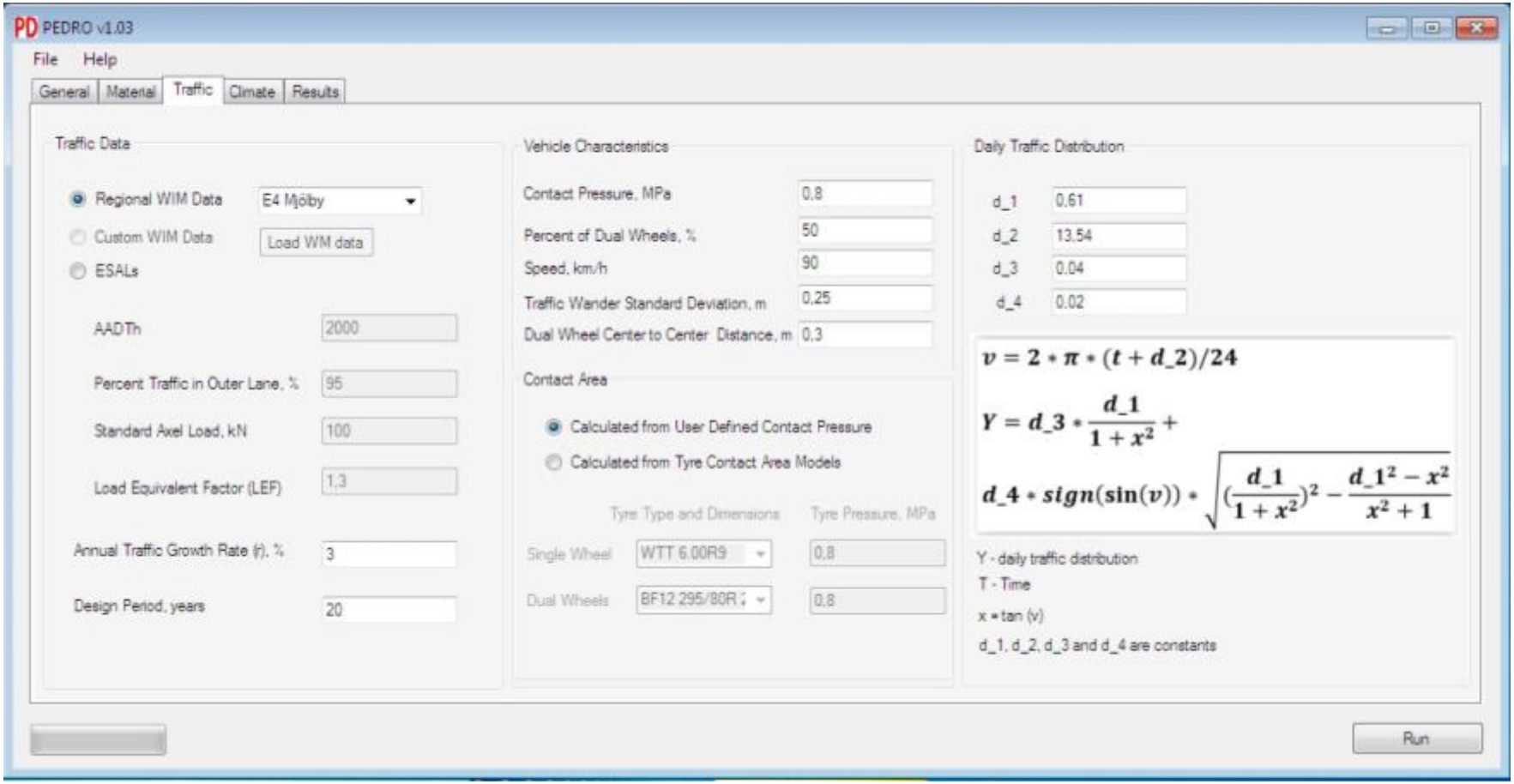
PEDRO v1.03
File
Help
General
Material
Traffic
Climate
Results
Traffic Data
Regional WIM Data
E4 Mjölby
Custom WIM Data
Load WM data
ESALs
AADTh
2000
Percent Traffic in Outer Lane, %
95
Standard Axel Load, kN
100
Load Equivalent Factor (LEF)
1,3
Annual Traffic Growth Rate (r), %
3
Design Period, years
20
Vehicle Characteristics
Contact Pressure, MPa
0,8
Percent of Dual Wheels, %
50
Speed, km/h
90
Traffic Wander Standard Deviation, m
0,25
Dual Wheel Center to Center Distance, m
0,3
Contact Area
Calculated from User Defined Contact Pressure
Calculated from Tyre Contact Area Models
Tyre Type and Dimensions
Tyre Pressure, MPa
Single Wheel
WTT 6.00R9
0,8
Dual Wheels
0,8
Daily Traffic Distribution
d_1
0,61
d_2
13,54
d_3
0,04
d_4
0,02
$v = 2 * \pi * (t + d\_2)/24$
$Y = d\_3 * \frac{d\_1}{1 + x^2} +$
$d\_4 * sign(\sin(v)) * \sqrt{(\frac{d\_1}{1 + x^2})^2 - \frac{d\_1^2 - x^2}{x^2 + 1}}$
Y - daily traffic distribution
T - Time
x = tan (v)
d_1, d_2, d_3 and d_4 are constants
Run

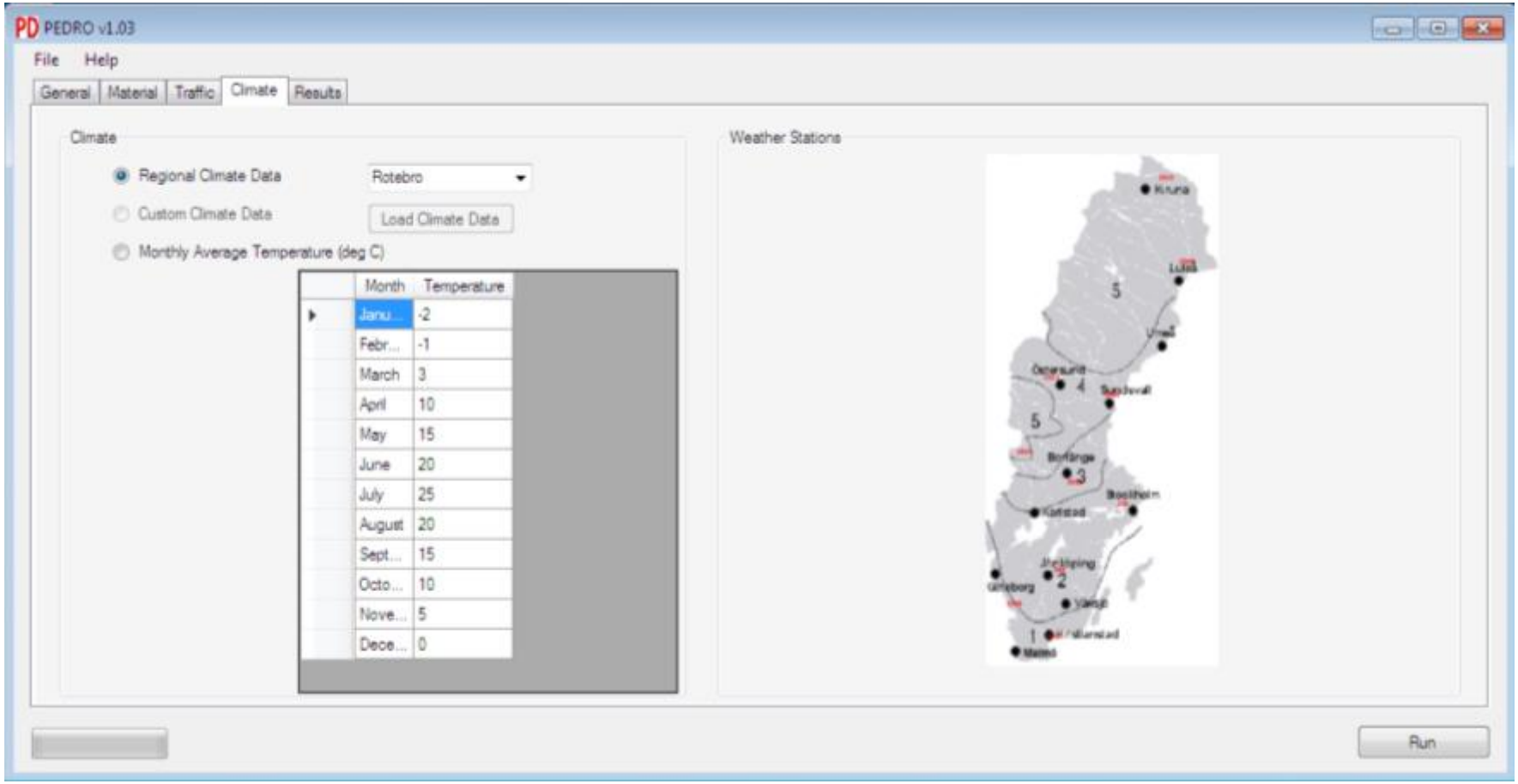
PD PEDRO v1.03
File
Help
General
Material
Traffic
Climate
Results
Climate
Regional Climate Data
Rotebro
Custom Climate Data
Load Climate Data
Monthly Average Temperature (deg C)
Month
Temperature
Janu...
-2
Febr...
-1
March
3
April
10
May
15
June
20
July
25
August
20
Sept...
15
Octo...
10
Nove...
5
Dece...
0
Weather Stations
Run

PD PEDRO v1.03
File
Help
General
Material
Traffic
Climate
Results
Year
Layer 1
Layer 2
Layer 3
Layer 4
Layer 5
Total
Profile
Legend
Layer 1
Layer 2
Layer 3
Layer 4
Layer 5
Total
Run

Appendix V – Input data

General input data

	Thickness [m]	Construction date	Test date
Reference structure			
ABS16	0.04	1996-12-03	2017-03-05
AG22	0.09	1996-12-02	2017-03-05
AG22	0.105	1996-12-01	2017-03-05
FAS structure			
Viacotop	0.04	1996-12-03	2017-03-30
Viacobind	0.08	1996-12-02	2017-03-30
Viacobase	0.115	1996-12-01	2017-03-30

Material input data

Poisson's ratio			
y_{span}	y_{min}	λ	x_{shift}
0.35	0.16	0.08	15.18

Viscosity parameters				
Reference structure				
	a_1	a_2	a_3	**n**
ABS16	0.0004	-0.1323	6.4099	0.08
AG22	0.0004	-0.1323	6.9110	0.08
FAS structure				
Viacotop	0.0004	-0.1323	6.5269	0.08
Viacobind	0.0004	-0.1323	7.0072	0.08
Viacobase	0.0004	-0.1402	6.9952	0.08

Traffic input data

BWIM		E6 Löddeköpinge
Annual traffic growth [%]		4.09
Design period [years]		20
Amount of dual wheels [%]		52
Speed [km/h]		91.2
Traffic wander standard deviation [m]		0.2909
Dual wheel centre to centre distance [m]		0.3155
Widebase tire	Tyre type	G165 425/65R22.5
	Inflation pressure [kPa]	800
Dual tire	Tyre type	BF12 295/80R22.5
	Inflation pressure [kPa]	800
Traffic distribution factors	d_1	0.61
	d_2	13.54
	d_3	0.04
	d_4	0.02

Appendix VI – Temperature data

Falkenberg temperature measurements, average based on measurements from 4 years

Depth [m]	Time [h]	Jan	Feb	Mar	Apr	May	June	July	Aug	Sep	Oct	Nov	Dec
0.02	0	-2.02	-1.70	1.62	7.33	13.40	19.50	22.15	19.52	13.75	7.96	4.74	-0.80
0.02	1	-2.11	-1.83	1.30	6.78	12.64	18.60	21.38	18.97	13.36	7.75	4.65	-0.77
0.02	2	-2.19	-1.96	0.97	6.35	12.03	18.23	20.76	18.49	13.01	7.55	4.57	-0.80
0.02	3	-2.28	-2.07	0.76	5.90	11.49	17.18	20.21	18.08	12.75	7.41	4.50	-0.81
0.02	4	-2.36	-2.17	0.55	5.51	11.03	16.68	19.71	17.71	12.45	7.24	4.45	-0.82
0.02	5	-2.42	-2.24	0.38	5.22	10.60	16.19	19.31	17.41	12.18	7.12	4.43	-0.86
0.02	6	-2.46	-2.29	0.22	4.95	10.31	15.87	18.99	17.12	11.92	7.02	4.39	-0.90
0.02	7	-2.49	-2.31	0.20	4.94	10.54	15.98	19.02	17.00	11.72	6.95	4.36	-0.90
0.02	8	-2.49	-2.26	0.67	5.49	11.49	16.68	19.50	17.09	11.78	6.95	4.36	-0.89
0.02	9	-2.44	-2.03	1.77	6.78	12.85	17.80	20.43	17.67	12.39	7.26	4.51	-0.84
0.02	10	-2.20	-1.41	3.27	8.65	14.59	19.34	21.69	18.66	13.64	8.06	4.85	-0.66
0.02	11	-1.71	-0.58	5.07	10.62	16.55	21.10	23.25	20.00	15.18	9.27	5.42	-0.32
0.02	12	-1.14	0.29	6.68	12.78	18.50	22.85	24.78	21.39	16.79	10.47	5.91	0.11
0.02	13	-0.71	1.02	8.03	14.52	20.28	24.50	26.34	22.79	18.25	11.49	6.26	0.35
0.02	14	-0.52	1.44	8.72	15.82	21.72	26.05	27.67	24.18	19.39	12.10	6.30	0.37
0.02	15	-0.60	1.44	8.77	16.46	22.56	26.97	28.68	25.30	19.97	12.23	6.11	0.25
0.02	16	-0.83	1.05	8.21	16.15	22.38	27.57	29.16	25.88	20.02	11.82	5.77	0.04
0.02	17	-1.10	0.50	7.14	15.60	22.20	27.60	29.13	25.64	19.52	11.27	5.45	-0.15
0.02	18	-1.31	-0.04	5.83	14.56	21.37	27.60	28.80	25.25	18.57	10.40	5.23	-0.28
0.02	19	-1.49	-0.43	4.66	13.01	20.14	26.72	28.20	24.40	17.30	9.68	5.06	-0.38
0.02	20	-1.63	-0.71	3.77	11.31	18.59	25.50	27.10	23.20	16.18	9.13	4.93	-0.44
0.02	21	-1.76	-0.94	3.09	9.93	17.04	23.97	25.78	21.92	15.22	8.76	4.82	-0.57
0.02	22	-1.90	-1.15	2.54	8.95	15.65	22.33	24.40	20.79	14.55	8.38	4.71	-0.67
0.02	23	-2.01	-1.36	2.08	8.19	14.49	20.84	23.13	19.90	14.02	8.11	4.60	-0.72

VViS 1336 temperature measurements, average based on measurements from 3 years

Depth [m]	Time [h]	Jan	Feb	Mar	Apr	May	June	July	Aug	Sep	Oct	Nov	Dec
0.002	0	-0.75	0.97	3.14	8.14	12.54	16.87	19.93	17.22	18.90	9.01	4.36	2.58
0.002	1	-0.82	0.88	2.88	8.07	11.84	15.85	18.95	16.71	18.47	8.71	4.27	2.43
0.002	2	-0.97	0.77	2.60	7.98	11.24	15.10	18.14	16.24	17.99	8.48	4.23	2.33
0.002	3	-0.95	0.73	2.43	7.78	10.77	14.55	17.58	15.61	17.33	8.26	4.27	2.32
0.002	4	-1.04	0.69	2.26	7.55	10.45	14.11	17.09	15.04	16.60	7.96	4.12	2.33
0.002	5	-1.08	0.66	2.16	7.39	10.37	13.99	16.73	14.82	16.07	7.89	4.13	2.27
0.002	6	-1.06	0.64	2.30	7.19	10.76	14.36	16.67	14.94	15.74	7.87	4.22	2.26
0.002	7	-1.03	0.62	2.88	7.26	12.10	16.02	17.42	15.69	15.39	7.87	4.35	2.33
0.002	8	-0.97	0.70	4.12	8.38	15.05	18.06	19.04	17.34	15.33	8.11	4.57	2.41
0.002	9	-0.82	1.29	5.89	10.27	17.78	20.48	21.02	19.53	15.84	8.64	5.00	2.70
0.002	10	-0.47	2.29	7.82	12.38	21.02	22.79	23.67	21.95	16.58	9.57	5.69	3.22
0.002	11	0.07	3.32	9.58	14.42	23.91	24.91	26.35	24.17	17.27	10.61	6.29	3.76
0.002	12	0.53	4.20	11.02	15.87	26.29	27.00	28.22	26.34	17.67	11.66	6.75	4.21
0.002	13	0.94	4.70	11.80	17.02	27.56	28.41	30.34	27.72	18.03	12.44	6.91	4.35
0.002	14	1.07	4.77	11.91	17.61	27.86	29.35	31.90	28.46	18.06	12.77	6.74	4.12
0.002	15	0.91	4.43	11.29	17.26	27.67	29.43	32.55	28.37	17.55	12.77	6.37	3.76
0.002	16	0.57	3.73	9.97	16.72	26.47	29.15	32.74	28.32	17.52	12.63	5.83	3.45
0.002	17	0.21	2.98	8.48	15.58	24.86	28.26	32.17	27.53	17.84	12.11	5.35	3.29
0.002	18	-0.09	2.38	7.05	13.90	23.05	27.31	30.93	26.16	17.92	11.48	5.01	3.18
0.002	19	-0.27	1.94	5.93	12.02	20.86	25.77	29.47	24.48	18.04	10.77	4.80	3.10
0.002	20	-0.40	1.63	5.10	10.39	18.48	23.90	27.41	22.50	18.20	10.21	4.64	2.99
0.002	21	-0.50	1.40	4.51	9.51	16.31	21.82	25.19	20.64	19.41	9.85	4.50	2.89
0.002	22	-0.59	1.24	4.04	8.92	14.70	19.91	23.09	19.15	18.99	9.50	4.32	2.83
0.002	23	-0.66	1.08	3.60	8.66	13.63	18.35	21.33	18.37	19.13	9.22	4.21	2.76